TWO-DIMENSIONAL AND RADIAL LAMINAR FREE JETS AND WALL JETS

A THESIS

Presented to

The Faculty of the Graduate Division

by

John Patrick Crenshaw

In Partial Fulfillment

of the Requirements for the Degree

Doctor of Philosophy in the

School of Aerospace Engineering

Georgia Institute of Technology

July, 1966

In presenting the dissertation as a partial fulfillment of the requirements for an advanced degree from the Georgia Institute of Technology, I agree that the Library of the Institute shall make it available for inspection and circulation in accordance with its regulations governing materials of this type. I agree that permission to copy from, or to publish from, this dissertation may be granted by the professor under whose direction it was written, or, in his absence, by the Dean of the Graduate Division when such copying or publication is solely for scholarly purposes and does not involve potential financial gain. It is understood that any copying from, or publication of, this dissertation which involves potential financial gain will not be allowed without written permission.

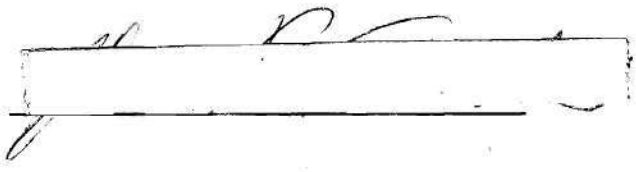

3/17/65
b

TWO-DIMENSIONAL AND RADIAL

LAMINAR FREE JETS AND WALL JETS

Approved:

Chairman

Date approved by Chairman Aug 22, 1966

ACKNOWLEDGMENTS

The author is extremely grateful for the understanding and support of many of his friends and family throughout his academic career. Without their assistance his educational endeavor would have been impossible.

To Mr. James E. Hubbartt, who suggested this problem, the author owes a special debt of gratitude. Mr. Hubbartt's willingness to stay in the main stream of the work, dedicating many hours to unglamourous trouble shooting as well as offering valuable suggestions, is unparalleled to the author's knowledge. The time and suggestions contributed by the other members of the author's thesis reading committee, Dr. Howard M. McMahon and Dr. Robin B. Gray, are gratefully acknowledged. The author is grateful to Mr. Calvin H. Wiser, whose skill, patience, and enthusiasm for his work made the experimental apparatus possible. To Dr. Arnold L. Ducoffe, who encouraged the author to continue his education, deep appreciation is expressed.

The author is indebted to his mother, who has been the guiding light of his academic endeavor. He is particularly grateful to his wife, Carolyn, whose influence has been an inspiration to him through a trying period of his life.

The author also wishes to express his appreciation to the National Aeronautics and Space Administration and the Ford Foundation for the financial assistance that made his education possible.

TABLE OF CONTENTS

TABLE OF CONTENTS (Continued)

LIST OF ILLUSTRATIONS

LIST OF ILLUSTRATIONS (Continued)

LIST OF ILLUSTRATIONS (Continued)

SUMMARY

The subject of this study is the downstream development of constant pressure free jets and wall jets. The wall jet is defined as a jet which is restricted on one side by a solid surface (wall) extending parallel to the direction of the flow and is unrestricted on the other side. Both two-dimensional and radial free jets and wall jets are analyzed for several typical initial and boundary conditions. In each case the solutions approach asymptotic, or similar, solutions as the downstream development length approaches infinity. This study is concerned with evaluating the development region between the initial conditions and the asymptotic solutions. Two methods are used for obtaining analytical solutions to the jets in the development region. The first is a numerical solution of the compressible boundary layer equations for a Prandtl number of unity. The second is an approximate integral solution for the velocity distributions obtained by assuming these distributions can be approximated by simple polynomials.

The boundary layer equations for the two-dimensional and radial jets are transformed first from the physical co-ordinates to equivalent incompressible co-ordinates using a Howarth type transformation. Further, the assumption that the viscosity is proportional to the temperature allows the separation of the momentum equation from the energy equation. Under this assumption the velocity and temperature distributions are obtained one at a time rather than simultaneously. The equations for the radial jets are reduced to the equations of the two-dimensional jets

through another transformation of the Mangler type. The resulting equations are identical to those for the two-dimensional incompressible flow with constant viscosity. They are applicable to either free jets or wall jets according to the boundary conditions chosen. The numerical scheme selected to solve these equations uses an explicit forward difference in the downstream co-ordinate and an implicit central difference in the normal co-ordinate. The implicit difference technique requires a finite range of the normal co-ordinate, a condition satisfied by an additional transformation of the normal co-ordinate to a momentum co-ordinate. The resulting equations were solved on a Burroughs 5500 computer for both free jets and wall jets.

The purpose of the approximate solution is to investigate the possibility of using a relatively simple integral technique, as opposed to the complicated finite difference technique, to obtain the velocity distributions of these jets. The cases investigated are the free jet and the wall jet with uniform initial velocity distributions. The development region of the jets is subdivided into two parts. The first part extends downstream from the initial conditions to the point of initial decay of the maximum velocity. The second part extends downstream from this point to the asymptotic condition. The velocity distributions are represented by simple polynomials which satisfy boundary conditions, the integral momentum equation, and the F integral relation which was introduced by Glauert for the asymptotic solution for the wall jet. The F integral relation is modified to apply to the free jet as well as the wall jet.

An experiment of limited scope was conducted for the two-dimensional wall jet. The experimentally measured velocity distributions in the

laminar development region are compared to the results of the exact theory. From this comparison, the approximate distance downstream to transition from laminar to turbulent flow is established. Although this transition data is limited to a single test condition, it is, to the author's knowledge, the first determination of transition for a wall jet.

Results of the numerical solutions of the momentum equation for both free jets and wall jets with various initial velocity distributions are presented as working plots. These results approach the asymptotic solution far downstream of the initial condition. Further, this comparison shows that the asymptotic solutions are good approximations to the exact solutions only after the maximum velocities of the jets have decayed to about one half of their original values for the free jets and one third of their original values for the wall jets. The results for free jets and wall jets show that the solutions for the uniform initial velocity distributions are better approximations to the solutions for the other initial velocity distributions than are the asymptotic solutions. Further, it is argued that this will generally be the case regardless of the initial conditions of the jets. A comparison of the wall shear in the development region of the wall jet for several initial conditions yields a good correlation of the wall shear for a wide range of jet initial conditions.

The approximate integral solutions for the free jet and the wall jet of uniform initial velocity distributions result in a closed form solution for the free jet and a simple numerical solution for the wall jet. These solutions predict the maximum velocity and general shape of

the velocity distribution well but do not predict the thickness of the viscous layer as well. The wall shear for the wall jet predicted by this method is very close to the exact solution. These results show the approximate method to be an adequate method for obtaining jet characteristics relatively easily.

The theoretical results from the exact solution for the wall jet compare well with the experimentally measured velocity distributions until the jet becomes turbulent. The transition Reynolds number is 450 based on the initial jet width and is 12,600 based on the downstream distance to transition from the nozzle exit. These transition Reynolds numbers are an order of magnitude above that for the free jet and below that for the boundary layer. Therefore, the wall has a stabilizing effect on the wall jet as compared to the free jet, whereas the finite dimension of the jet width has a destabilizing effect on the wall jet as compared to the boundary layer.

NOMENCLATURE

Roman Symbols

A	- constant in the approximate velocity distributions dependent on the boundary conditions
$A(i,j)$	- coefficient in the finite difference equations
B	- constant in the approximate velocity distributions dependent on the boundary conditions
$B(i,j)$	- coefficient in the finite difference equations
C	- constant in the approximate velocity distribution dependent on the boundary conditions
c	- Chapman's viscosity constant; equation (2.6)
c_p	- coefficient of specific heat at constant pressure
C_1, C_2	- constants in Crocco solution to the conservation of energy equation; equation (2.44)
$C(i,j)$	- the inhomogeneous term in the finite difference equations
D	- constant in the approximate velocity distributions dependent on the boundary conditions
d	- height of initial velocity distribution; Figures 2 and 3
F	- integral relation; equation (2.26)
g	- dummy function
h	- enthalpy
K	- dummy variable in finite difference equations
L	- dummy variable in finite difference equations
M^*	- momentum co-ordinate; equation (2.29)
M_o	- total momentum integral; equation (2.22)
N	- dummy variable in finite difference equations
Pr	- Prandtl number

NOMENCLATURE (Continued)

q	- heat transfer
R	- gas constant
S	- constant in viscosity relation dependent on the gas
s	- radial downstream co-ordinate; equation (2.15)
T	- static temperature
T_o	- stagnation temperature
u	- velocity component in x direction
v	- velocity component in y direction
$\tilde{v}$	- dummy velocity variable
X	- compressible downstream co-ordinate; equation (2.9)
x	- physical downstream co-ordinate
Y	- compressible normal co-ordinate; equation (2.10)
y	- physical normal co-ordinate
z	- transformed normal co-ordinate; equation (2.16)

Greek Symbols

α, β	- momentum grid control variables
ΔM	- momentum grid increment
ΔS	- downstream grid increment
δ	- layer thickness
η	- dummy variable
Θ	- temperature cubed
$\bar{\Theta}$	- mean cubed temperature

μ - dynamic viscosity

ν - velocity cubed

$\bar{\nu}$ - mean cubed velocity

ξ - dummy variable

ρ - density

τ - wall shear stress

Superscript

* - referring to dimensionless variables

Subscripts

a - referring to particular portion of jet; Figures 2 and 3

b - referring to particular portion of jet; Figures 2 and 3

e - referring to external fluid condition

f - referring to free jet

i - difference index in downstream co-ordinate

in - referring to initial condition

j - difference index in normal co-ordinate

m - mean

max - maximum

r - referring to reference condition

w - referring to wall jet or wall

CHAPTER I

INTRODUCTION

For the purpose of this work, a jet is defined as a finite laminar stream of a viscous fluid discharging into the same fluid at rest. The static pressure of the jet fluid is the same as the pressure of the fluid at rest. An unrestricted jet is termed a "free jet." If the jet is restricted parallel to the direction of the flow by a solid surface (wall), then the jet is termed a "wall jet."

The free jets are the more familiar of the two types of jets and can have any number of different geometries. Three of the most familiar geometries are the axisymmetric free jet, the two-dimensional free jet, and the radial free jet. The radial free jet is defined as one issuing radially from the slit between two parallel circular disks. Each of these jets can be restricted in one dimension by a wall to form the corresponding wall jet. The axisymmetric wall jet surrounds a cylindrical center body. The two-dimensional wall jet is restricted by a plane wall extending in the direction of the flow (e.g., an extension of a nozzle wall downstream of the nozzle exit). The radial wall jet is restricted by a plane wall extending radially in the direction of the flow (e.g., an extension of one nozzle wall downstream of the nozzle exit). This study is concerned with the two-dimensional and radial free jet and wall jet as described above. The axisymmetric jets are not investigated.

The free jets, as the more common and practical of the two types of jets, have attracted the most attention in the past. Interest in the

wall jet, however, arises through such problems as the direct impingement of a jet on a surface, the flow from beneath ground effect machines, and the flows in separated regions and cavities. Asymptotic solutions for the two-dimensional laminar incompressible free jet, and for the two-dimensional and radial laminar incompressible wall jets, exist in the literature (1, 2, 3). These references present the solutions of Prandtl's partial differential equations for the boundary layer, which are obtained through a similarity analysis for each kind of jet. Under the condition of similarity the partial differential equations are reduced to ordinary differential equations. Each resulting solution holds for wall jets of a particular kind and strength far enough downstream such that the details of the initial conditions of the jets no longer affect the solutions. The asymptotic solution to the radial free jet is obtained from the two-dimensional solution through a transformation presented herein. The asymptotic solutions for the wall jets have been extended by Riley to include the effects of compressibility (4). A summary of the work on free jet flow is found in reference (5).

The asymptotic solutions offer results for the jets far downstream of the starting region but are not useful for predicting the flow characteristics close to the initial condition. Furthermore, the extent of the region affected by the initial condition is unknown. The research reported herein concentrates on the downstream development of the jets for various initial conditions until they have essentially reached the asymptotic conditions. This region of nonsimilar shear flow is hereafter termed the "development region."

Two methods are used for obtaining solutions to the jets in the

development region. The first is referred to as the exact solution and involves a numerical solution of the compressible boundary layer equations for a Prandtl number of unity. The second is referred to as the approximate solution and is an integral technique for obtaining the velocity distribution by assuming these distributions can be approximated by simple polynomials.

The boundary layer equations of the exact solution for the two-dimensional and radial jets are transformed first from the physical co-ordinates to equivalent incompressible co-ordinates using a Howarth type transformation (6). Further, the assumption that the viscosity is proportional to the temperature allows the separation of the momentum equation from the energy equation (7). Under this assumption the velocity and temperature distributions are obtained one at a time rather than simultaneously. The equations for the radial jets are reduced to the equations of the two-dimensional jets through another transformation of the Mangler type. The new co-ordinates are referred to as the transformed co-ordinates. The resulting equations are identical to those for the two-dimensional incompressible flow with constant viscosity. They are applicable to either free jets or wall jets according to the boundary conditions chosen. The numerical scheme selected to solve these equations is explicit in the downstream co-ordinate and implicit in the normal co-ordinate. The explicit difference is a forward difference and the implicit difference is an averaged central difference. The implicit difference technique requires a finite range of the normal co-ordinate, a condition satisfied by a transformation of the normal co-ordinate to a momentum co-ordinate. The resulting equations were solved on a Burroughs 5500

computer for both free jets and wall jets of various initial and boundary conditions.

The purpose of the approximate solution is to investigate the possibility of using the relatively simple integral techniques, as opposed to the complicated finite difference technique, to obtain the velocity distributions of these jets. The cases considered are the free jet and the wall jet with uniform initial velocity conditions. The method consists of studying the development region of the jets in two parts. The first part extends downstream from the initial conditions to the point of initial decay of the maximum velocity. The second part extends downstream from this point to the asymptotic condition. The relations satisfied are the integral momentum equation and the F integral relation introduced by Glauert for the wall jet (3). The F integral relation is modified to apply to the free jet as well as to the wall jet.

An experiment of limited scope was conducted for the two-dimensional wall jet. The experimentally measured velocity distributions in the laminar development region are compared to the results of the exact theory. From this comparison the approximate distance downstream to transition from laminar to turbulent flow is established. Although this transition data is limited to a single test condition, it is, to the author's knowlege, the first determination of transition for a wall jet.

CHAPTER II

THEORETICAL ANALYSIS

The development of the velocity distributions for a free jet and a wall jet with uniform initial velocity conditions is illustrated in Figure 1. The x and y co-ordinates are the downstream and normal co-ordinates, respectively. The $y = 0$ line corresponds to the center-line of a symmetrical free jet and to the wall of a wall jet. All the free jets considered in this study are symmetrical with respect to the line $y = 0$. Then, only that portion of the free jet for $y \geq 0$ must be considered in order to completely determine the free jet. All properties and distributions presented for the free jet throughout this study will refer to that portion of the jet from $y = 0$ to $y \to \infty$. The reference properties, denoted by the subscript r, refer to the specified properties of the jet at the maximum velocity of the initial condition.

Equations and Assumptions

The equations required to study the flow of a viscous compressible fluid are as follows:

(i) momentum equation

(ii) energy equation

(iii) continuity equation

(iv) thermodynamic equation of state

(v) viscosity relationship

The momentum and energy equations used in this work are the classic

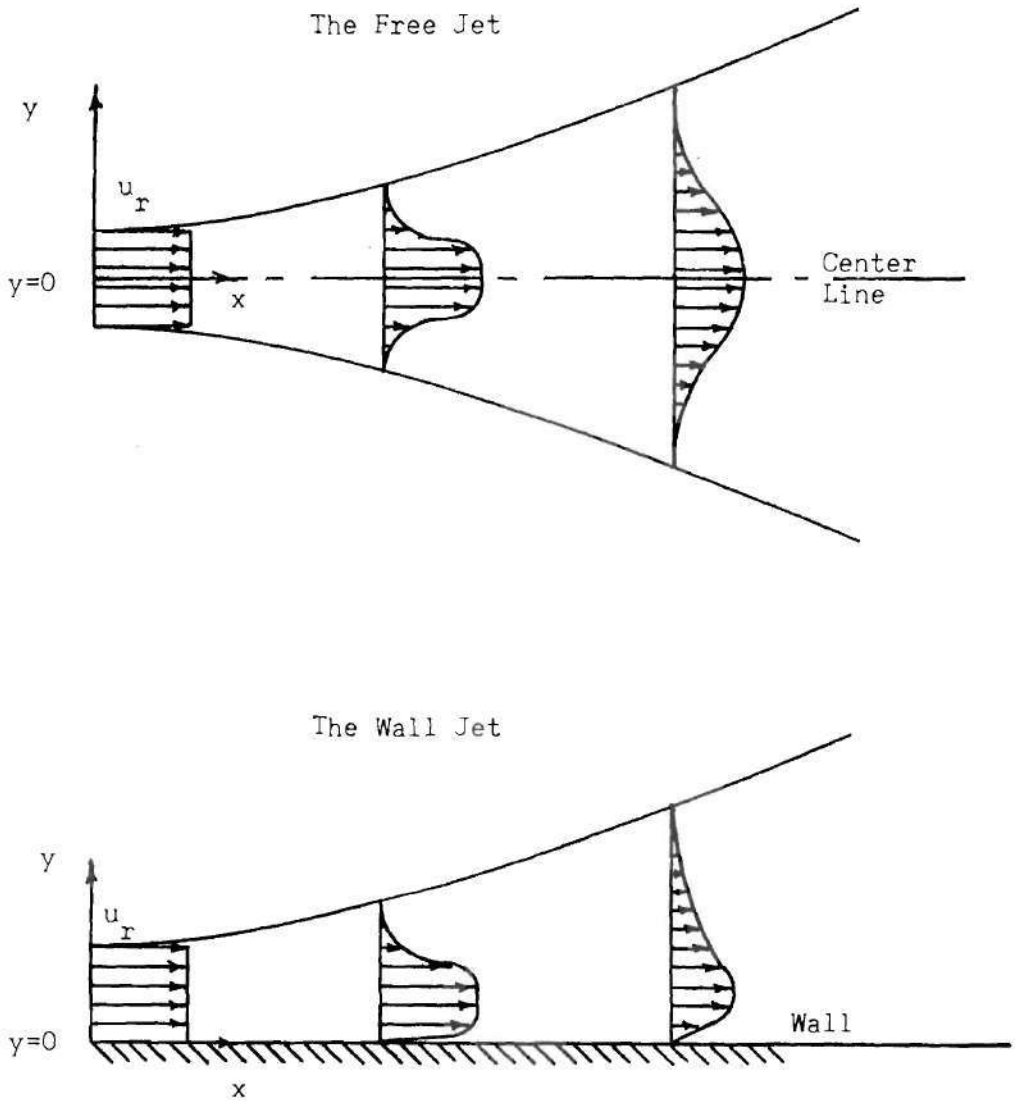

Figure 1. Illustration of the Development of the Free Jet and the Wall Jet.

equations used to study the flow of a fluid of small viscosity. They were introduced by Prandtl as simplifications of the Navier-Stokes equations and are termed the boundary layer equations (8). The thermodynamic equation of state used is that for a calorically and thermally perfect gas, and the viscosity is assumed to vary in direct proportion to the temperature. Further, the static pressure is assumed constant, and the Prandtl number of the gas is assumed equal to unity. These five equations relate the five unknowns

(i) the velocity component in the x direction, u

(ii) the velocity component in the y direction, v

(iii) the temperature, T

(iv) the density, ρ

(v) the viscosity, μ

to the physical co-ordinates of the field, x and y. They are expressed as follows:

the momentum equation,

$$\rho\left(u \frac{\partial u}{\partial x} + v \frac{\partial u}{\partial y}\right) = \frac{\partial}{\partial y}\left(\mu \frac{\partial u}{\partial y}\right) \tag{2.1}$$

the energy equation,

$$\rho\left(u \frac{\partial T}{\partial x} + v \frac{\partial T}{\partial y}\right) = \frac{\partial}{\partial y}\left(\mu \frac{\partial T}{\partial y}\right) + \frac{\mu}{c_p}\left(\frac{\partial u}{\partial y}\right)^2 \tag{2.2}$$

the continuity equation,

$$\frac{\partial(\rho u x^k)}{\partial x} + \frac{\partial(\rho v x^k)}{\partial y} = 0 \tag{2.3}$$

the equation of state,

$$\rho T = \rho_r T_r \tag{2.4}$$

and the viscosity equation,

$$\frac{\mu}{T} = c \frac{\mu_r}{T_r} \tag{2.5}$$

For the two-dimensional cases, $k = 0$, and for the radial cases, $k = 1$. The Chapman constant, c, is derived from the Sutherland viscosity relation and is expressed as

$$c = \sqrt{\frac{T_m}{T_r}} \quad \frac{T_r + S}{T_m + S} \tag{2.6}$$

where T_m is a mean flow temperature, and S is an empirical constant related to the gas (7). This form of the viscosity relation yields satisfactory results and leads to an uncoupling of the momentum equation from the energy equation (7). Under this condition, an independent solution of the velocity distribution can be obtained without involving the temperature distribution. This result can then be used in the solution of the temperature distribution. The specific heat at constant pressure, c_p, is assumed to be a specified constant (i.e., the fluid is a calorically perfect gas). This condition can be eliminated by substituting enthalpy for temperature in the results presented in this study. The physical co-ordinates of the jets, however, can only be obtained if the expression for c_p is known. The results for the physical co-ordinates presented here are for c_p equal to a specified constant and are not

applicable to the more general case.

The unknowns of interest are the velocity, u, and the temperature, T. Since the line $y = 0$ is either the centerline of the free jet or the wall of the wall jet, then at $y = 0$, $v = 0$. The velocity, v, can be eliminated from equations (2.1) and (2.2) by substitution from equation (2.3). The resulting equations combined with the above condition are

$$\rho \left[u \frac{\partial u}{\partial x} - \frac{1}{x^k} \left(\int_o^y \frac{\partial(\rho u x^k)}{\partial x} dy \right) \frac{\partial u}{\partial y} \right] = \frac{\partial}{\partial y} \left(\mu \frac{\partial u}{\partial y} \right) \tag{2.7}$$

$$\rho \left[u \frac{\partial T}{\partial x} - \frac{1}{x^k} \left(\int_o^y \frac{\partial(\rho u x^k)}{\partial x} dy \right) \frac{\partial T}{\partial y} \right] = \frac{\partial}{\partial y} \left(\mu \frac{\partial T}{\partial y} \right) + \frac{\mu}{c_p} \left(\frac{\partial u}{\partial y} \right)^2 \tag{2.8}$$

Since the density is related to the temperature through equation (2.4), then equations (2.7) and (2.8) are two equations for the two unknowns of interest, u and T. The initial and boundary conditions for these equations that pertain to the jets studied here are as follows:

for the free jets,

initial conditions

$$u(x_{in}, y) = u_{in}(y) \text{ and } T(x_{in}, y) = T_{in}(y)$$

boundary conditions

$$y = 0, \frac{\partial u}{\partial y} = \frac{\partial T}{\partial y} = 0$$

$$y = \infty, u = 0 \text{ and } T = T_e$$

for the wall jets,

initial conditions

$$u(x_{in},y) = u_{in}(y) \text{ and } T(x_{in},y) = T_{in}(y)$$

boundary conditions

$$y = 0, \quad u = 0 \text{ and } T = T_w \text{ or } \frac{\partial T}{\partial y} = 0$$

$$y = \infty, \quad u = 0 \text{ and } T = T_e$$

The temperatures T_e and T_w are the exterior fluid temperature and wall temperature, respectively, and are constants for the case of a particular jet. The boundary condition that the slope of the temperature at the wall is equal to zero describes the adiabatic or insulated wall case.

Transformation to Incompressible Form

The compressible flow problem can be simplified through a transformation of the physical co-ordinates as demonstrated by Howarth (6). Let

$$X = cx \tag{2.9}$$

$$Y = \int_o^y \frac{\rho}{\rho_r} \, dy = \int_o^y \frac{T_r}{T} \, dy \tag{2.10}$$

be the new co-ordinates. As shown in Appendix A, equations (2.7) and (2.8) under this transformation combined with equations (2.4) and (2.5) become

$$u \frac{\partial u}{\partial X} - \frac{1}{X^k} \left(\int_o^Y \frac{\partial (uX^k)}{\partial X} \, dY \right) \frac{\partial u}{\partial Y} = \frac{\mu_r}{\rho_r} \frac{\partial^2 u}{\partial Y^2} \tag{2.11}$$

$$u \frac{\partial T}{\partial X} - \frac{1}{X^k} \left(\int_o^Y \frac{\partial (uX^k)}{\partial X} \, dY \right) \frac{\partial T}{\partial Y} = \frac{\mu_r}{\rho_r} \frac{\partial^2 T}{\partial Y^2} + \frac{\mu_r}{\rho_r c_p} \left(\frac{\partial u}{\partial Y} \right)^2 \tag{2.12}$$

The boundary and initial conditions for equations (2.11) and (2.12) in terms of X and Y are the same as those for equations (2.7) and (2.8) in terms of x and y. Equation (2.11) is identical to the momentum equation of an incompressible flow with a constant viscosity if X and Y are the physical co-ordinates of the flow. It can be solved independently for $u(X,Y)$. This solution can then be used in equation (2.12) to obtain $T(X,Y)$. The velocity and temperature distributions can be expressed in terms of the physical co-ordinates of the jets by inverting the transformation equations (2.9) and (2.10). That is

$$x = \frac{X}{c} \tag{2.13}$$

$$y = \int_o^Y \frac{T}{T_r} \, dY \tag{2.14}$$

combined with equation (2.6) for the Chapman constant, c, yields the physical co-ordinates of the jets. The transformed compressible co-ordinates, X and Y, will hereafter be referred to as the incompressible co-ordinates.

Transformation to Two-Dimensional Form

It is not necessary to solve the equations of viscous flow for both the two-dimensional and radial flow conditions. A transformation of the

independent variables, as shown in Appendix A, allows both the two-dimensional and radial problems to be solved simultaneously. Let

$$s = \frac{X^{2k+1} - X_{in}^{2k+1}}{2k+1} \tag{2.15}$$

$$z = X^{k}Y \tag{2.16}$$

where X_{in} is the initial axial location in the incompressible co-ordinate. Under this transformation, equations (2.11) and (2.12) become

$$u \frac{\partial u}{\partial s} - \left(\int_o^z \frac{\partial u}{\partial s} \, dz \right) \frac{\partial u}{\partial z} = \frac{\mu_r}{\rho_r} \frac{\partial^2 u}{\partial z^2} \tag{2.17}$$

$$u \frac{\partial T}{\partial s} - \left(\int_o^z \frac{\partial u}{\partial s} \, dz \right) \frac{\partial T}{\partial z} = \frac{\mu_r}{\rho_r} \frac{\partial^2 T}{\partial z^2} + \frac{\mu_r}{\rho_r c_p} \left(\frac{\partial u}{\partial z} \right)^2 \tag{2.18}$$

The variable k does not appear in equations (2.17) and (2.18). Further, these equations are of the same form as equations (2.11) and (2.12) for $k = 0$ (i.e., the two-dimensional flow case). The initial and boundary conditions in terms of these new co-ordinates are identical to those of the incompressible two-dimensional problem.

As a consequence of this transformation, only the two-dimensional cases need to be investigated, since solutions to the radial problems can be obtained directly from solutions to the two-dimensional problems with the aid of equations (2.15) and (2.16). This same correspondence can be obtained as a special case of the Mangler transformation, which transforms the axisymmetric boundary layer equations into approximately

equivalent two-dimensional equations (9). In fact, Riley used the Mangler transformation to show that the asymptotic solution for the radial wall jet could be derived from the two-dimensional solution (10). Unlike the general Mangler transformation, however, the transformation for the radial flow case, as developed herein, is exact and does not require that the thickness of the viscous layer be small compared to the radial distance to a point in the flow. The radial flow transformation is particularly significant, since for any given initial velocity and temperature condition there exists an infinite number of problems corresponding to an infinite number of initial radial distances to the initial condition. All of these, however, map into the single two-dimensional solution through equations (2.15) and (2.16).

The transformations of compressible flow (equations (2.9) and (2.10)) and of radial flow (equations (2.15) and (2.16)) can finally be combined to give a single set of equations relating the physical co-ordinates of two-dimensional or radial compressible flows to the transformed co-ordinates of equations (2.17) and (2.18). These final transformation equations are

$$s = \frac{(cx)^{2k+1} - (cx_{in})^{2k+1}}{2k + 1} \tag{2.19}$$

$$z = (cx)^{k} \int_{o}^{y} \frac{T_r}{T}\, dy \tag{2.20}$$

where x and y are, again, the physical co-ordinates of the flow. The co-ordinates s and z will, hereafter, be referred to as the transformed co-ordinates. Solutions of equations (2.19) and (2.20) for x and y

combined with the solutions of equations (2.17) and (2.18) for u and T with the appropriate initial and boundary conditions constitute the exact solutions of the jets considered in this study.

Asymptotic Solutions

As mentioned in Chapter I, both the free jet and the wall jet problems have asymptotic solutions (similar solutions) which correspond to the exact solutions of the jets only as the downstream distances from the initial conditions become infinite. These solutions were developed in references (1) and (2) for the free jet and in reference (3) for the wall jet. They are important to this study as checks on the solutions far downstream and as indications of the extent of the development regions covered. Furthermore, the present study is concerned with determining the upstream limit of applicability of these simple asymptotic solutions. These solutions also give rise to some jet conservation integrals which will prove useful in the approximate analysis presented later.

Free Jet

The asymptotic solution of reference (2) in terms of the present nomenclature, and thus for both two-dimensional and radial free jets, is given by

$$u = \frac{3^{1/3}}{2}\left(\frac{M_o^2}{\rho_r \mu_r s}\right)^{1/3} \operatorname{sech}^2\left[\frac{1}{2(3)^{1/3}}\left(\frac{\rho_r M_o}{\mu_r}\right)^{1/3}\left(\frac{z}{s^{2/3}}\right)\right] \qquad (2.21)$$

where M_o is the total momentum of the jet from $y = 0$ to $y = \infty$ defined by the expression

$$M_o = \rho_r \int_o^\infty u^2 dz \tag{2.22}$$

This integral expression for the total momentum is a measure of the strength of the free jet and, as shown in Appendix B, is constant for every downstream location along the jet. The value of M_o is dependent upon the initial condition for the free jet. Equation (2.21) is in terms of M_o and, therefore, the results from this expression depend upon the initial condition of the jet. This dependence can be removed by defining the following dimensionless variables:

$$u^* = \frac{u}{u_r}$$

$$s_f^* = \frac{\rho_r \mu_r u_r^3}{M_o^2} s$$

$$z_f^* = \frac{\rho_r u_r^2}{M_o} z$$

In terms of these variables, equation (2.21) becomes

$$u^* = \frac{(3^{1/3}/2)}{s_f^{*1/3}} \operatorname{sech}^2 \left(\frac{1}{2(3)^{1/3}} \frac{z_f^*}{s_f^{*2/3}} \right) \tag{2.23}$$

Wall Jet

The asymptotic solution of reference (3) in terms of the present nomenclature, and thus for both two-dimensional and radial wall jets, is

given by

$$u = \left(\frac{5F}{2\rho_r \mu_r s}\right)^{1/2} f'(\eta) \tag{2.24}$$

where

$$\eta = \left(\frac{5\rho_r F}{32\mu_r^3 s^3}\right)^{1/4} z \tag{2.25}$$

The function $f'(\eta)$ is given by the expressions

$$f'(\eta) = \frac{2}{3} g(1-g^3)$$

and

$$\eta = \log \frac{\sqrt{(1 + g + g^2)}}{1 - g} + \sqrt{3} \tan^{-1}\left(\frac{\sqrt{3}}{2 + g} g\right)$$

The F relation in equations (2.24) and (2.25) is given by

$$F = \rho_r^2 \int_0^\infty u \int_z^\infty u^2 dzdz \tag{2.26}$$

Glauert (3) shows that the F relation remains constant for the wall jet at every downstream location along the jet (see Appendix B). The total momentum of the wall jet is not conserved downstream, as it is in the case of the free jet, since there is a shear force on the wall.

The F relation, however, is conserved for the wall jet and serves as a measure of the strength of the wall jet in the same manner that the total momentum serves as a measure of the strength of the free jet.

The dependence of equations (2.24) and (2.25) upon the initial condition of the wall jet can be removed by defining the following dimensionless variables:

$$u^* = \frac{u}{u_r}$$

$$s_w^* = \frac{\rho_r \mu_r u_r^2}{F} s$$

$$z_w^* = \left(\frac{\rho_r u_r^3}{F}\right)^{1/2} z$$

The asymptotic solution for the wall jet becomes

$$u^* = \left(\frac{5}{2s_w^*}\right)^{1/2} f'(\eta) \qquad (2.27)$$

where

$$\eta = \left(\frac{5}{32}\right)^{1/4} \frac{z_w^*}{s_w^{*3/4}} \qquad (2.28)$$

The F relation can be used as a conservation integral in approximate analyses just as the expression for the total momentum and the moment of momentum have been used in the past. It is applicable

not only for a wall jet analysis, but with some modification it is useful for other jet-related problems as well. This usage will be demonstrated later in this chapter.

The Exact Solution

The general case of a laminar viscous free jet or wall jet in the development region involves a solution of equations (2.17) and (2.18) for the initial and boundary conditions appropriate for the jet. The general method of solution employed here is an implicit finite difference technique, which previously has been used successfully on a problem in heat transfer in a finite solid and on a viscous free layer problem (11, 12). This method requires a finite range of the normal co-ordinate. The z co-ordinate of equations (2.17) and (2.18) has an infinite range and, therefore, must be transformed into a normal co-ordinate with a finite range. For the jets studied here, a momentum co-ordinate serves this purpose. The transformation employed is

$$M^* = \frac{\rho_r}{M_o} \int_o^z u^2 dz \tag{2.29}$$

M_o is, as defined in equation (2.22), the total momentum from $y=0$ to $y = \infty$ at the particular station downstream. The new co-ordinate, M^*, is a dimensionless momentum co-ordinate with a range from zero to unity. As shown in Appendix A, equations (2.17) and (2.18), for either the free jet or the wall jet in terms of this new co-ordinate, become

$$\frac{M_o^2}{\rho_r \mu_r} u \frac{\partial u}{\partial s} = u^2 \frac{\partial}{\partial M^*} \left(u^2 \frac{\partial u}{\partial M^*} \right) + \left[(1 - M^*) \left(u^2 \frac{\partial u}{\partial M^*} \right)_{M^*=0} \right. \tag{2.30}$$

$$\left. - u^2 \frac{\partial u}{\partial M^*} \right] u \frac{\partial u}{\partial M^*}$$

$$\frac{M_o^2}{\rho_r \mu_r} u \frac{\partial T}{\partial s} = u^2 \frac{\partial}{\partial M^*} \left(u^2 \frac{\partial T}{\partial M^*} \right) + \left[(1-M^*) \left(u^2 \frac{\partial u}{\partial M^*} \right)_{M^*=0} \right. \tag{2.31}$$

$$\left. - u^2 \frac{\partial u}{\partial M^*} \right] u \frac{\partial T}{\partial M^*} + \frac{1}{c_\rho} \left(u^2 \frac{\partial u}{\partial M^*} \right)^2$$

where

$$M_o^2 = M_{o_{in}}^2 - 2\rho_r \mu_r \int_o^s \left(u^2 \frac{\partial u}{\partial M^*} \right)_{M^*=0} ds \tag{2.32}$$

The remainder of this section will be devoted to the methods of solution of equations (2.30), (2.31), and (2.32) for the cases of the free jet and the wall jet.

Free Jet

The boundary condition at $y = 0$ for the free jet is

$$\left(\frac{\partial u}{\partial y} \right)_{y=0} = \left(\frac{u^2}{M_o} \frac{\partial u}{\partial M^*} \right)_{M^*=0} = 0$$

Using this expression in equations (2.30), (2.31), and (2.32) gives

$$\frac{M_o^2}{\rho_r \mu_r} u \frac{\partial u}{\partial s} = u^2 \frac{\partial}{\partial M^*}\left(u^2 \frac{\partial u}{\partial M^*}\right) - u^3 \left(\frac{\partial u}{\partial M^*}\right)^2 \tag{2.33}$$

$$\frac{M_o^2}{\rho_r \mu_r} u \frac{\partial T}{\partial s} = u^2 \frac{\partial}{\partial M^*}\left(u^2 \frac{\partial T}{\partial M^*}\right) - u^3 \frac{\partial u}{\partial M^*}\frac{\partial T}{\partial M^*} \tag{2.34}$$

$$+ \frac{1}{c_\rho}\left(u^2 \frac{\partial u}{\partial M^*}\right)^2$$

It is convenient to introduce the following dimensionless variables as suggested by the asymptotic solution:

$$u^* = \frac{u}{u_r}$$

$$T^* = \frac{2h_r}{u_r^2}\,\frac{T-T_r}{T_r}$$

$$s_f^* = \frac{\rho_r \mu_r u_r^3}{M_o^2}\, s$$

$$z_f^* = \frac{\rho_r u_r^2}{M_o}\, z$$

where h_r is the enthalpy based on the reference initial condition. In terms of these variables, equations (2.33) and (2.34) become

$$u^* \frac{\partial u^*}{\partial s_f^*} = u^{*2} \frac{\partial}{\partial M^*} \left(u^{*2} \frac{\partial u^*}{\partial M^*} \right) - u^{*3} \left(\frac{\partial u^*}{\partial M^*} \right)^2 \tag{2.35}$$

$$u^* \frac{\partial T^*}{\partial s_f^*} = u^{*2} \frac{\partial}{\partial M^*} \left(u^{*2} \frac{\partial T^*}{\partial M^*} \right) - u^{*3} \frac{\partial u^*}{\partial M^*} \frac{\partial T^*}{\partial M^*} + 2 \left(u^{*2} \frac{\partial u^*}{\partial M^*} \right)^2 \tag{2.36}$$

with initial and boundary conditions

$$u^*(0,M^*) = u^*_{in}(M^*), \quad T^*(0,M^*) = T^*_{in}(M^*)$$

$$M^* = 0, \quad u^{*2} \frac{\partial u^*}{\partial M^*} = u^{*2} \frac{\partial T^*}{\partial M^*} = 0$$

$$M^* = 1, \quad u^* = 0 \quad \text{and} \quad T^* = T^*_e$$

The transformed normal co-ordinate, from equation (2.29), is

$$z_f^* = \frac{\rho_r u_r^2}{M_o} X^k Y = \int_o^{M^*} \frac{dM^*}{u^{*2}} \tag{2.37}$$

The physical normal co-ordinate, from equations (2.20) and (2.29), is given by

$$\frac{2h_r}{u_r^2} \left[\frac{\rho_r u_r^2}{M_o} (cx)^k \, y - z_f^* \right] = \int_o^{M^*} \frac{T^*}{u^{*2}} \, dM^* \tag{2.38}$$

when combined with equation (2.37).

Momentum Equation. The momentum equation for the free jet (equation (2.35)) is simplified somewhat if the dependent variable, u^*, is changed to u^{*3}. Let

$$\nu^* = u^{*3},$$

and equation (2.35) becomes

$$\frac{\partial \nu^*}{\partial s_f^*} = \nu^* \frac{\partial^2 \nu^*}{\partial M^{*2}} - \frac{1}{3}\left(\frac{\partial \nu^*}{\partial M^*}\right)^2 \qquad (2.39)$$

for the free jet in terms of the new dependent variable. The initial and boundary conditions for (2.39) are

$$\nu^*(0, M^*) = \nu^*_{in}(M^*)$$

$$M^* = 0, \quad \frac{\partial \nu^*}{\partial M^*} = 0$$

$$M^* = 1, \quad \nu^* = 0$$

Solutions to equation (2.39) are obtained through an implicit finite difference technique using a forward difference in s^* and an averaged central difference in M^*. The grid is varied in both the s^* and M^* directions. A very fine increment of s^* (10^{-8}) is used for s^* close to the initial condition. This increment is progressively increased as the solution proceeds downstream. The grid in the M^* coordinate is one hundred equal increments through the layer with the last grid increment subdivided into one hundred additional equal increments

in order to obtain a better solution as $y \to \infty$.

The details of the finite difference approximation to equation (2.39) are presented in Appendix C. The difference approximations used for the derivatives are

$$\left.\frac{\partial \nu^*}{\partial s_f^*}\right|_{M^*} \approx (\nu^*_{i,j+1} - \nu^*_{i,j})/\Delta s_f^* \tag{2.40}$$

$$\left.\frac{\partial \nu^*}{\partial M^*}\right|_{s_f^*} \approx \frac{1}{4\Delta M^*}\left[(\nu^*_{i+1,j+1} + \nu^*_{i+1,j} - \nu^*_{i,j+1} - \nu^*_{i,j})/\alpha + (\nu^*_{i,j+1} + \nu^*_{i,j} - \nu^*_{i-1,j+1} - \nu^*_{i-1,j})/\beta\right] \tag{2.41}$$

$$\left.\frac{\partial^2 \nu^*}{\partial M^{*2}}\right|_{s_f^*} \approx \frac{1}{(\alpha+\beta)\Delta M^{*2}}\left[(\nu^*_{i+1,j+1} + \nu^*_{i+1,j} - \nu^*_{i,j+1} - \nu^*_{i,j})/\alpha - (\nu^*_{i,j+1} + \nu^*_{i,j} - \nu^*_{i-1,j+1} - \nu^*_{i-1,j})/\beta\right] \tag{2.42}$$

where Δs_f^* is the downstream increment, ΔM^* is the smallest increment in the momentum grid, 10^{-4}, i is the M^* index, j is the s_f^* index, and the momentum grid control variables, α and β, are

$$\alpha = \beta = 100 \quad \text{for} \quad 0 < i < 100$$

$$\alpha = 100, \beta = 1 \quad \text{for} \quad i = 100$$

$$\alpha = \beta = 1 \quad \text{for} \quad 100 < i < 199$$

The j conditions in these expressions are the known conditions at the

previous s_f^* station, and the $j + 1$ conditions are the unknowns except at the boundaries. The non-linear coefficients of equation (2.39) are approximated by the values at the previous s_f^* station initially then improved through averaging the values at the previous s_f^* station with the newly computed values and iterating until the change is less than one per cent of the previous value. Equation (2.39) in difference form then becomes

$$\frac{\Delta M^{*2}}{\Delta s^*}(\nu^*_{i,j+1} - \nu^*_{i,j}) = \frac{1}{(\alpha+\beta)}\bar{\nu}^*_i\Big[(\nu^*_{i+1,j+1} + \nu^*_{i+1,j} - \nu^*_{i,j+1} - \nu^*_{i,j})/\alpha$$

$$- (\nu^*_{i,j+1} + \nu^*_{i,j} - \nu^*_{i-1,j+1} - \nu^*_{i-1,j})/\beta\Big]$$

$$- \frac{1}{24}\Big[(\bar{\nu}^*_{i+1} - \bar{\nu}^*_i)/\alpha + (\bar{\nu}^*_i - \bar{\nu}^*_{i-1})/\beta\Big] \times$$

$$\Big[(\nu^*_{i+1,j+1} + \nu^*_{i+1,j} - \nu^*_{i,j+1} - \nu^*_{i,j})/\alpha + (\nu^*_{i,j+1} + \nu^*_{i,j} - \nu^*_{i-1,j+1}$$

$$- \nu^*_{i-1,j})/\beta\Big]$$

where the bars indicate the averaged variables in the non-linear coefficients which are improved through iteration. Simplification of this equation yields

$$\nu^*_{i-1,j+1} + A(i,j)\nu^*_{i,j+1} + B(i,j)\nu^*_{i+1,j+1} = C(i,j) \qquad (2.43)$$

where $A(i,j)$, $B(i,j)$, and $C(i,j)$ are known functions of the previous

step in s_f^* and iteration. This equation is considered at every interior grid point yielding 198 simultaneous equations for the 198 unknown $v^*_{i,j+1}$. The matrix of coefficients governing these equations is tridiagonal, however, and so subject to a relatively quick and easy solution.

Energy Equation. The energy equation in transformed co-ordinates (equation (2.18)) is linear in temperature. Then, solutions of this equation expressed in terms of the incompressible transformed co-ordinates can be added linearly to obtain new solutions. The linearity property of the energy equation allows many results to be obtained from relatively few solutions.

Crocco has shown that if the Prandtl number equals unity, a solution of the energy equation exists of the form expressed by

$$T_o^* = C_1 + C_2 u^* \tag{2.44}$$

where C_1 and C_2 are constants depending on the initial and boundary conditions of the energy equation (13, 14). The momentum equation still must be solved for u^*, but with this solution, equation (2.44) will furnish solutions to the energy equation for particular initial and boundary conditions. In particular, if the initial and boundary conditions on T_o^* are exactly the same as those on u^*, then equation (2.44) yields

$$T_o^* = u^*$$

or in terms of the static temperature,

$$T^* = u^*(1 - u^*) \tag{2.45}$$

Further, if the initial and boundary conditions on T_o^* are unity, then equation (2.44) yields

$$T_o^* = 1$$

or in terms of the static temperature,

$$T^* = 1 - u^{*2} \tag{2.46}$$

Equations (2.45) and (2.46) combined with the solution of the momentum equations are useful solutions for the temperature distributions in both free jets and wall jets.

Additional solutions of the energy equation for initial and boundary conditions other than those of the Crocco solutions can be obtained through a numerical solution of the energy equation given by equation (2.36). This equation is simplified somewhat if the solutions are carried out in terms of the stagnation temperature,

$$T_o = T + \frac{1}{2c_p} u^2$$

rather than the static temperature. The dimensionless form of the stagnation temperature is

$$T_o^* = T^* + u^{*2}$$

Further, the dependent variable, T_o^*, is transformed to T_o^{*3} as was

done with u^* in the momentum equation. Defining

$$\theta^* = T_o^{*3}$$

equation (2.36) in terms of ν^* and θ^* becomes

$$\frac{\partial \theta^*}{\partial s_f^*} = \nu^* \frac{\partial^2 \theta^*}{\partial M^{*2}} + \frac{1}{3}\left(\frac{\partial \nu^*}{\partial M^*} - 2 \frac{\nu^*}{\theta^*} \frac{\partial \theta^*}{\partial M^*} \right) \frac{\partial \theta^*}{\partial M^*} \qquad (2.47)$$

The initial and boundary conditions for equation (2.47) are

$$\theta^*(0, M^*) = \theta_{in}^*(M^*)$$

$$M^* = 0, \qquad \frac{\partial \theta^*}{\partial M^*} = 0$$

$$M^* = 1, \qquad \theta^* = \theta_e^*$$

The details of the finite difference approximation to equation (2.47) are contained in Appendix C. The difference approximations used for the derivatives are those given by equations (2.40), (2.41), and (2.42) with ν^* replaced by θ^*. The resulting difference approximation to equation (2.47) is

$$\theta_{i-1,j+1}^* + A(i,j)\, \theta_{i,j+1}^* + B(i,j)\, \theta_{i+1,j+1}^* = C(i,j) \qquad (2.48)$$

where the $A(i,j)$, $B(i,j)$, and $C(i,j)$ are known functions of the previous step in s^* and iteration, and $\theta_{i-1,j+1}^*$, $\theta_{i,j+1}^*$, and $\theta_{i+1,j+1}^*$ are the unknowns. Equation (2.48) is considered at every interior grid point

to yield a set of simultaneous equations for the $\theta^*_{i,j+1}$.

Wall Jet

It is convenient to introduce the following dimensionless variables as suggested by the asymptotic solution:

$$u^* = \frac{u}{u_r}$$

$$s_w^* = \frac{\rho_r \mu_r u_r^2}{F} s$$

$$M_o^* = \frac{M_o}{M_{o_{in}}}$$

$$z_w^* = \left(\frac{\rho_r^2 u_r^3}{F} \right)^{1/2} z$$

$$F^* = \frac{u_r F}{M_{o_{in}}^2}$$

$$T^* = \frac{2h_r}{u_r^2} \frac{T - T_w}{T_r} \qquad \text{for the constant temperature wall case}$$

or

$$T^* = \frac{2h_r}{u_r^2} \frac{T - T_r}{T_r} \qquad \text{for the adiabatic wall case}$$

The temperature variable for the constant wall temperature case is chosen to remove a singularity at the wall. The variable F is defined by

equation (2.26). Then, equations (2.30), (2.31), and (2.32) become

$$\frac{M_o^{*2}}{F^*} u^* \frac{\partial u^*}{\partial s_w^*} = u^{*2} \frac{\partial}{\partial M^*} \left(u^{*2} \frac{\partial u^*}{\partial M^*} \right) + \left[(1-M^*) \left(u^{*2} \frac{\partial u^*}{\partial M^*} \right)_{M^*=0} - u^{*2} \frac{\partial u^*}{\partial M^*} \right] u^* \frac{\partial u^*}{\partial M^*} \tag{2.49}$$

$$\frac{M_o^{*2}}{F^*} u^* \frac{\partial T^*}{\partial s_w^*} = u^{*2} \frac{\partial}{\partial M^*} \left(u^{*2} \frac{\partial T^*}{\partial M^*} \right) + \left[(1-M^*) \left(u^{*2} \frac{\partial u^*}{\partial M^*} \right)_{M^*=0} - u^{*2} \frac{\partial u^*}{\partial M^*} \right] u^* \frac{\partial T^*}{\partial M^*} + 2 \left(u^{*2} \frac{\partial u^*}{\partial M^*} \right)^2 \tag{2.50}$$

$$M_o^{*2} = 1 - 2F^* \int_o^{s^*} \left(u^{*2} \frac{\partial u^*}{\partial M^*} \right)_{M^*=0} ds_w^* \tag{2.51}$$

The initial and boundary conditions for the wall jet are

$$u^*(0,M^*) = u_{in}^*(M^*), \qquad T^*(0,M^*) = T_{in}^*(M^*)$$

$$M^* = 0, \qquad u^* = 0 \text{ and } T^* = 0 \text{ or } u^{*2} \frac{\partial T^*}{\partial M^*} = 0$$

$$M^* = 1, \qquad u^* = 0 \text{ and } T^* = T_e^*$$

The transformed normal co-ordinate, from equation (2.29), is

$$z_w^* = \left(\frac{\rho_r^2 u^3 r}{F} \right)^{1/2} X^k Y = \frac{1}{(F^*)^{1/2}} \int_o^{M^*} \frac{dM^*}{u^{*2}} \tag{2.52}$$

The physical normal co-ordinate, from equations (2.20) and (2.29), is given by

$$\frac{2h_r}{u_r^2}\left[\left(\frac{\rho_r^2 u_r^3}{F}\right)^{1/2}(cx)^{k_\gamma - z_w^*}\right] = \frac{1}{(F^*)^{1/2}}\int_o^{M^*}\frac{(T^* - T_r^*)}{u^{*2}}\,dM^* \qquad (2.53)$$

when combined with equation (2.52).

Momentum Equation. The dependent variable of the momentum equation for the wall jet (equations (2.49) and (2.51)) is transformed from u^* to u^{*3} as was done for the free jet. Again, let

$$\nu^* = u^{*3}$$

and equations (2.49) and (2.51) become

$$\frac{M_o^{*2}}{F^*}\frac{\partial \nu^*}{\partial s_w^*} = \nu^*\frac{\partial^2 \nu^*}{\partial M^{*2}} + \frac{1}{3}\left[(1 - M^*)\left(\frac{\partial \nu^*}{\partial M^*}\right)_{M^*=0} - \frac{\partial \nu^*}{\partial M^*}\right]\frac{\partial \nu^*}{\partial M^*} \qquad (2.54)$$

$$M_o^{*2} = 1 - \frac{2}{3}F^*\int_o^{s_w^*}\left(\frac{\partial \nu^*}{\partial M^*}\right)_{M^*=0} ds_w^* \qquad (2.55)$$

The initial and boundary conditions on equation (2.54) are

$$\nu^*(0, M^*) = \nu_{in}^*(M^*)$$

$$M^* = 0, \qquad \nu^* = 0$$

$$M^* = 1, \qquad \nu^* = 0$$

The transformation from u^* to ν^* is necessary for the wall jet in order to remove a singularity at the wall (i.e., at $z^*=M^*=0$). Under the momentum transformation, the derivative of the velocity with respect to the transformed normal co-ordinate at the wall is given by

$$\left(\frac{\partial u^*}{\partial z^*}\right)_{z^*=0} = F^{*1/2} \left(u^{*2} \frac{\partial u^*}{\partial M^*}\right)_{M^*=0} \tag{2.56}$$

Since there is a shear force on the wall, the left hand side of this equation is not zero. The velocity, u^*, is zero at the wall, however, and therefore

$$\left(\frac{\partial u^*}{\partial M^*}\right)_{M^*\to 0} \longrightarrow \infty$$

This derivative occurs in equations (2.49), (2.50), and (2.51) for the wall jet. A finite difference technique, however, requires that the derivatives are always finite. Equation (2.56) for the derivative at the wall in terms of ν^* is

$$\left(\frac{\partial u^*}{\partial z^*}\right)_{z^*=0} = F^{*1/2} \left(u^{*2} \frac{\partial u^*}{\partial M^*}\right)_{M^*=0} = F^{*1/2} \frac{1}{3} \left(\frac{\partial \nu^*}{\partial M^*}\right)_{M^*=0}$$

The derivative in terms of ν^* remains finite since $F^* \neq 0$, and this condition on the difference approximation is satisfied for equations (2.54) and (2.55).

Solutions to equation (2.54) for various initial and boundary

conditions are obtained through the implicit finite difference technique described for the free jet. Again, the grid is varied in both the s^* and M^* directions. A very fine increment of s^* (10^{-8}) is used for s^* close to the initial condition and this is progressively increased as the solution progresses downstream. The M^* co-ordinate grid is one hundred equal increments, with both the first and last grid increment subdivided into one hundred equal increments in order to obtain a better solution at the wall and as $y \to \infty$.

The details of the finite difference approximation to equations (2.54) and (2.55) are presented in Appendix C. The difference approximations for the derivatives are the same as those used on the momentum equation of the free jet (equations (2.40), (2.41) and (2.42)), and the result is a set of simultaneous equations of the form of equation (2.43) for the $\nu^*_{i,j+1}$.

Energy Equation. The Crocco solutions of the energy equation for the free jet, given by equations (2.45) and (2.46), apply also to the wall jet. Results for other initial and boundary conditions are obtained through a numerical solution of equations (2.50) and (2.51). As in the case of the free jet, the dependent variables, u^* and T^*, are transformed to

$$\nu^* = u^{*3}$$

and

$$\theta^* = T_o^{*3}$$

where

$$T_o^* = T^* + u^{*2}$$

is the dimensionless stagnation temperature. The transformation to θ^* again removes a singularity at the wall. Equations (2.50) and (2.51), in terms of ν^* and θ^*, are

$$\frac{M_o^{*2}}{F^*}\frac{\partial\theta^*}{\partial s_w^*} = \nu^*\frac{\partial^*\theta^*}{\partial M^{*2}} + \frac{1}{3}\left[(1 - M^*)\left(\frac{\partial\nu^*}{\partial M^*}\right)_{M^*=0} + \frac{\partial\nu^*}{\partial M^*} - 2\frac{\nu^*}{\theta^*}\frac{\partial\theta^*}{\partial M^*}\right]\frac{\partial\theta^*}{\partial M^*} \tag{2.57}$$

$$M_o^* = 1 - \frac{2}{3}F^*\int_o^{s_w^*}\left(\frac{\partial\nu^*}{\partial M^*}\right)_{M^*=0} ds_w^* \tag{2.58}$$

The initial and boundary conditions on equation (2.57) are

$$\theta^*(0,M^*) = \theta_{in}^*(M^*)$$

$$M^* = 0, \quad \theta^* = 0 \text{ or } \frac{\partial\theta^*}{\partial M^*} = 0$$

$$M^* = 1, \quad \theta^* = \theta_e^*$$

The details of the finite difference approximation to equations (2.57) and (2.58) are presented in Appendix C. The difference approximations of the derivatives are the same as those used for the momentum equation (equations (2.40), (2.41), and (2.42)) with ν^* replaced by θ^*.

The result is a set of simultaneous equations of the form of equation (2.48) for the $\theta^*_{i,j+1}$.

The Approximate Solutions

A solution of the momentum equations for the free jet and the wall jet can be obtained through an integral technique much easier to solve than the finite difference scheme used in the exact solution. The free jet and wall jet with initially uniform velocity distributions are treated as examples of the method. The object of these examples is to illustrate a use and to explore the accuracy of the simple integral method. The velocity distributions are approximated by simple polynomials which are selected to satisfy boundary conditions as well as the total momentum integral defined by equation (2.22) and the F integral defined by equation (2.26).

Free Jet

Figure (2) defines two downstream regions (region (I) and region (II)) of the development of a free jet with a uniform initial condition. In region (I), the maximum velocity of the jet does not change from its initial value. The viscous layer develops as a free layer at the external fluid boundary. As the jet development continues downstream, the free layer grows until it reaches the jet centerline. At this point, the maximum velocity of the jet begins to decay, and the development is no longer that of a free layer. Here, region (I) ends and region (II) begins. Whereas region (I) can be treated as a free layer flow, region (II) must take account of the decay of the maximum velocity. These two regions of the jet development will be treated separately.

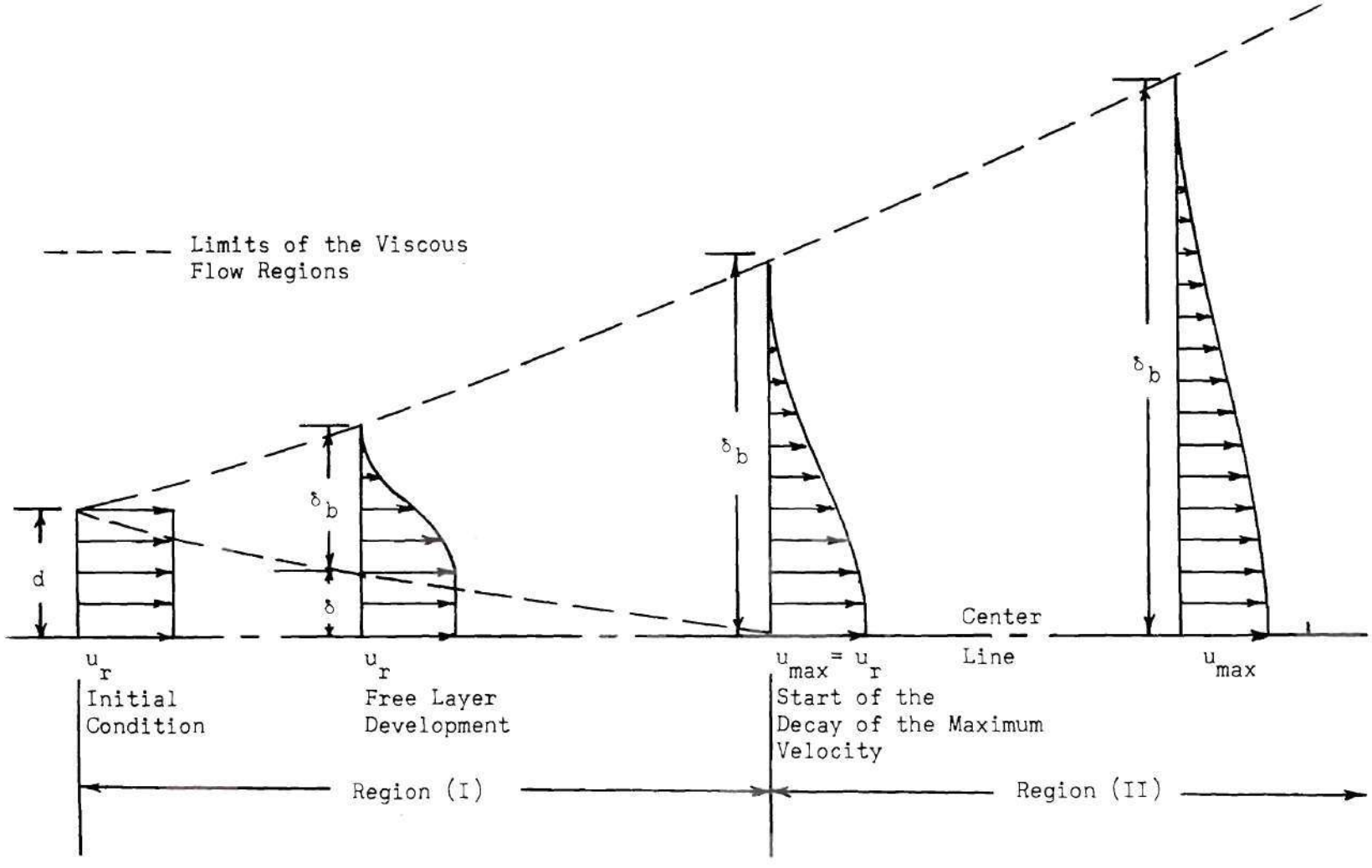

Figure 2. Illustration of the Development of a Free Jet From a Uniform Initial Velocity Distribution.

Region (I). The velocity distribution in the viscous layer of region (I) is assumed of the form

$$\frac{u_b}{u_r} = A\left(\frac{z-\delta}{\delta_b}\right)^3 + B\left(\frac{z-\delta}{\delta_b}\right)^2 + C\left(\frac{z-\delta}{\delta_b}\right) + D \qquad (2.59)$$

where δ is the transformed thickness of the constant velocity region of the jet, δ_b is the transformed thickness of the viscous layer, and the constants A, B, C, and D are selected such that the following boundary conditions are satisfied:

$$z = \delta, \qquad \frac{u_b}{u_r} = 1 \quad \text{and} \quad \frac{\partial(u_b/u_r)}{\partial z} = 0$$

$$z = \delta + \delta_b, \qquad \frac{u_b}{u_r} = \frac{\partial(u_b/u_r)}{\partial z} = 0$$

The expression for the velocity with these boundary conditions then becomes

$$\frac{u_b}{u_r} = 2\left(\frac{z-\delta}{\delta_b}\right)^3 - 3\left(\frac{z-\delta}{\delta_b}\right)^2 + 1 \qquad (2.60)$$

The unknown quantities δ and δ_b are obtained from the integral momentum equation and F relation over the viscous layer.

As shown in Appendix B for the free layer, the integral momentum equation is given by

$$\frac{M_o}{\rho_r} = (d - \delta)u_r^2 = \int_{\delta}^{\infty} u_b^2 dz \tag{2.61}$$

and the F relation is given by

$$\frac{F_{in}}{\rho_r^2} = \int_o^{\infty} u_b \int_z^{\infty} u_b^2 \, dzdz + \frac{1}{2}\frac{\mu_r}{\rho_r} u_r^2 s$$

From the jet initial condition,

$$\frac{F_{in}}{\rho_r^2} = \int_o^{d} u_r \int_z^{d} u_r^2 \, dzdz = \frac{1}{2} u_r^3 d^2$$

and the F relation becomes

$$\frac{1}{2} u_r^3 d^2 = \int_o^{\infty} u_b \int_z^{\infty} u_b^2 \, dzdz + \frac{1}{2}\frac{\mu_r}{\rho_r} u_r^2 s \tag{2.62}$$

Equations (2.61) and (2.62) can be integrated for the velocity distribution given by equation (2.60) and then solved simultaneously to obtain the solution for δ_b and δ for the free layer, or region (I) of the free jet of Figure 2. The results are

$$\frac{\delta_b}{d} = 8.518 \left(\frac{\mu_r}{\rho_r u_r s} \right)^{1/2} \left(\frac{s}{d} \right) \tag{2.63}$$

$$\frac{\delta}{d} = 1 - 3.164 \left(\frac{\mu_r}{\rho_r u_r s} \right)^{1/2} \left(\frac{s}{d} \right) \tag{2.64}$$

Region (II). The condition that $\delta = 0$ in equation (2.64) determines the distance downstream such that the jet maximum velocity begins to decay. This point then marks the end of region (I) and the beginning of region (II). The velocity distribution of region (II) is again assumed to be a cubic of the form

$$\frac{u_b}{u_{max}} = A\left(\frac{z}{\delta_b}\right)^3 + B\left(\frac{z}{\delta_b}\right)^2 + C\left(\frac{z}{\delta_b}\right) + D \tag{2.65}$$

with the boundary conditions

$$z = 0, \qquad \frac{u_b}{u_{max}} = 1 \quad \text{and} \quad \frac{\partial(u_b/u_{max})}{\partial z} = 0$$

$$z = 1, \qquad \frac{u_b}{u_{max}} = \frac{\partial(u_b/u_{max})}{\partial z} = 0$$

where u_{max} is the maximum velocity in the jet, and δ_b is again the transformed thickness of the viscous layer. The expression for the velocity distribution satisfying these boundary conditions is

$$\frac{u_b}{u_{max}} = 2\left(\frac{z}{\delta_b}\right)^3 - 3\left(\frac{z}{\delta_b}\right)^2 + 1 \tag{2.66}$$

In this region, the integral momentum equation is

$$\frac{M_o}{\rho_r} = u_r^2 d = \int_o^\infty u_b^2 dz \tag{2.67}$$

and the F relation is (see Appendix B),

$$\frac{F_{in}}{\rho_r^2} = \frac{1}{2} u_r^3 d^2 = \int_o^\infty u_b \int_z^\infty u_b^2 \, dzdz + \frac{1}{2} \frac{\mu_r}{\rho_r} \int_o^s u_{max}^2 ds \tag{2.68}$$

Equations (2.67) and (2.68) can be integrated for the velocity distribution given by equation (2.66) to obtain the solution for region (II) of the free jet of Figure 2. The result for the two unknowns, u_{max} and δ_b, is

$$\frac{u_{max}}{u_r} = \left(\frac{1}{2.727 \frac{\mu_r}{\rho_r u_r d} \left(\frac{x}{d} \right) + 1} \right)^{1/3} \tag{2.69}$$

$$\frac{\delta_b}{d} = \frac{2.692 \, u_r^2}{u_{max}^2} \tag{2.70}$$

These expressions hold from the start of the decay of the maximum velocity on downstream.

Wall Jet

The wall jet is analyzed in a similar manner. The result, however, is more complicated. The wall jet development from a uniform initial velocity condition on downstream is illustrated in Figure 3. Again, the flow is divided into two regions: (I) the region from the initial condition

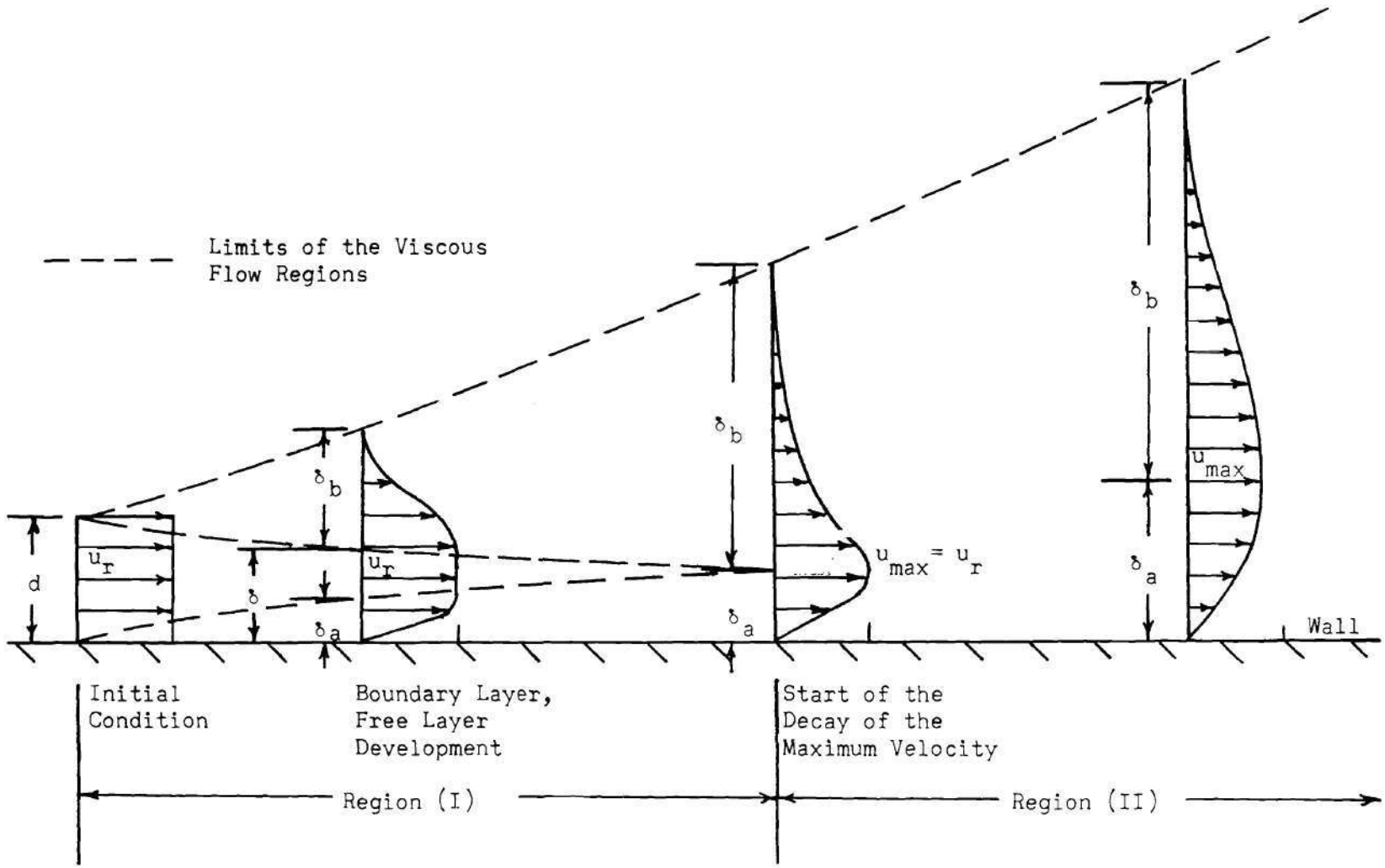

Figure 3. Illustration of the Development of a Wall Jet From a Uniform Initial Velocity Distribution.

until the maximum velocity begins to decay and (II) the region from the point of initial decay of the maximum velocity on downstream. The velocity profile in region (I) develops as a boundary layer next to the wall, and as a free layer for $y \to \infty$. Region (I) ends, and region (II) begins when the free layer and boundary layer merge, and the maximum velocity begins to decay.

Region (I). An integral solution for the boundary layer is obtained by assuming a velocity distribution of the form expressed by

$$\frac{u_a}{u_r} = A\left(\frac{z}{\delta_a}\right)^3 + B\left(\frac{z}{\delta_a}\right)^2 + C\left(\frac{z}{\delta_a}\right) + D$$

subject to the boundary conditions

$$z = 0, \qquad \frac{u_a}{u_r} = \frac{\partial^2\left(\frac{u_a}{u_r}\right)}{\partial z^2} = 0$$

$$z = 1, \qquad \frac{u_a}{u_r} = 1 \quad \text{and} \quad \frac{\partial\left(\frac{u_a}{u_r}\right)}{\partial z} = 0$$

and requiring that this profile satisfy the momentum integral expressed as

$$\frac{M_o}{\rho_r} = \delta_a u_r^2 = \int_o^\infty u_a^2 dz + \frac{\mu_r}{\rho_r} \int_o^s \frac{\partial u_a}{\partial z}\, ds \qquad (2.71)$$

The equation for the velocity profile becomes

$$\frac{u_a}{u_r} = \frac{3}{2}\left(\frac{z}{\delta_a}\right) - \frac{1}{2}\left(\frac{z}{\delta_a}\right)^3 \tag{2.72}$$

and the integration of equation (2.71) for this velocity distribution yields

$$\frac{\delta_a}{d} = 4.64\left(\frac{\mu_r}{\rho_r u_r s}\right)^{1/2}\left(\frac{s}{d}\right) \tag{2.73}$$

for the thickness of the layer (15). The solution for the free layer is the same as that which was derived for region (I) of the free jet (equation (2.63) and (2.64)).

Equations (2.64) and (2.73) can be used to find the distance downstream such that the boundary layer and free layer solutions merge. That is, the distance downstream such that

$$\delta_a = \delta \tag{2.74}$$

This distance then determines the division between region (I) and region (II) of the wall jet.

Region (II). The solution of region (II) is obtained by dividing the velocity distribution into two parts: the boundary layer type of flow (from the maximum velocity to the wall) and the free layer type (from the maximum velocity away from the wall). These two solutions are patched together at the point of maximum velocity. The boundary layer velocity distribution of equation (2.72) with u_r replaced by u_{max} is used for the part of the layer next to the wall. The free layer velocity distribution of equation (2.60) again with u_r replaced by u_{max} is assumed

for the part of the layer away from the wall. These velocity distributions are

$$\frac{u_a}{u_{max}} = \frac{3}{2}\left(\frac{z}{\delta_a}\right) - \frac{1}{2}\left(\frac{z}{\delta_a}\right)^3 \tag{2.75}$$

and

$$\frac{u_b}{u_{max}} = 2\left(\frac{z-\delta_a}{\delta_b}\right)^3 - 3\left(\frac{z-\delta_a}{\delta_b}\right)^2 + 1 \tag{2.76}$$

where u_a and u_b denote the velocity distributions of the boundary layer and free layer portions of the wall jet, respectively. Together they represent the velocity distribution of the wall jet. The three unknowns, u_{max}, δ_a, and δ_b are found from equations expressing the F relation and momentum integral for the entire wall jet and the momentum integral for the free layer portion of the wall jet. These equations are expressed

$$\frac{F}{\rho_r^2} = \frac{1}{2} u_r^3 d^2 = \int_o^{\delta_a+\delta_b} u \int_z^{\delta_a+\delta_b} u^2 dz dz \tag{2.77}$$

$$\frac{d}{ds}\left[\int_o^{\delta_a+\delta_b} u^2 dz\right] = -\frac{\mu_r}{\rho_r}\left(\frac{\partial u}{\partial z}\Big|_s\right)_{z=0} \tag{2.78}$$

$$\frac{d}{ds}\left[\int_{\delta_a}^{\delta_a+\delta_b} u_b^2\, dz\right] = -u_{max}\frac{d}{ds}\left[\int_o^{\delta_a} u_a dz\right] \tag{2.79}$$

Integration of equations (2.77), (2.78), and (2.79) for the velocity distribution of equations (2.75) and (2.76) yields, after simplifications,

$$u_{max} \frac{d\delta_a^2}{ds} = 29.7446 \frac{\mu_r}{\rho_r} \left\{ \frac{0.04118}{0.12758} - \frac{\left[0.028358 + 6.5906 \left(\frac{u_r}{u_{max}}\right)^3 \left(\frac{d}{\delta_a}\right)^2\right]^{1/2} + 2.3925 \left(\frac{u_r}{u_{max}}\right)^3 \left(\frac{d}{\delta_a}\right)^2}{\left[0.028358 + 6.5906 \left(\frac{u_r}{u_{max}}\right)^3 \left(\frac{d}{\delta_a}\right)^2\right]^{1/2} + 3.3035 \left(\frac{u_r}{u_{max}}\right)^3 \left(\frac{d}{\delta_a}\right)^2} \right\} \tag{2.80}$$

$$\delta_a^2 \frac{du_{max}}{ds} = 0.2010\, u_{max} \frac{d\delta_a^2}{ds} - \frac{\mu_r}{\rho_r} 4.330 \tag{2.81}$$

$$\frac{\delta_b}{\delta_a} = -1.530 + \left[0.028358 + 6.5906 \left(\frac{u_r}{u_{max}}\right)^3 \left(\frac{d}{\delta_a}\right)^2\right]^{1/2} \tag{2.82}$$

These three equations relate the three unknowns δ_a, δ_b, and u_{max}. After solving region (I) for the initial conditions in region (II), this solution for region (II) can be solved easily with an explicit finite difference technique. Equation (2.80) is first solved for $\frac{d\delta_a^2}{ds}$ using the known values at the previous s station for all the variables. Then, equation (2.81) can be solved for $\frac{du_{max}}{ds}$ using the result of equation (2.80) and the known values at the previous s station for the other variables. These two expressions can then be integrated to obtain δ_a and u_{max} at the new s station, and equation (2.82) is solved for δ_b. This process can then be repeated step by step downstream. The details

of the individual approximate solutions used in these analyses are presented in Appendix D.

CHAPTER III

EXPERIMENTAL APPARATUS AND PROCEDURE

The experimental apparatus was designed to generate a two-dimensional laminar wall jet of air and to allow measurement of the velocity distribution of the jet at various axial positions. The velocities were computed from Bernoulli's equation for compressible flow. These results were compared to the results of the exact solution and were used to determine the approximate location of transition from a laminar to a turbulent wall jet for the one case studied.

The laminar wall jet can only be obtained for a very low Reynolds number. Also, for the most accurate determination of the velocity distribution, the dynamic pressure in the jet must be maintained as high as possible. Further, to avoid supersonic expansion the Mach number at the nozzle exit must be maintained less than unity. The condition of low Reynolds number for highest possible dynamic pressure under subsonic flow conditions was met by reducing the density of the air (i.e., by operating the jet under a partial vacuum inside of a vacuum tank). The jet issued from a chamber at a pressure of 0.0944 pounds per square inch into the vacuum tank at a pressure of 0.0511 pounds per square inch. These pressures were maintained by continuous pumping, and the jet was studied under a steady state condition. An illustration of the chamber and tank is presented in Figure 4.

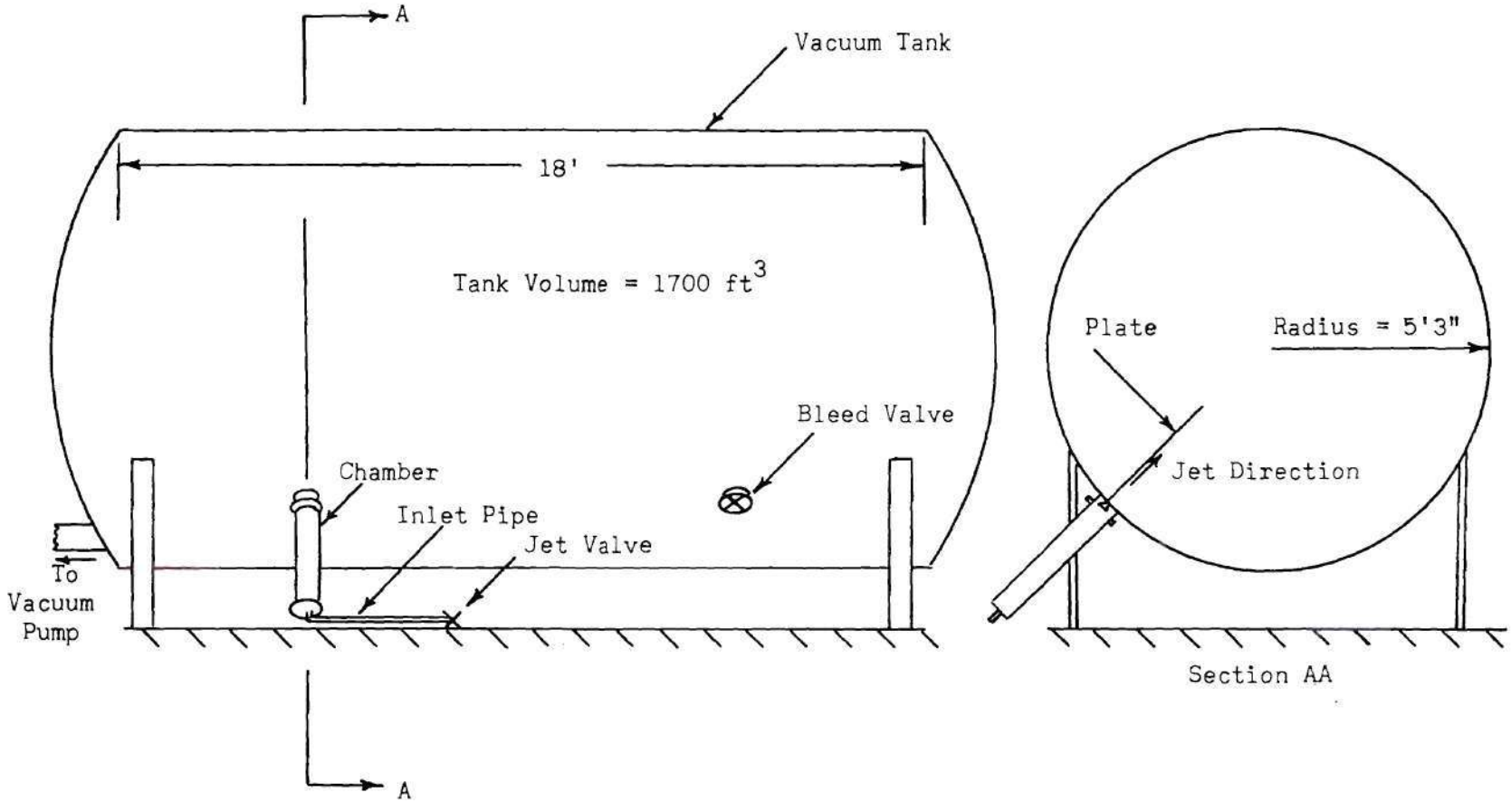

Figure 4. Illustration of the Over-All Physical Size of the Experimental Apparatus.

Equipment and Instrumentation

The air forming the wall jet passed from the atmosphere through a valve, termed the jet valve, into a forty-three inch length of two-inch inner-diameter pipe. This pipe served to dissipate the velocity of the air entering from the atmosphere. The air flowed from this pipe into a forty-two inch length of six inch inner-diameter pipe termed the chamber. A series of wire mesh was installed in the chamber to straighten the flow and act as a turbulence damper. The flow passed out of the chamber through a nozzle which forms the two-dimensional jet. The construction of the chamber and nozzle is illustrated in Figure 5. The nozzle exit was rectangular with a height of one quarter of an inch and a width of four inches. The nozzle was located in one port of the vacuum tank, and a valve, termed the bleed valve, was located in another port of the tank. A flat plate extended from the nozzle exit, downstream and served as the wall of the wall jet. Vertical side walls were mounted on the plate parallel to the flow to form a three inch channel in the middle of the jet. The channel preserved the two-dimensionality of the wall jet. The entire system was pumped down and held under the condition of a partial vacuum at constant pressure throughout the test by continuous pumping. The pressure inside the tank was measured by a McLeod gauge, and the pressure difference between the tank and the chamber was measured by a micromanometer using a silicon oil as the manometer fluid. These two pressure measurements were held at specified values during the test by properly adjusting the jet and bleed valves. A thermometer located outside of the tank measured the temperature of the air before it entered the jet valve.

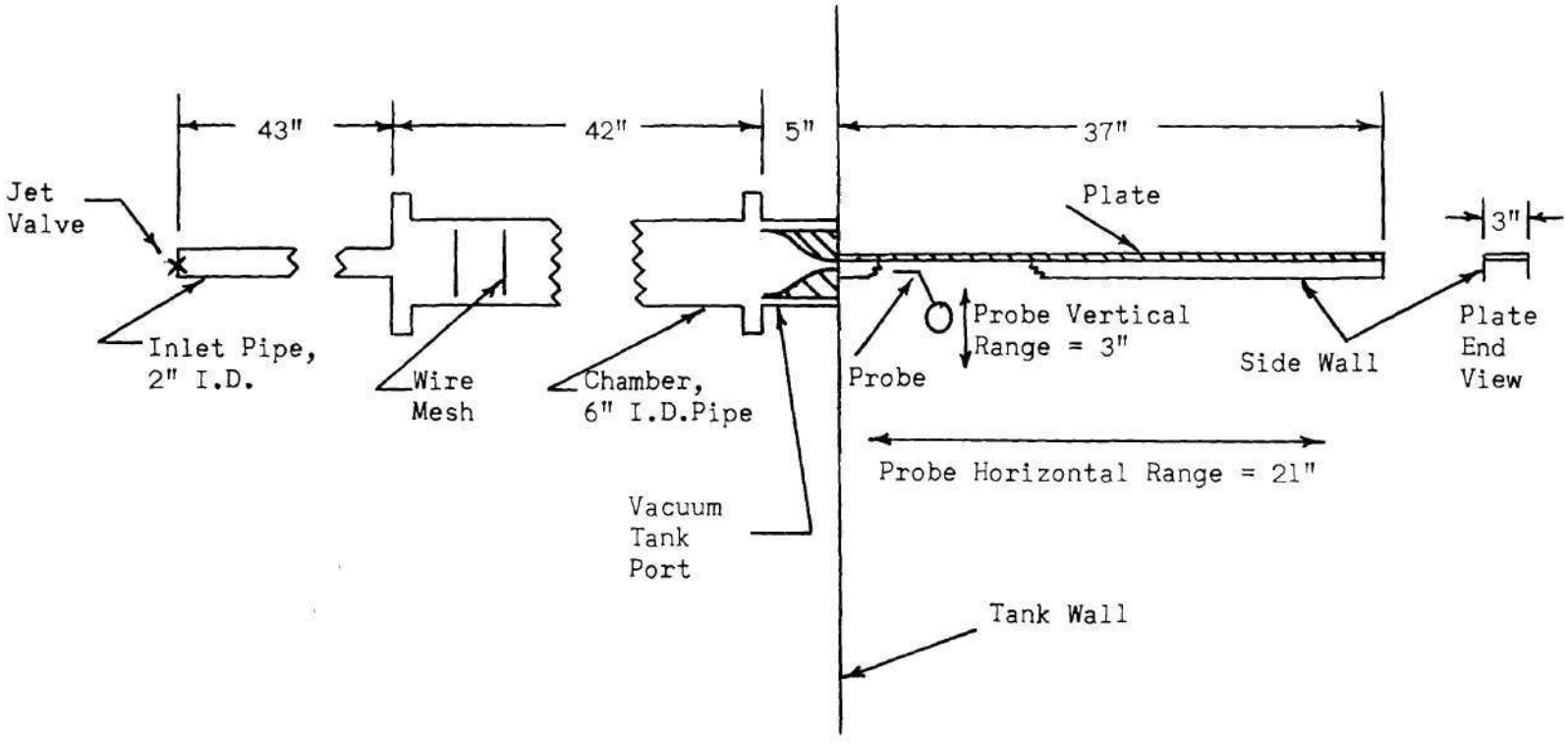

Figure 5. Illustration of the Chamber and Nozzle of the Experimental Apparatus.

The probe used to measure the jet total pressures was made of 0.018 inch inner-diameter aluminum tubing with a 0.007 inch wall, which was flattened to give an approximately rectangular opening 0.005 inches in height and 0.025 inches in width. The probe was attached to a 0.1 pounds per square inch maximum pressure differential Ultradyne variable reluctance differential transducer which was referenced to the pressure in the vacuum tank. The transducer was mounted on a traversing mechanism which allowed motion in the directions parallel and normal to the jet flow. The location of the probe, for these two degrees of freedom, was controlled by a hydraulic system operated from a pump, which was located outside of the tank. A variable-resistance potentiometer, contained in one leg of a Wheatstone bridge, was used to measure the location of the probe in the vertical direction. The longitudinal position of the probe was calibrated in terms of the longitudinal distance traversed by each full stroke of the hydraulic pump.

Calibration and Procedure

The pressure transducers were calibrated using a micromanometer. Checks of the transducers under both vacuum and atmospheric conditions did not reveal any effect of vacuum, so the transducers were calibrated outside of the tank under atmospheric conditions and then installed for the tests. The pressure measurements were repeatable within an accuracy of 7×10^{-5} pounds per square inch. The calibration of the positioning potentiometer allowed the determination of the probe within approximately 0.02 inches. The hydraulic pump stroke calibration allowed the determination of the longitudinal position of the probe within 0.05 inches.

The pressure measured by the probe under the low density flow conditions was not the true total pressure of the stream but a value greater than the true total pressure. A calibrated correction of the total pressure was obtained for the probe. A one inch diameter circular nozzle was constructed for these calibrations to maximize the core of isentropic flow in the nozzle. The probe was placed in the center of this nozzle, and total pressures for a range of Reynolds numbers and Mach numbers were measured. These pressures were compared with the measured chamber pressure, and correction curves similar to those presented in reference (16) were obtained for the probe and included in the reduction of the experimental data. The correction factor was dependent upon the Reynolds number but not the Mach number for the range of conditions considered in this study. The magnitude of the corrections was around 2 per cent of the corrected pressure. A few corrections were greater but always less than 10 per cent of the corrected pressure.

The experimental procedure involved first setting the jet and bleed valves to obtain the desired pressure in the chamber and tank as determined from the readings of the micromanometer and the McLeod gauge. The longitudinal position of the probes was then established in the immediate exit plane of the jet, and the jet was surveyed at arbitrary intervals in the vertical direction. These surveys were repeated at three inch intervals longitudinally. All surveys were made midway between the two side walls. The pressure measurements were converted to velocities through the Bernoulli equation of compressible flow. The static pressures in the jet were assumed equal to the tank pressure, and the total temperatures in the jet were assumed equal to the temperature of the air before entering through the jet valve.

CHAPTER IV

DISCUSSION OF RESULTS

Free Jet

Exact Solutions

Momentum Equation. The exact solutions of the momentum equation for the free jet were carried out for the two jet initial conditions of a uniform initial velocity distribution and a parabolic initial velocity distribution. Figure 6 presents the results for the uniform initial velocity distribution in terms of the transformed co-ordinates for various downstream locations. Included also are the results from the asymptotic solution for the last three downstream locations (equation (2.23)). The asymptotic solution becomes a good approximation to the exact solution only after the maximum velocity has decayed to approximately one half of its original value. The convergence of the exact solution to the asymptotic solution is demonstrated more effectively in Figure 7. In this figure, the data of Figure 6 is plotted in terms of the similarity variables of the asymptotic solution. The asymptotic solution for all downstream stations then plots on a single curve, and the exact solution converges to that curve for increasing distance downstream (i.e., increasing s_f^*). Figure 8 presents the exact solution for the free jet with an initially parabolic velocity distribution in terms of the transformed co-ordinates for various downstream locations. Here again, the asymptotic solution is compared to the exact solution for the last three positions downstream with qualitatively the same results as presented for the case of a uniform

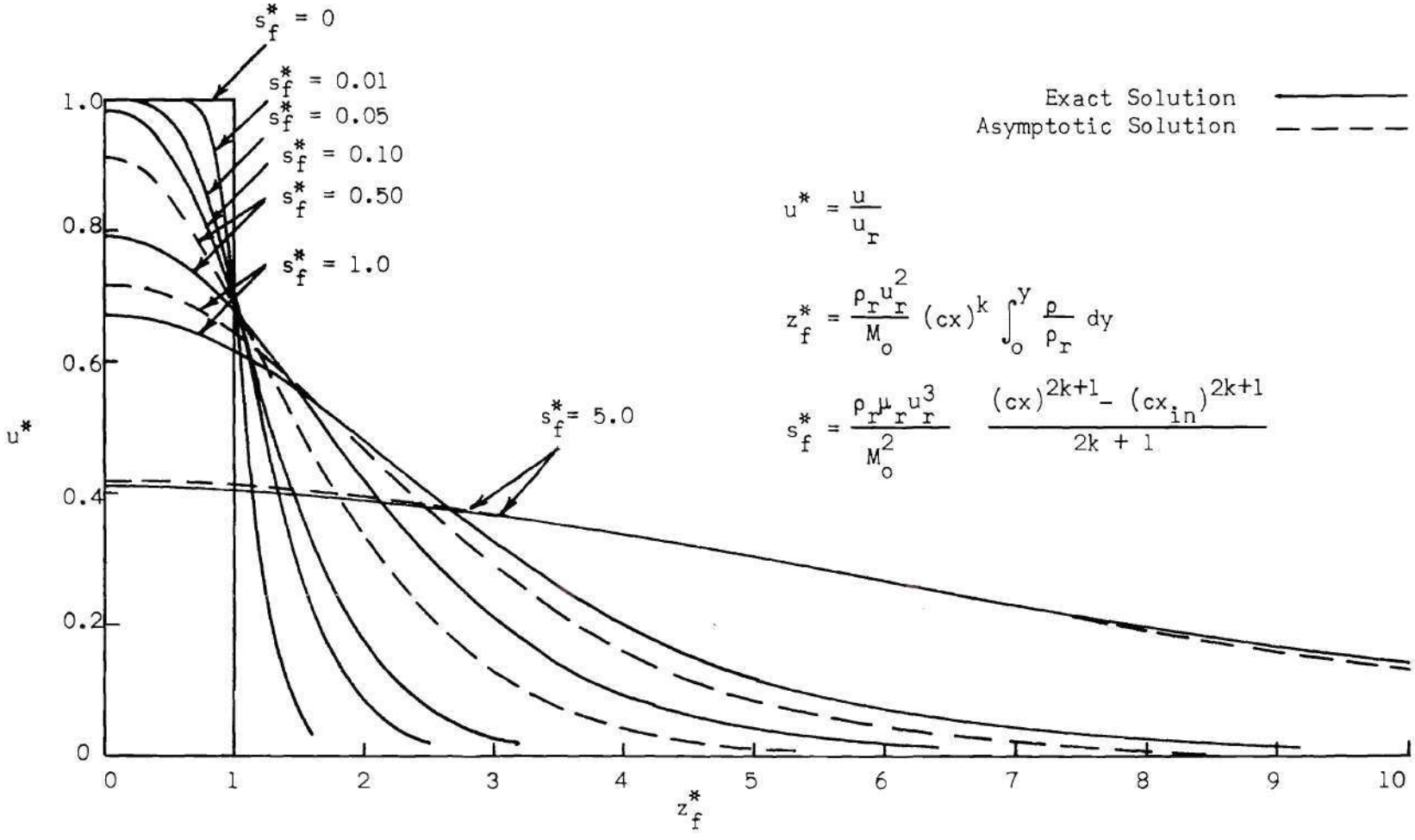

Figure 6. Velocity Distribution for the Free Jet at Several Locations Downstream, Uniform Initial Velocity Condition.

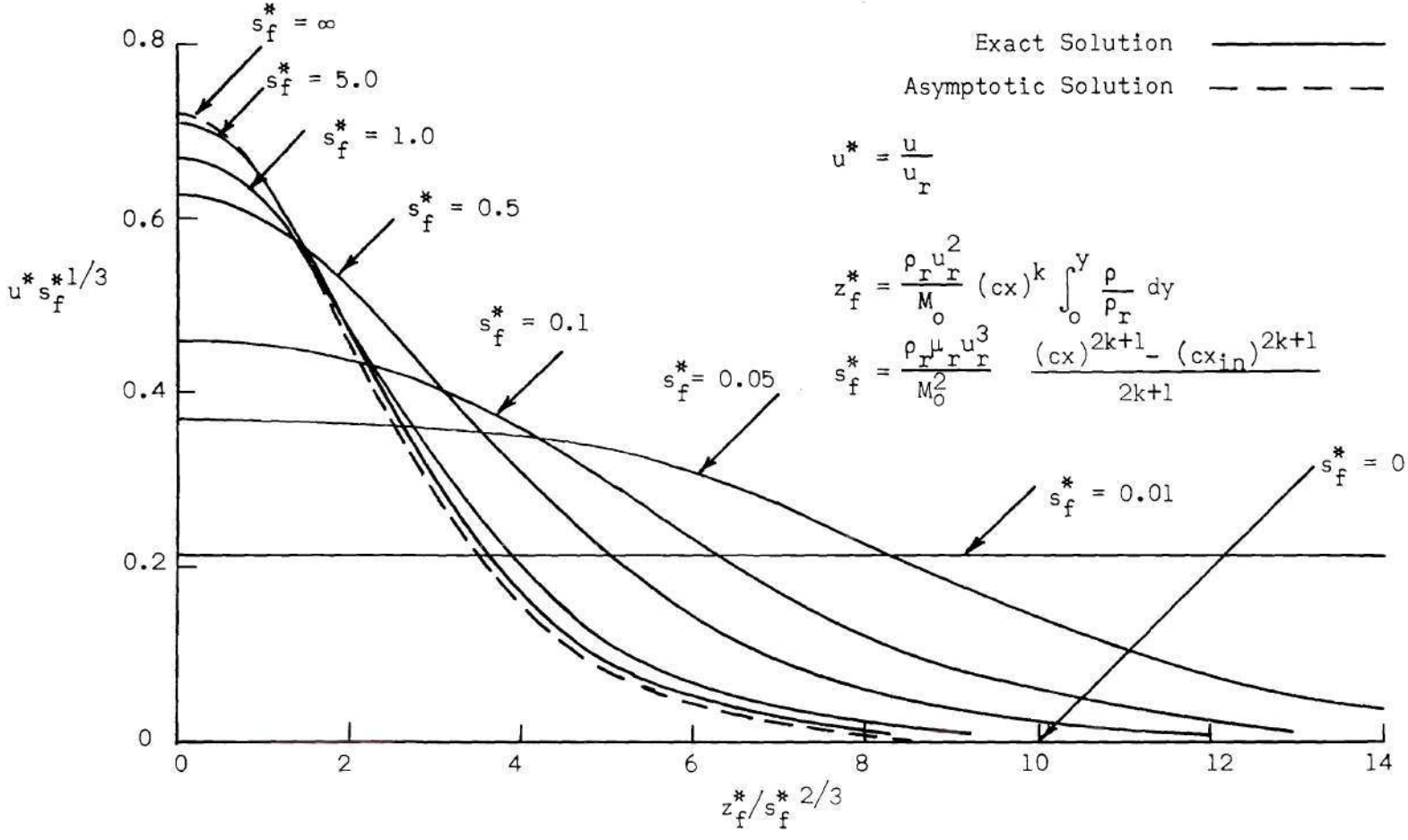

Figure 7. Velocity Distributions for the Free Jet in Terms of the Similarity Parameters at Several Locations Downstream, Uniform Initial Velocity Condition.

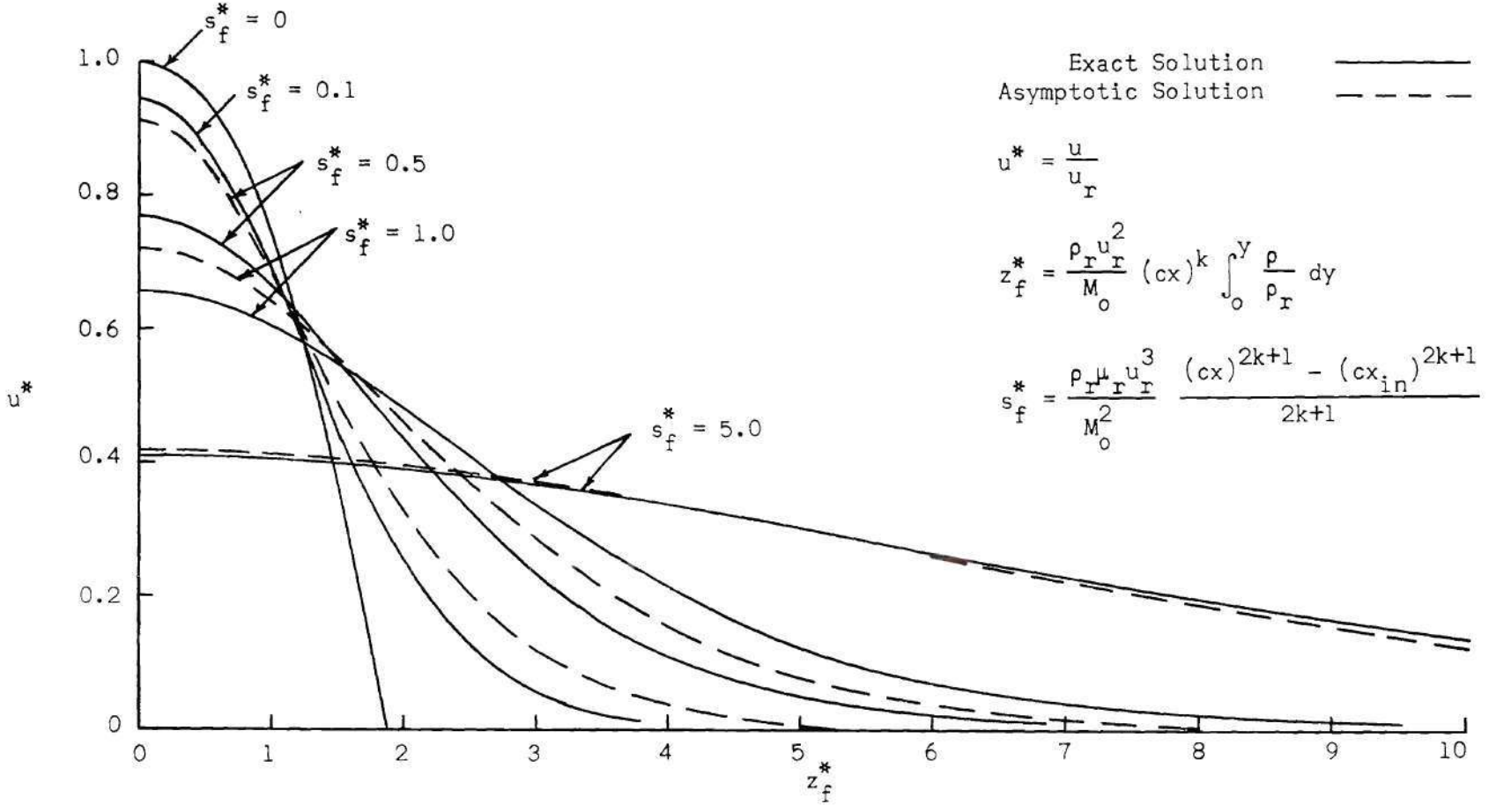

Figure 8. Velocity Distribution for the Free Jet at Several Locations Downstream, Parabolic Initial Velocity Condition.

initial velocity distribution.

A comparison of the solutions for the uniform and parabolic initial velocity distributions are presented in Figure 9. Initially, the velocity distributions do not compare well, as would be expected. However, the two solutions approach each other for increasing distance downstream. In fact, these solutions compare better with each other than with the asymptotic solution presented in Figures 6 and 8. Then, the solution for the uniform initial velocity distribution is a better approximation to the solution for the parabolic initial velocity distribution than is the asymptotic solution.

This idea can be generalized by considering the initial conditions of the asymptotic solution. Equation (2.23) predicts a jet with an infinitesimal initial thickness and an infinite initial velocity, such that the total momentum of the jet is finite. A jet with a finite initial velocity and a specified total momentum has the smallest possible initial thickness when the initial velocity distribution is uniform. Since the jet with a uniform initial velocity distribution comes closest to the initial condition of the asymptotic solution, then the asymptotic solution compares better with this jet than with any other jet. A measure of the degree of comparison of the asymptotic solution with any other solution is how well the maximum velocities compare as the jet developes downstream. The maximum velocity of the asymptotic solution is always greater than that for any other solution since it decays from an infinite value. The maximum velocity of the jet with a uniform initial velocity distribution must be greater than or equal to the maximum velocity of a jet with any other initial velocity distribution since this jet

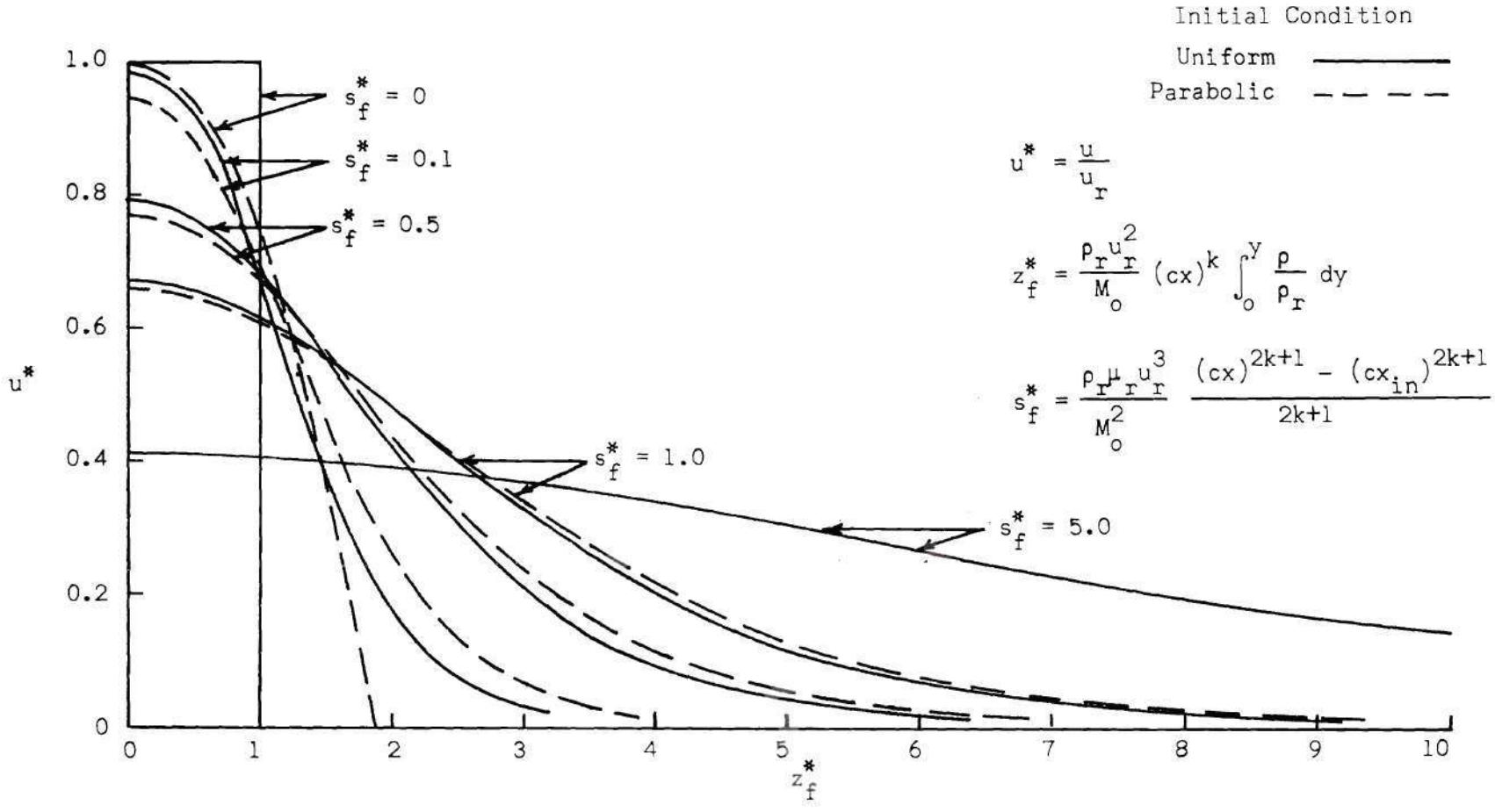

Figure 9. A Comparison of the Velocity Distributions for Free Jets with Two Initial Velocity Conditions at Several Locations Downstream.

compares better with the asymptotic solution than any other jet. Then, the maximum velocity for the jet with a uniform initial velocity distribution is between the solution for the jet with any other initial velocity distribution and the asymptotic solution. The maximum velocity and generally the entire velocity distribution for a jet of any initial condition compares better with the solution with a uniform initial velocity distribution than with the asymptotic solution for all positions downstream.

Energy Equation. The energy equation was solved for the free jet under the initial jet conditions of uniform velocity and temperature distributions. The boundary conditions of the external fluid considered are

$$\text{(i)} \qquad T_e^* = \frac{2h_r}{u_r^2} \frac{T_e - T_r}{T_r} = 0$$

$$\text{(ii)} \qquad T_e^* = \frac{2h_r}{u_r^2} \frac{T_e - T_r}{T_r} = 1$$

These initial and boundary conditions for the free jet correspond exactly to those leading to the Crocco solutions of the energy equations (2.45) and (2.46). Then

$$T^* = u^*(1 - u^*)$$

is the solution for case (i), and

$$T^* = 1 - u^{*2}$$

is the solution for case (ii).

Figure 10 illustrates the development of the temperature distribution for case (i). In this case, the temperature of the jet initially is the same as that of the exterior fluid. As the velocity of the jet is dissipated through viscous interaction with the external fluid, the kinetic energy of the jet is converted into thermal energy. In the early stages of development, only the portion of the jet close to the exterior fluid is affected by viscosity, so the temperature rises in the outer edge of the jet while remaining unchanged at the centerline. As the viscous development of the jet continues, then the entire velocity distribution decays, and the temperature of the jet rises accordingly. The hot jet cools off further downstream as more and more of the cooler external fluid is mixed with the jet fluid. The temperature distribution and the compressible physical co-ordinates in terms of the transformed co-ordinates for case (i) are presented in Figures 11 and 12. Figures 13 and 14 present the same results for case (ii).

Case (i) involves viscous dissipation with an external fluid having the same temperature that the jet had initially. Case (ii) includes the additional effect of an exterior fluid temperature different from the initial temperature of the jet. Since the energy equation expressed in terms of the transformed co-ordinates is linear in temperature, then these solutions can be added linearly to obtain solutions for different external fluid conditions. For example, suppose the solution of the energy equation is desired for the dimensionless external fluid temperature equal to -1/4 (i.e., a cold external fluid). Then denoting the solution for case (i) as $\{0\}$ and that for case (ii) as $\{1\}$, the solution for this example can be symbolically expressed as

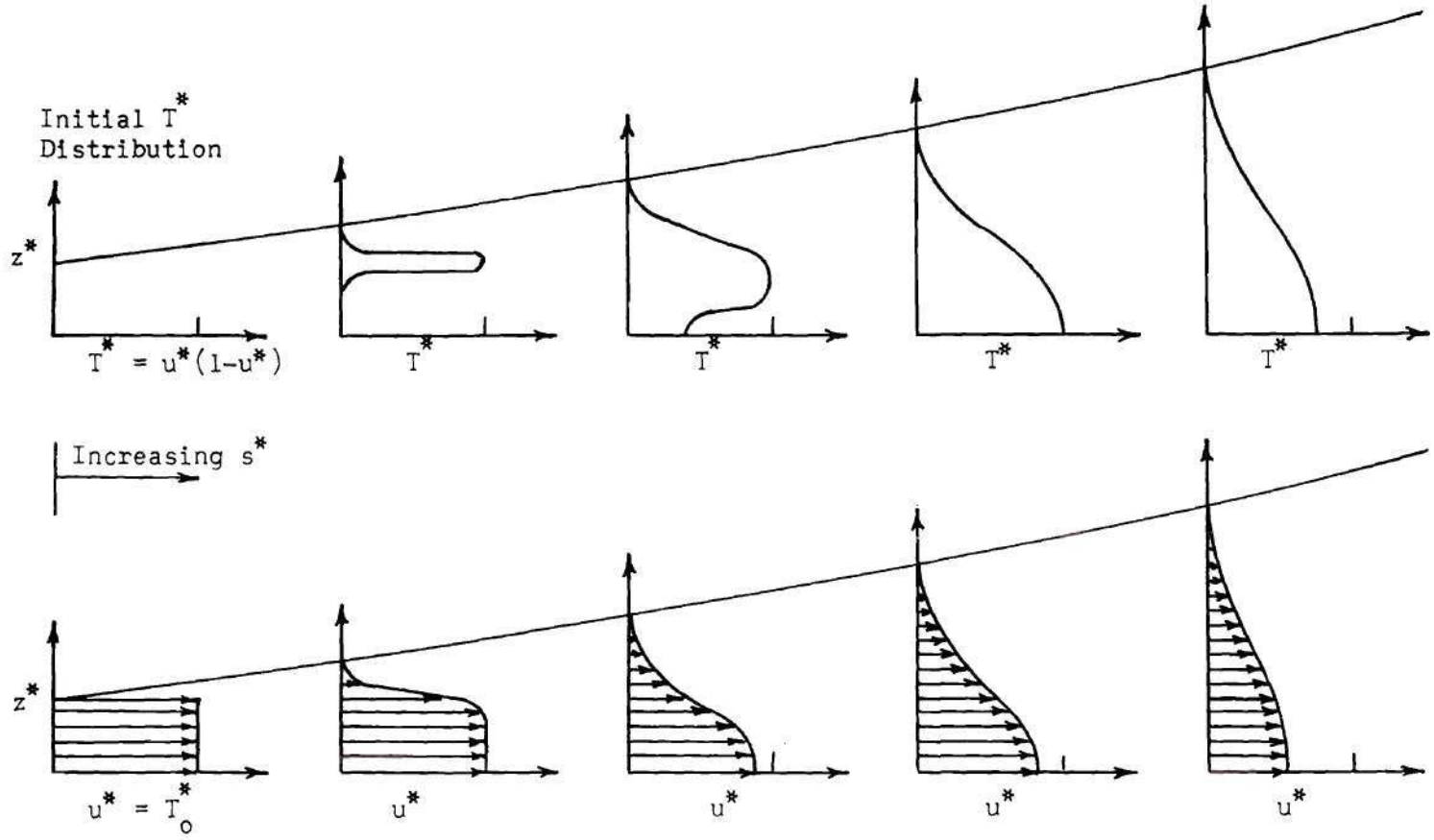

Figure 10. Illustration of the Development of the Temperature Distribution in a Free Jet.

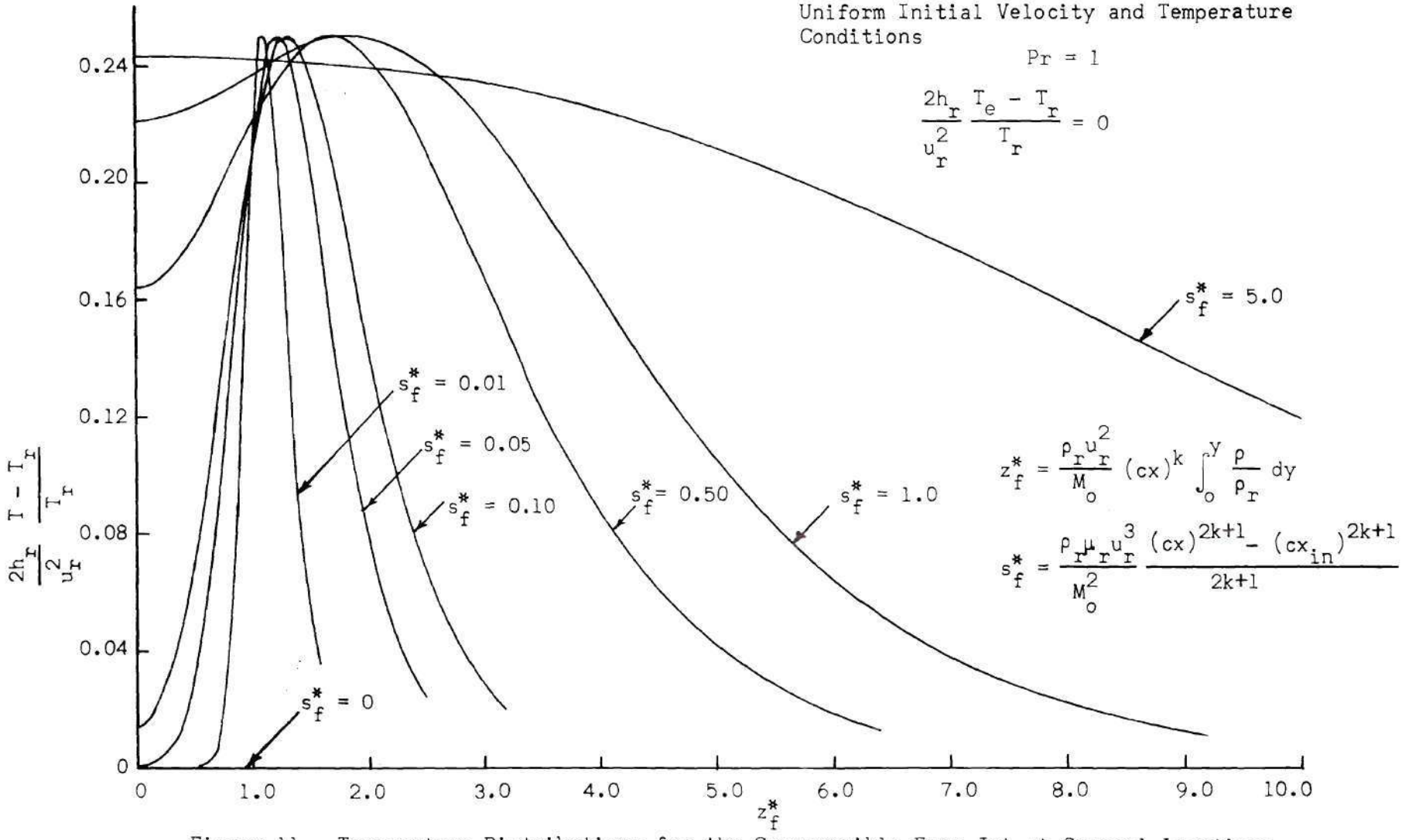

Figure 11. Temperature Distributions for the Compressible Free Jet at Several Locations Downstream, $T_e = T_r$.

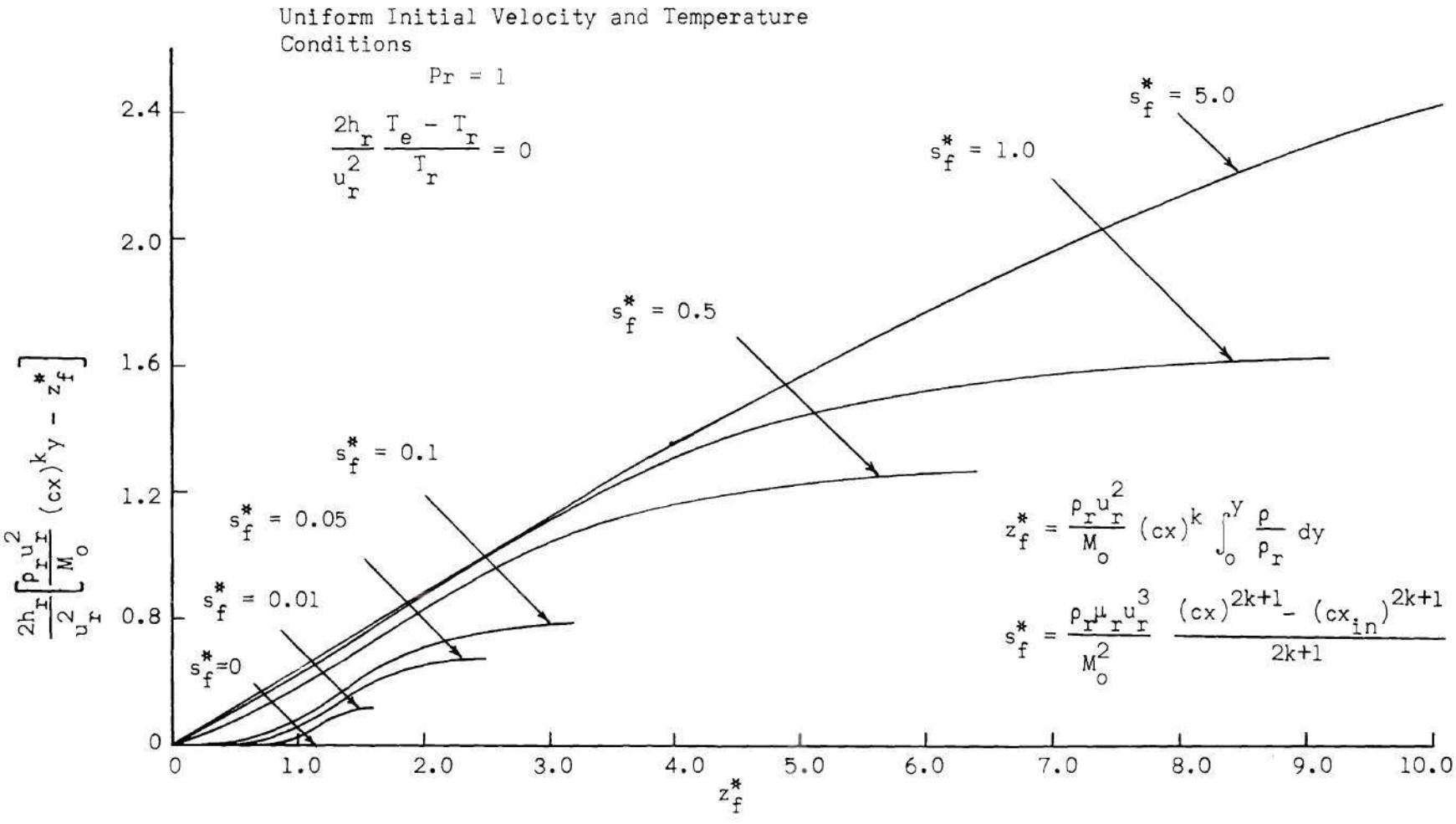

Figure 12. Normal Distance Parameter for the Compressible Free Jet at Several Locations Downstream, $T_e = T_r$.

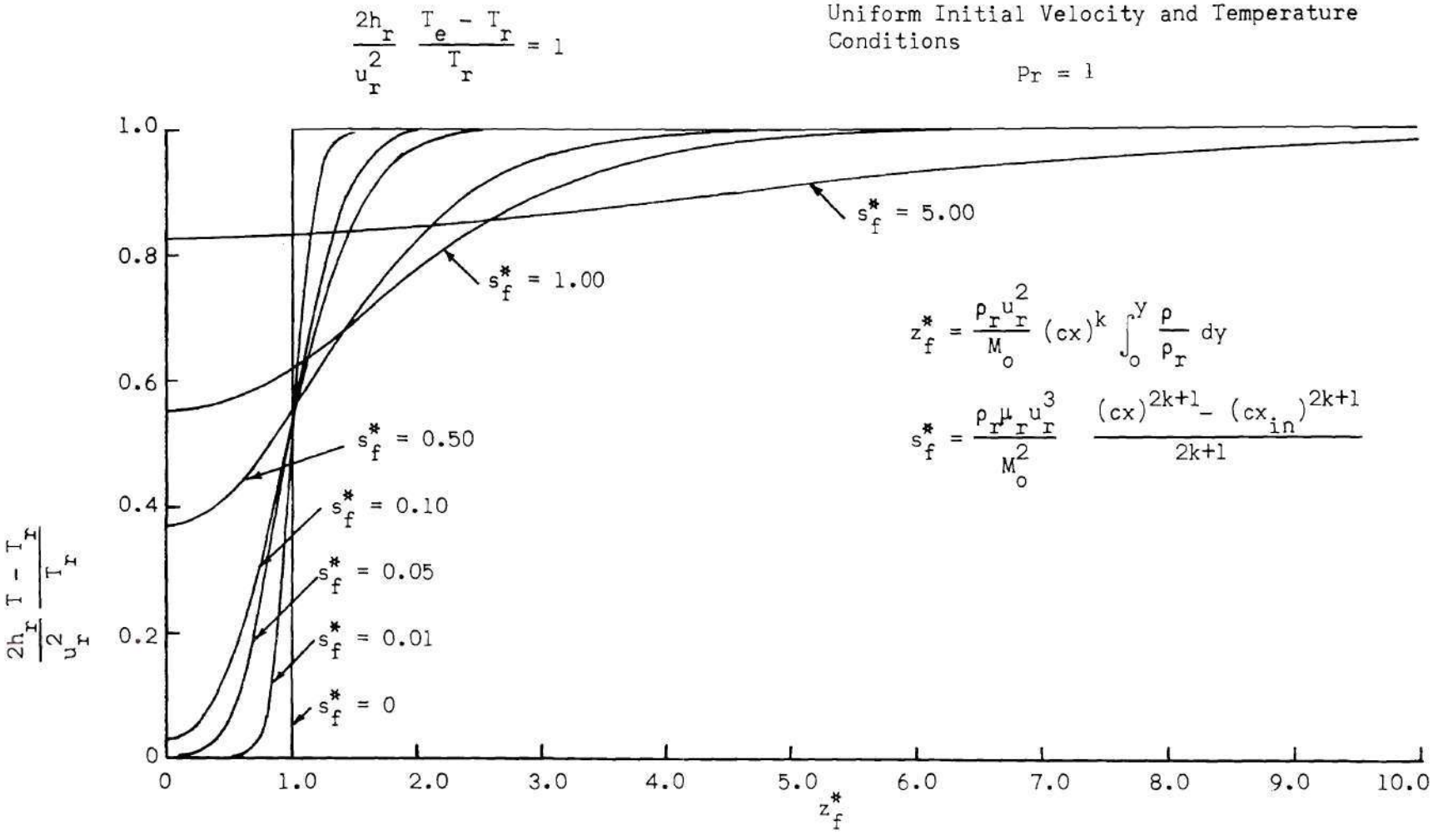

Figure 13. Temperature Distribution for the Compressible Free Jet at Several Locations Downstream, $T_e \neq T_r$.

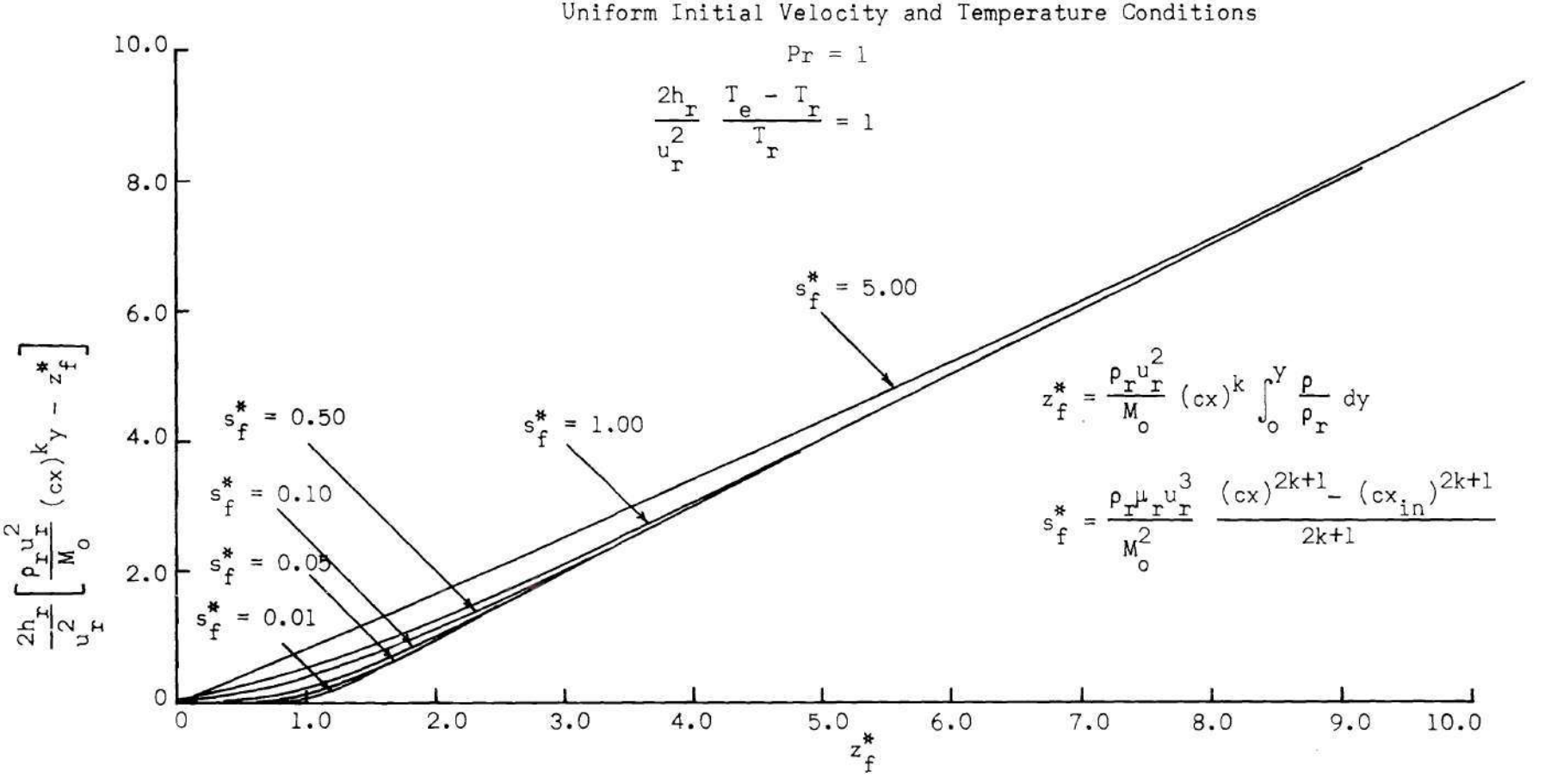

Figure 14. Normal Distance Parameter for the Compressible Free Jet at Several Locations Downstream, $T_e \neq T_r$.

$$\{-1/4\} = \{0\} + (-1/4)\left(\{1\} - \{0\}\right)$$

Here, the first term of this solution expresses the effect of the viscous dissipation of the jet, and the second term the effect of the cold external fluid. Since the transformation to the physical co-ordinates is linear in temperature, the physical co-ordinates of this example can be obtained by adding the physical co-ordinates of the known solutions in the same manner. The solution for other external fluid conditions can be obtained in the same way.

Approximate Solution

The approximate solution of the momentum equation for the free jet is divided into two downstream regions. The region from the initial condition to the point downstream at which the maximum velocity of the jet begins to decay is termed region (I), and the region from that point on downstream is termed region (II).

The approximate solution in dimensionless form of the free jet for region (I) is

$$x^* \leq 0.10$$

$$\frac{\delta_b}{d} \equiv \delta_b^* = 8.518x^{*1/2}$$

$$\frac{\delta}{d} \equiv \delta^* = 1 - 3.164x^{*1/2}$$

for $z^* \leq \delta^*$ then $u^* = 1$

$$\text{for } z^* > \delta^* \quad \text{then } u^* = 2\left(\frac{z^* - \delta^*}{\delta_b^*}\right)^3 - 3\left(\frac{z^* - \delta^*}{\delta_b^*}\right)^2 + 1$$

and for region (II) is

$$x^* > 0.10$$

$$u_{max}^* = \left(\frac{1}{2.727(x^* - 0.1) + 1}\right)^{1/3}$$

$$\delta_b^* = 2.692 \frac{1}{u_{max}^{*2}}$$

$$u^* = u_{max}^*\left[\, 2\left(\frac{z^*}{b^*}\right)^3 - 3\left(\frac{z^*}{b^*}\right)^2 + 1 \,\right]$$

This result is presented and compared to the exact result in Figure 15. The solutions compare well for the maximum velocity and general shape of the velocity distribution but not as well for the thickness of the jet.

Wall Jet

Exact Solution

Momentum Equation. The exact solution of the momentum equation for the wall jet is presented for the following three initial velocity conditions: (i) a uniform distribution, (ii) a parabolic distribution, and (iii) one half of an asymptotic free jet distribution. As in the case of the free jet, the solutions are presented in terms of the transformed co-ordinates for various downstream locations in Figures 16, 17, and 18. The velocity decay before the asymptotic solution becomes a good approximation to the exact result is greater in the case of a wall jet

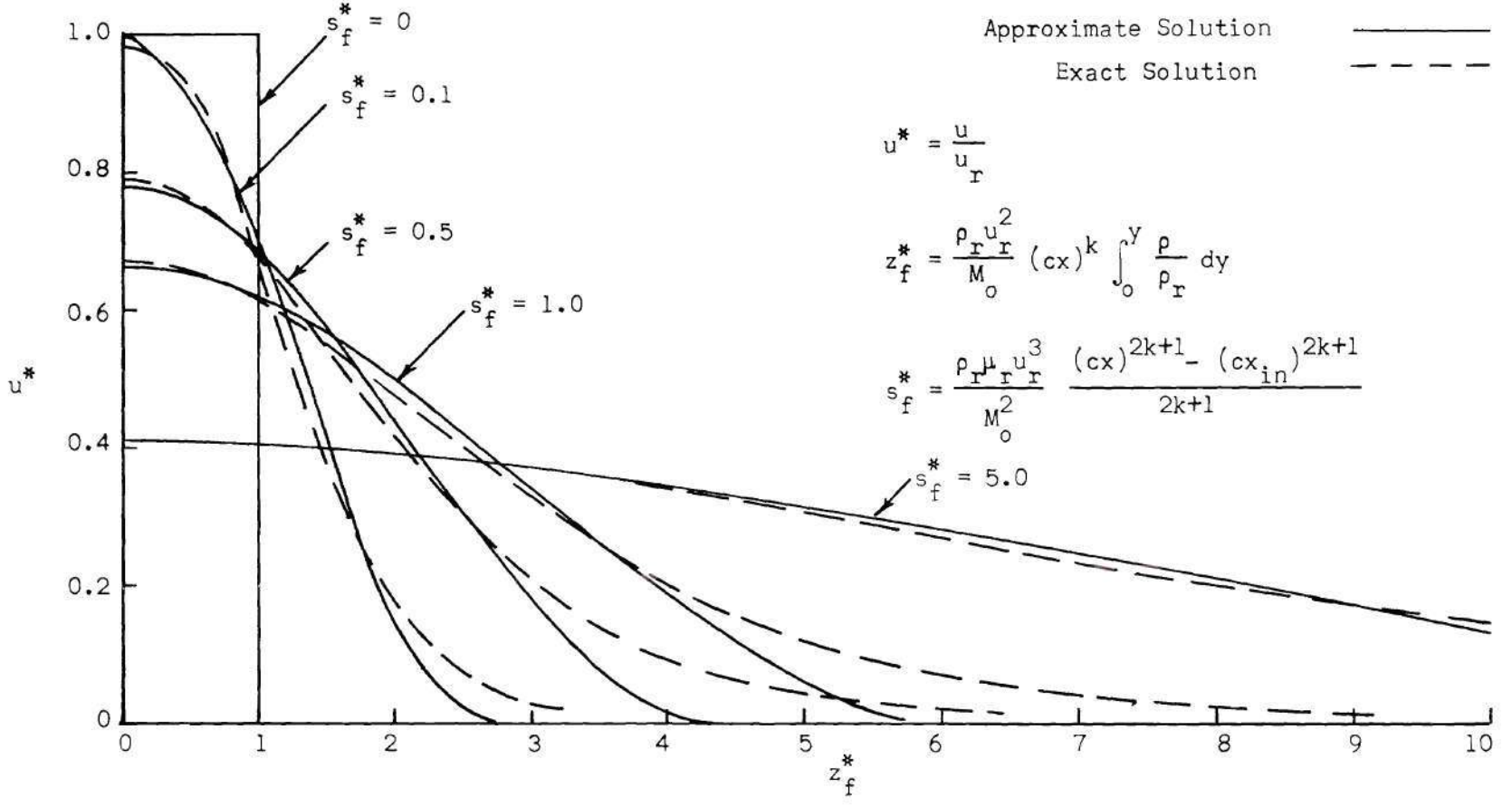

Figure 15. A Comparison of the Approximate and the Exact Velocity Distributions for the Free Jet at Several Locations Downstream, Uniform Initial Velocity Condition.

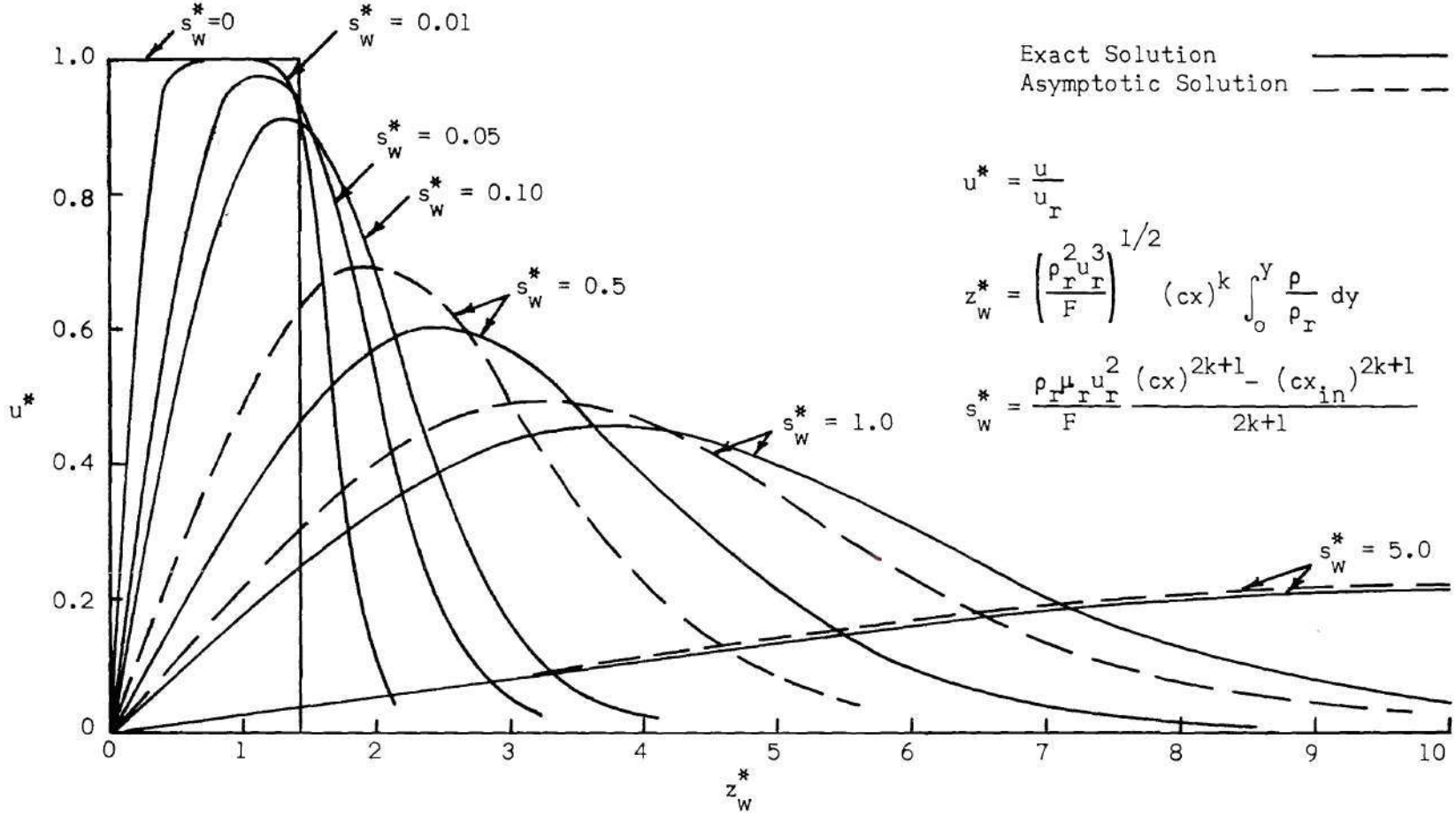

Figure 16. Velocity Distributions for the Wall Jet at Several Locations Downstream, Uniform Initial Velocity Condition.

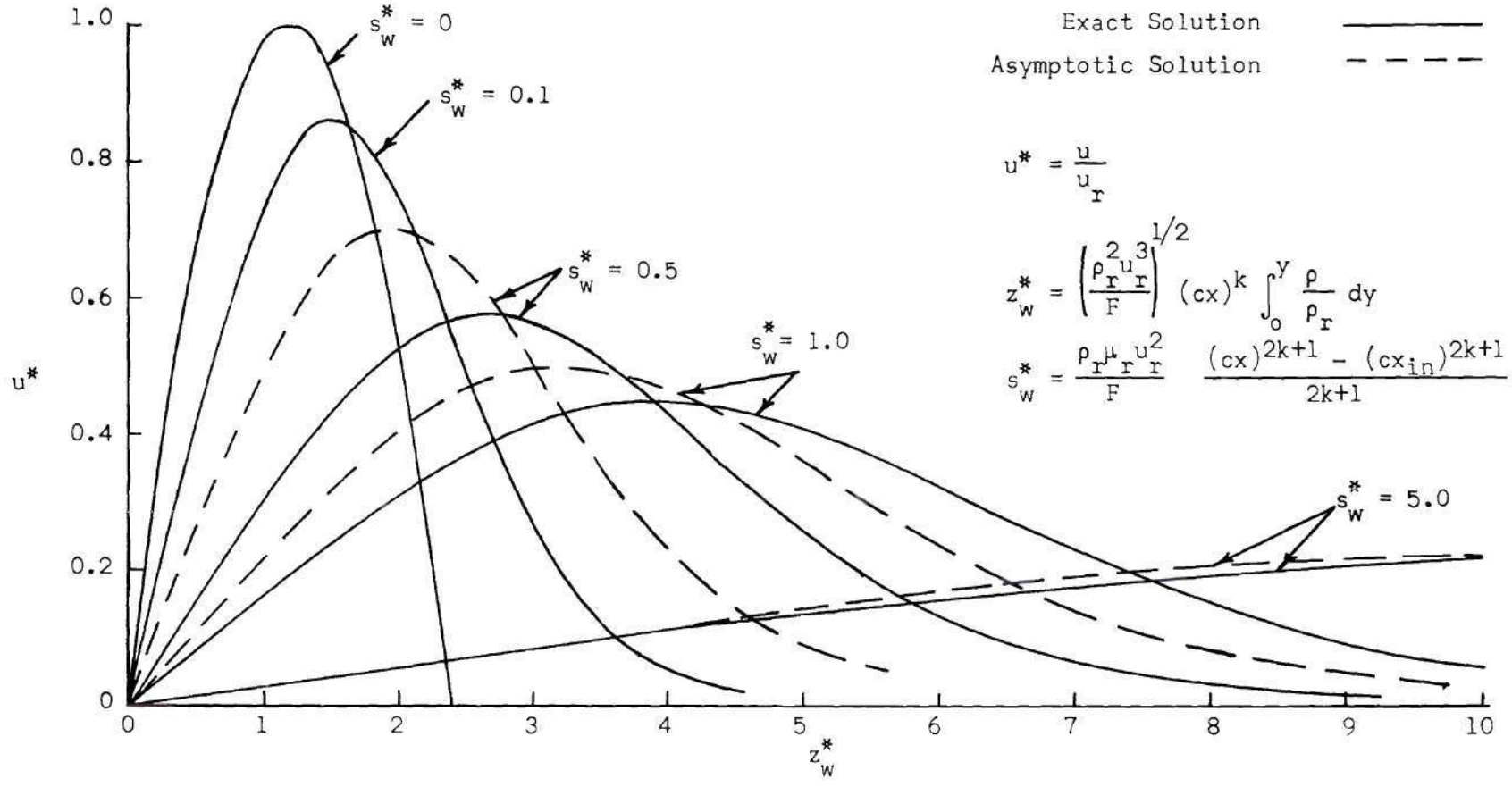

Figure 17. Velocity Distributions for the Wall Jet at Several Locations Downstream, Parabolic Initial Velocity Condition.

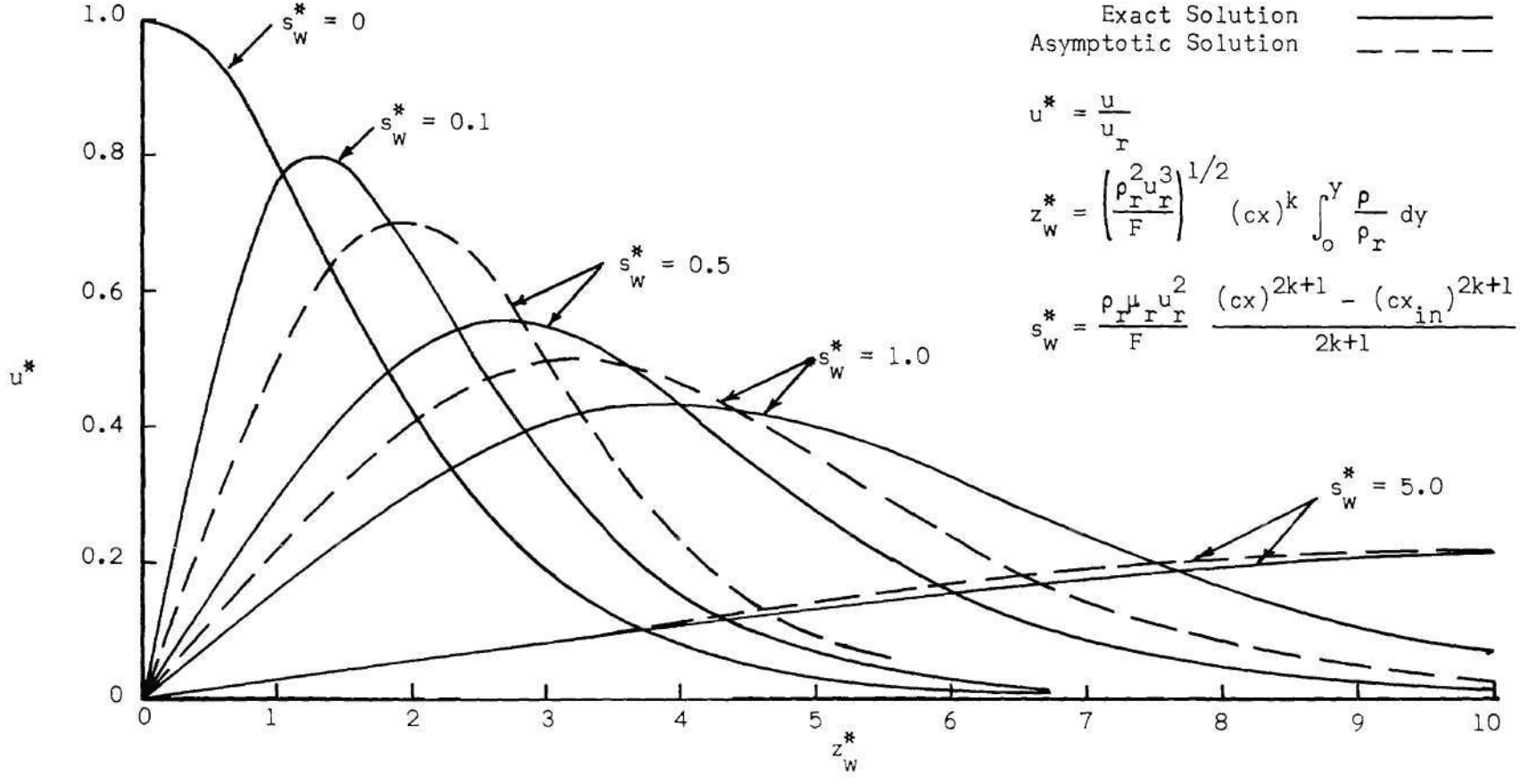

Figure 18. Velocity Distributions for the Wall Jet at Several Locations Downstream, Asymptotic Free Jet Initial Velocity Condition.

than in the case of a free jet. In these cases, the two solutions compare well only after the maximum velocity has decayed to about one third of its original value. Figure 19 presents the solution for the uniform initial velocity condition of Figure 16 in terms of the similarity variables of the asymptotic solution for various downstream locations. In Figure 19, the asymptotic solution for all downstream locations plots on a single curve, and the exact solution approaches this curve for increasing distance downstream.

In Figure 20, the solutions with the parabolic and one half of an asymptotic free jet initial velocity distributions are compared with the solution with the uniform initial velocity distribution. These solutions compare better with the uniform initial condition than with the asymptotic solution shown in Figures 17 and 18. The initial condition of the asymptotic wall jet solution is an infinitesimally thin jet with an infinite velocity. The argument presented in the case of the free jet applies as well for the wall jet, and thus the maximum velocity, and generally the entire velocity distribution, for the wall jet compares better with the solution with a uniform initial velocity distribution than with the asymptotic solution.

The wall shear is of practical interest and in dimensionless form is expressed by

$$\tau^* = \left(\frac{F}{c^2 \rho_r^2 \mu_r^2 u_r^5 (cx)^{2k}} \right)^{1/2} \qquad \tau = \left(\frac{\partial u^*}{\partial z^*} \bigg|_{s^*} \right)_{z^*=0}$$

This quantity is plotted in Figure 21 versus the downstream location for wall jets of three different initial velocity conditions. The initial

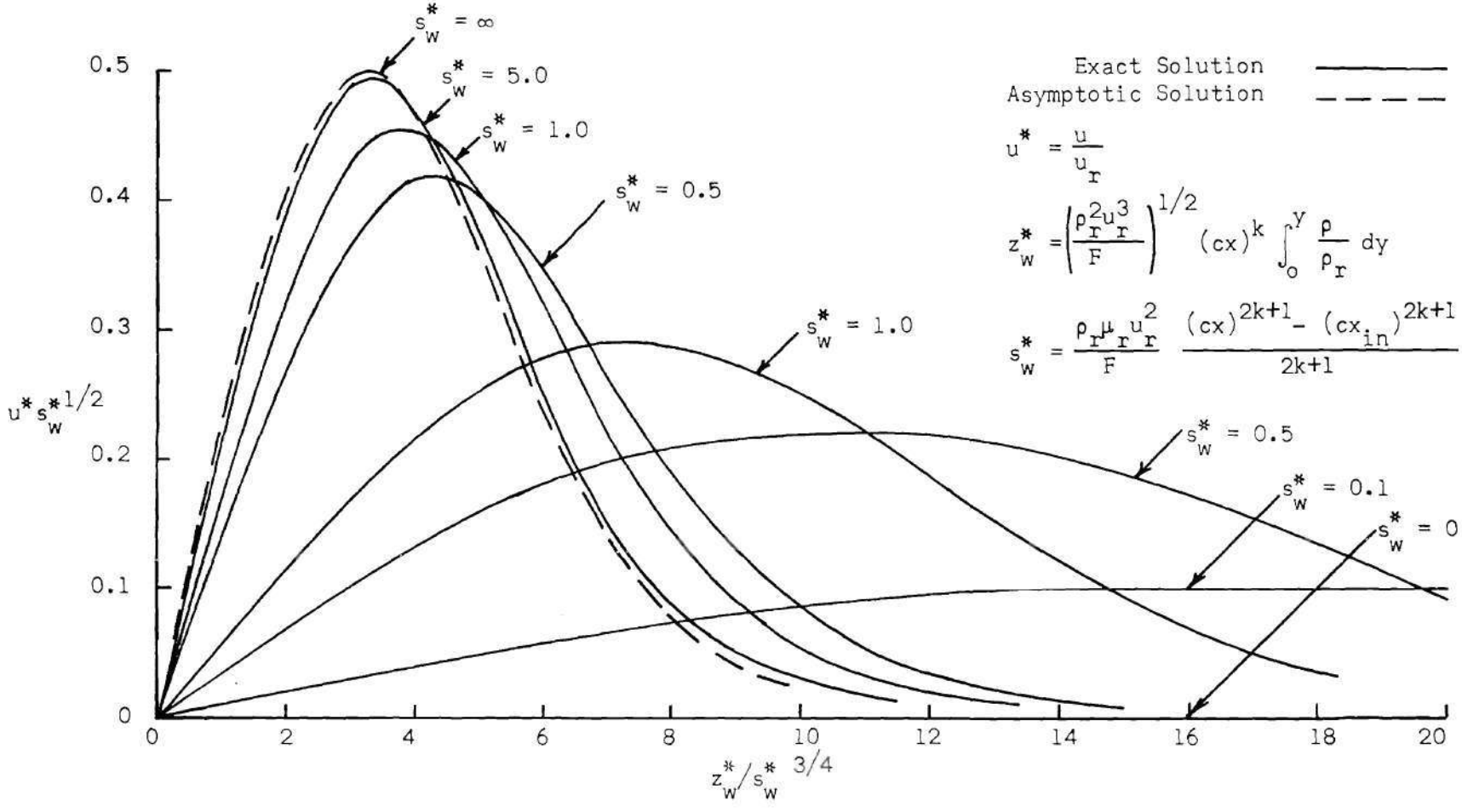

Figure 19. Velocity Distribution for the Wall Jet in Terms of the Similarity Parameters at Several Locations Downstream, Uniform Initial Velocity Condition.

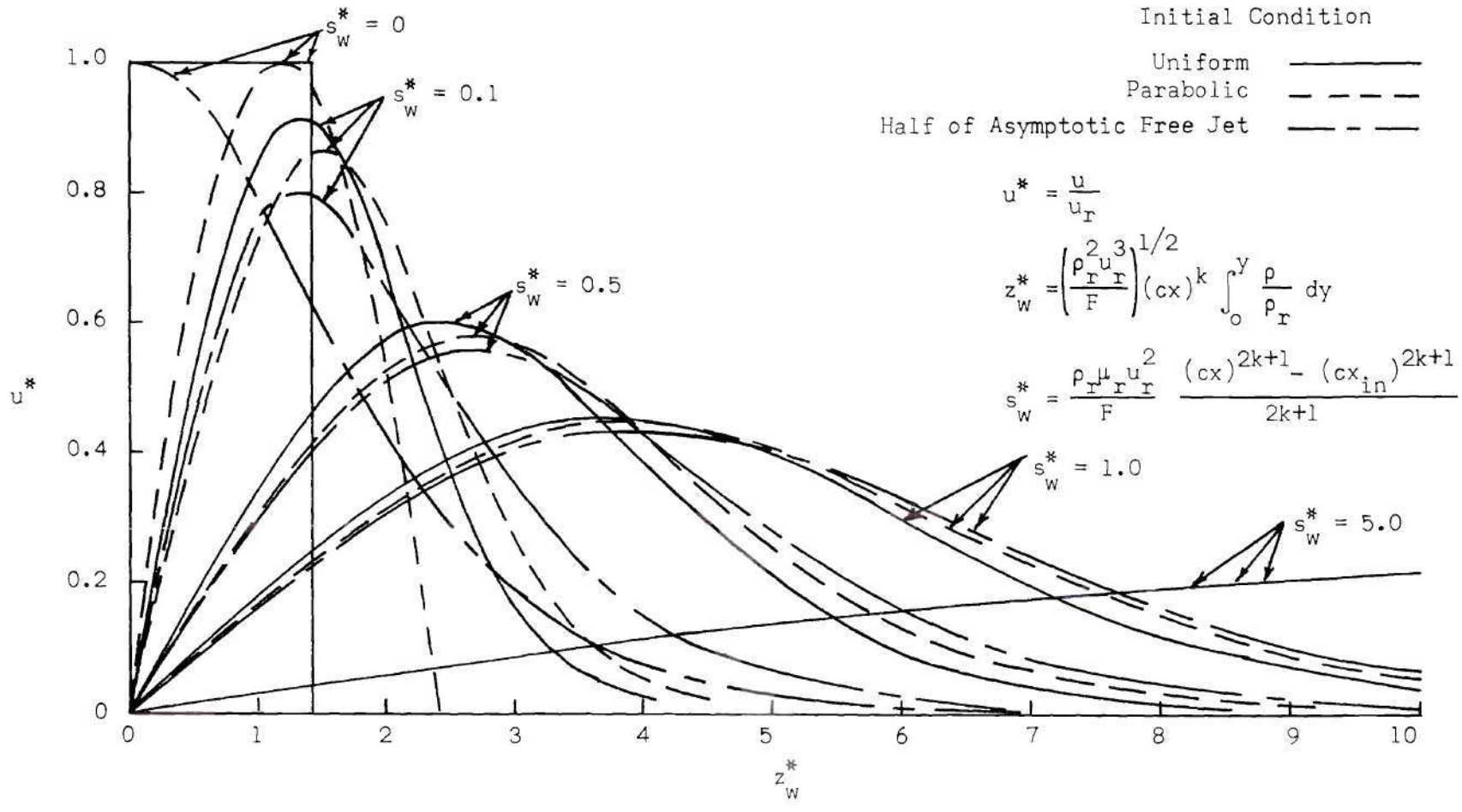

Figure 20. Comparison of Velocity Distributions for Wall Jets With Various Initial Velocity Conditions at Several Locations Downstream.

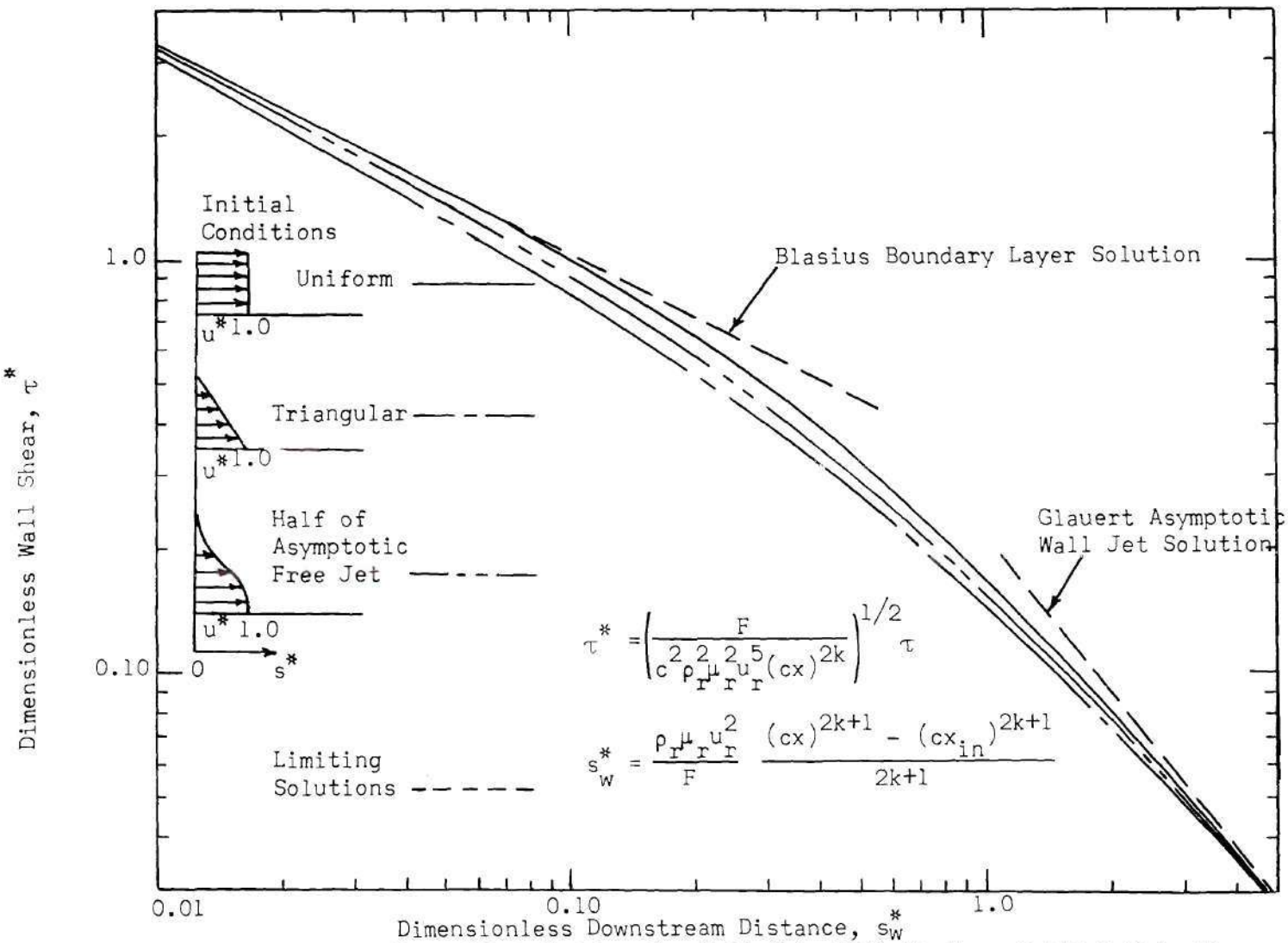

Figure 21. Wall Shear Distribution for Wall Jets With Various Initial Velocity Conditions.

velocity conditions treated are a uniform, triangular, and one half of an asymptotic free jet with the velocities for $z = 0$ equal to the maximum velocity in each distribution. Included on the plot are the results from the Blasius boundary layer solution and the Glauert asymptotic solution. The wall shear for the three cases presented in Figure 21, as well as for any other case with the maximum initial velocity at $z = 0$, are limited by the Blasius solution near the initial condition, since the initial development next to the wall is that of a boundary layer, and are limited by the Glauert solution far downstream. The wall shear for uniform and triangular initial conditions forms a narrow band between the two limiting solutions. The wall shear for all wall jets with initial conditions geometrically between the uniform and triangular conditions will be contained within this band. This correlation holds for many wall jets with initial conditions not geometrically between the uniform and triangular conditions. An example of such a case is the half of an asymptotic free jet initial condition presented in Figure 21. In fact, the wall shear for this case is approximately midway between the uniform and triangular initial condition cases. Then, a mean wall shear distribution, such as that shown by the one half of an asymptotic free jet case, will serve as a good approximation to the wall shear in the development region for wall jets with a wide range of initial velocity distributions.

Energy Equation. The energy equation for the wall jet was solved with the jet initial conditions of uniform velocity and temperature distributions. Several more cases for the wall jet were considered than for the free jet because of the additional freedom introduced by the boundary

conditions at the wall. If the wall is adiabatic, then the dimensionless temperature is the same as for the free jet, i.e.,

$$T^* = \frac{2h_r}{u_r^2} \frac{T - T_r}{T_r}$$

The boundary conditions considered are

$$\text{(i)} \quad T_e^* = 0, \quad \frac{\partial T_e^*}{\partial z^*} = 0 \qquad \begin{Bmatrix} 0 \\ - \end{Bmatrix}$$

$$\text{(ii)} \quad T_e^* = 1, \quad \frac{\partial T_e^*}{\partial z^*} = 0 \qquad \begin{Bmatrix} 1 \\ - \end{Bmatrix}$$

For the case of a constant wall temperature, the dimensionless temperature is

$$T^* = \frac{2h_r}{u_r^2} \frac{T - T_w}{T_r}$$

The boundary conditions considered are

$$\text{(iii)} \quad T_e^* = 0, \quad T_r^* = 0 \qquad \begin{Bmatrix} 0 \\ 0 \end{Bmatrix}$$

$$\text{(iv)} \quad \begin{matrix} T_e^* = 0 \\ T_r^* = 1 \end{matrix} \quad \left\{ \begin{matrix} 0 \\ 1 \end{matrix} \right\}$$

$$\text{(v)} \quad \begin{matrix} T_e^* = 1 \\ T_r^* = 0 \end{matrix} \quad \left\{ \begin{matrix} 1 \\ 0 \end{matrix} \right\}$$

The numbers contained within the brackets to the right of the five cases are the symbolic representations of the individual cases. The top number in the brackets denotes the external fluid condition and the bottom number the initial condition with the dash (-) denoting the adiabatic wall cases.

The conversion of the kinetic energy of the jet into thermal energy because of the viscous dissipation of the velocity distribution occurs with the wall jet as it did with the free jet. In the case of the wall jet, however, the velocity distribution decays initially in the boundary layer next to the wall as well as in the free layer next to the external fluid. Therefore, for the wall jet, the development of the temperature distribution initially occurs near the wall as well as near the external fluid.

Cases (ii) and (iii) correspond to the conditions of the two Crocco solutions of the energy equation, and thus the dimensionless temperature may be expressed as

$$T^* = 1 - u^{*2}$$

and

$$T^* = u^*(1 - u^*)$$

respectively. The other three cases, however, require a numerical solution of the energy equation. The temperature distribution and the physical co-ordinates in terms of the transformed co-ordinates for each of the five cases are presented in Figures 22 through 31.

The heat transfer in dimensionless form is expressed as

$$q^* = \frac{2F^{1/2}}{c\rho_r \mu_r u_r^{7/2} (cx)^k} \quad q = \left(\frac{\partial T^*}{\partial z^*}\right)_{z^*=0}$$

This parameter for cases (iii), (iv), and (v) is presented in Figure 32.

Since the energy equation in terms of the transformed co-ordinates is linear in temperature, these solutions can be added linearly to satisfy different conditions for the external fluid and for the wall. The effect of a cold external fluid on the adiabatic wall jet is analogous to the same case for the free jet already discussed. For example, if the dimensionless temperature of the external fluid is -1/4 the solution is symbolically expressed as

$$\begin{Bmatrix} -1/4 \\ - \end{Bmatrix} = \begin{Bmatrix} 0 \\ - \end{Bmatrix} + \left[-1/4\right]\left(\begin{Bmatrix} 1 \\ - \end{Bmatrix} - \begin{Bmatrix} 0 \\ - \end{Bmatrix} \right)$$

Solutions (iv) and (v) for the wall jet of constant wall temperature contain the viscous dissipation effect of solution (iii), plus, respectively, the additional effects of a wall temperature and exterior fluid temperature different from the initial jet temperature. For example,

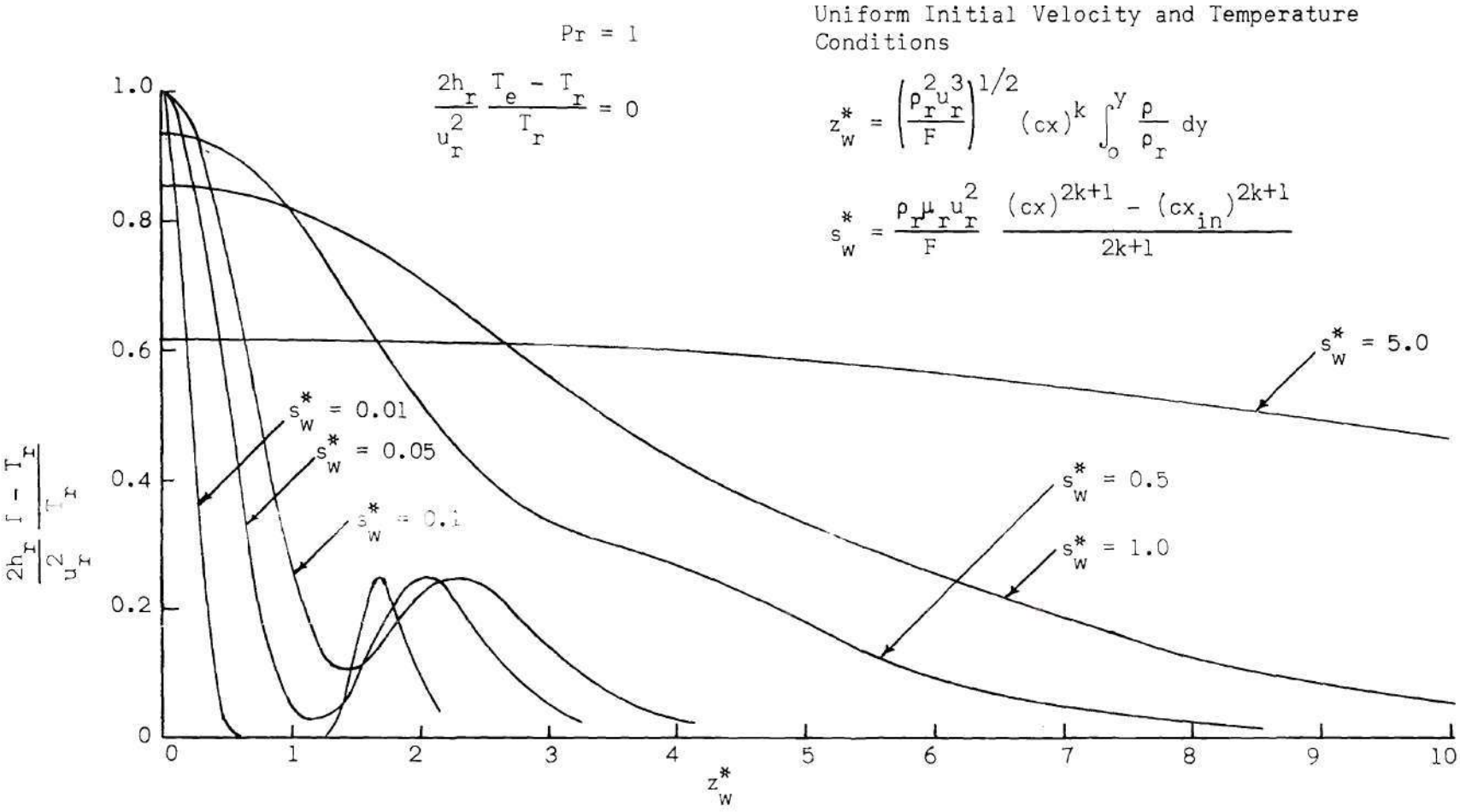

Figure 22. Temperature Distribution for the Compressible Wall Jet at Several Locations Downstream, $T_e = T_r$, Adiabatic Wall.

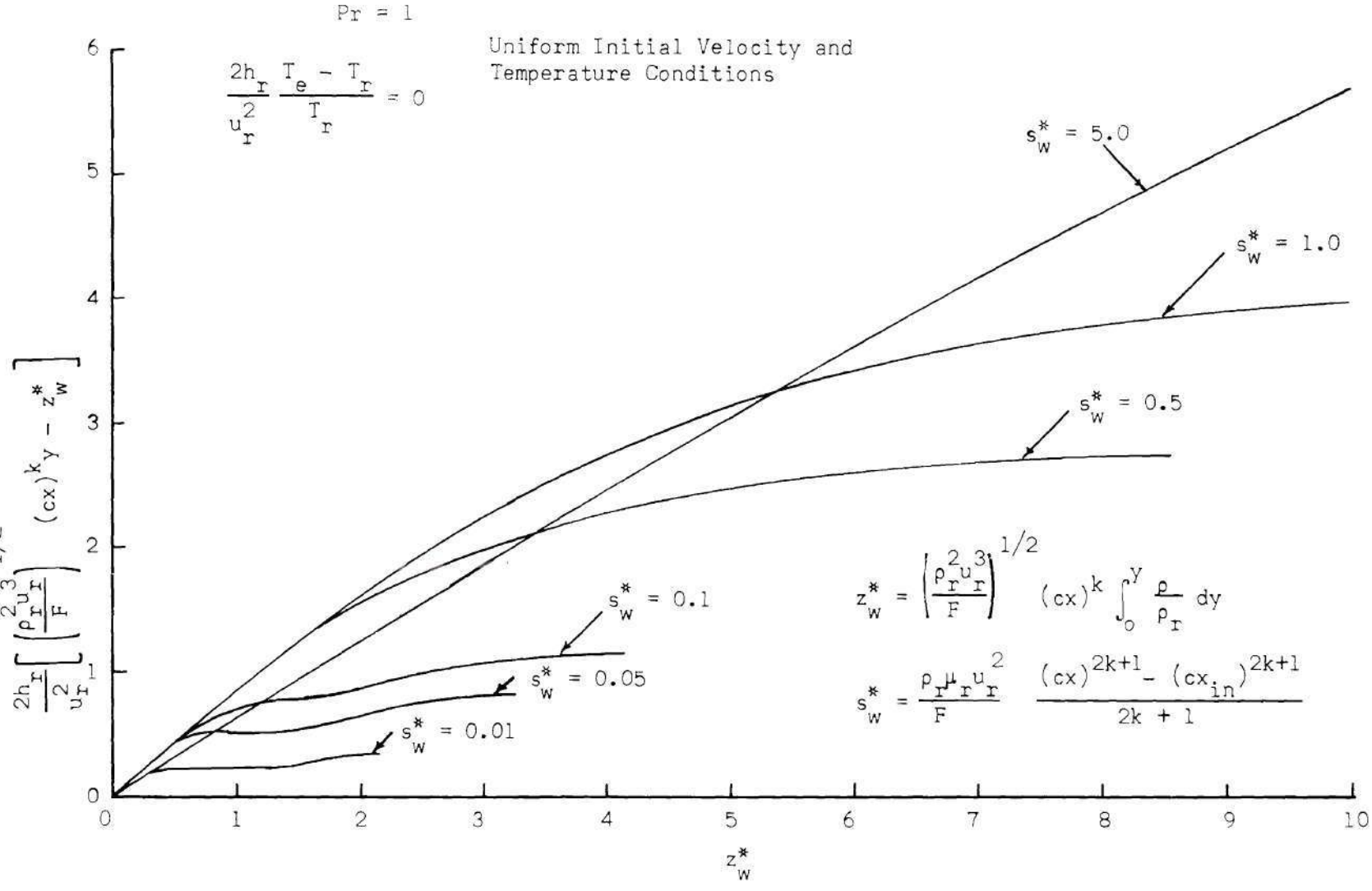

Figure 23. Normal Distance Parameter for the Compressible Wall Jet at Several Locations Downstream, $T_e = T_r$, Adiabatic Wall.

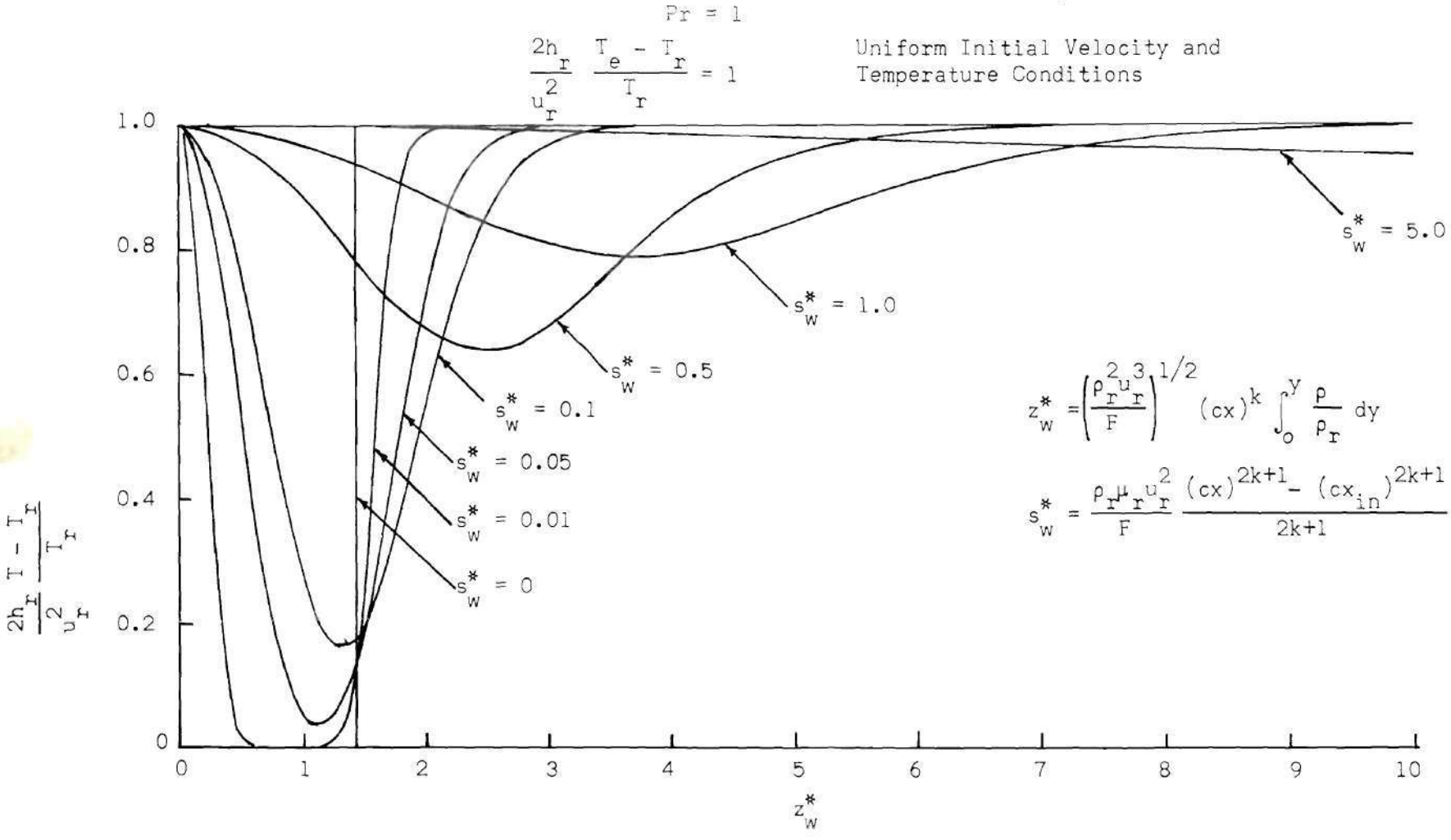

Figure 24. Temperature Distribution for the Compressible Wall Jet at Several Locations Downstream, $T_e \neq T_r$, Adiabatic Wall.

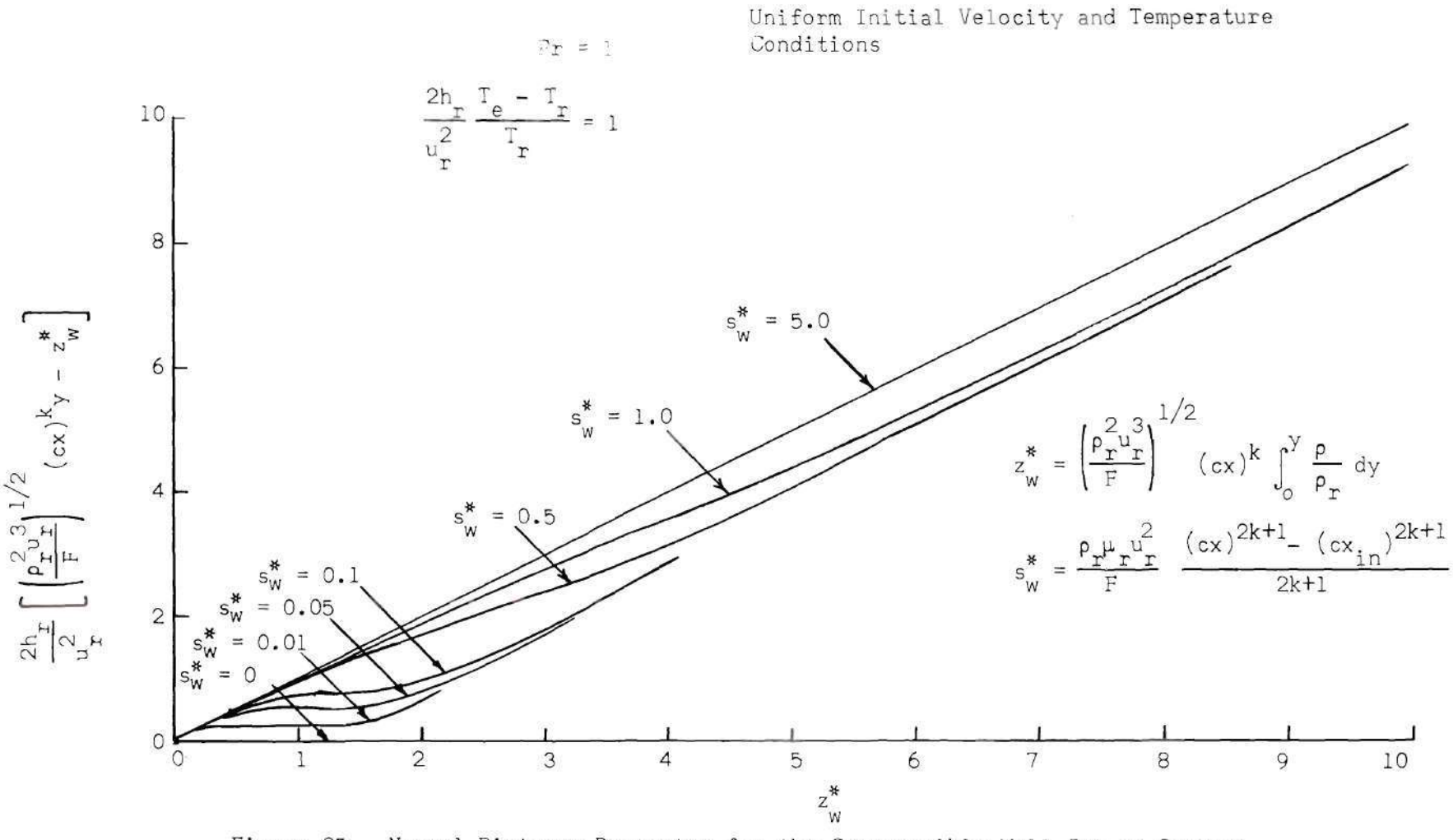

Figure 25. Normal Distance Parameter for the Compressible Wall Jet at Several Locations Downstream, $T_e \neq T_r$, Adiabatic Wall.

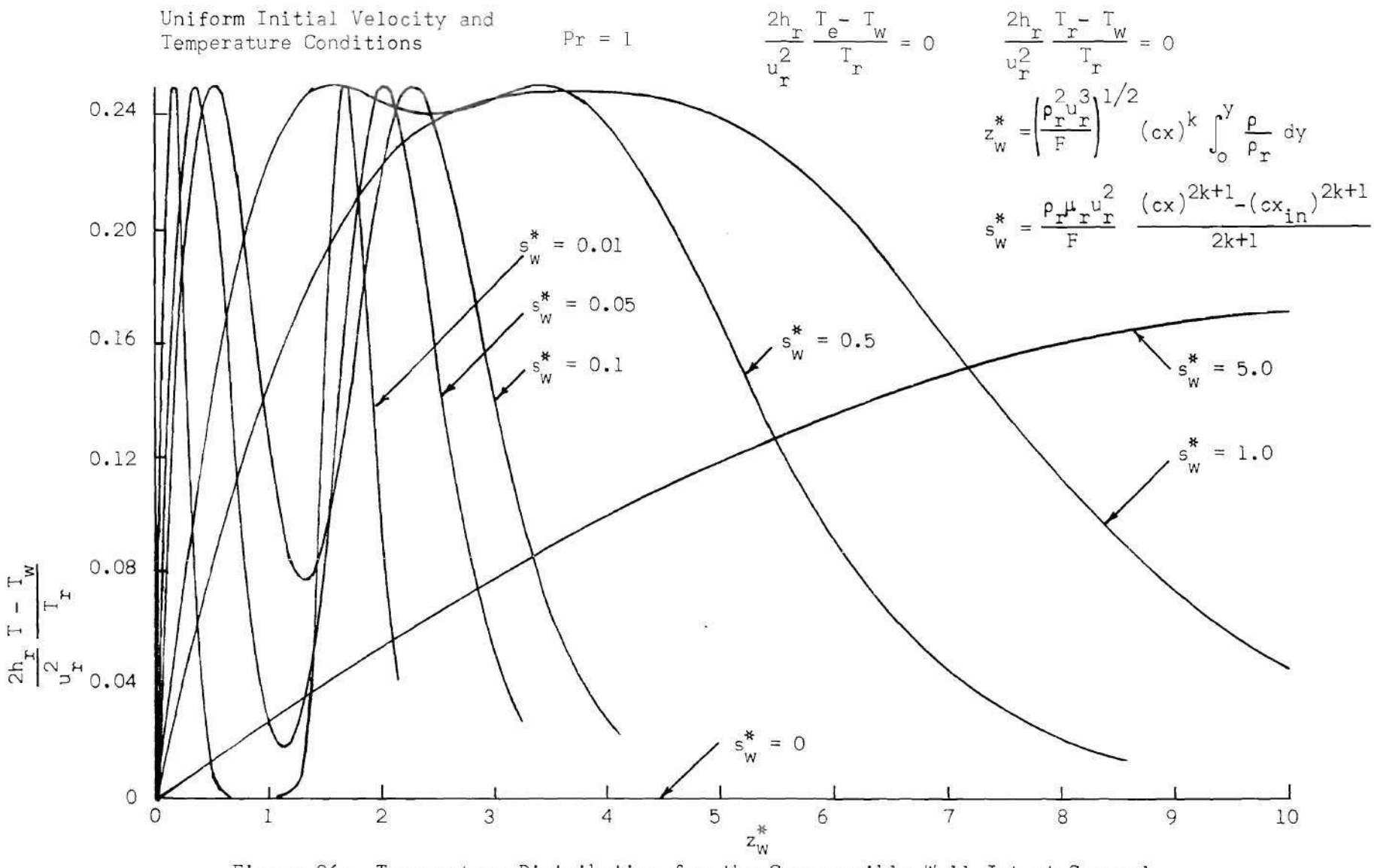

Figure 26. Temperature Distribution for the Compressible Wall Jet at Several Locations Downstream, $T_e = T_w$, $T_r = T_w$.

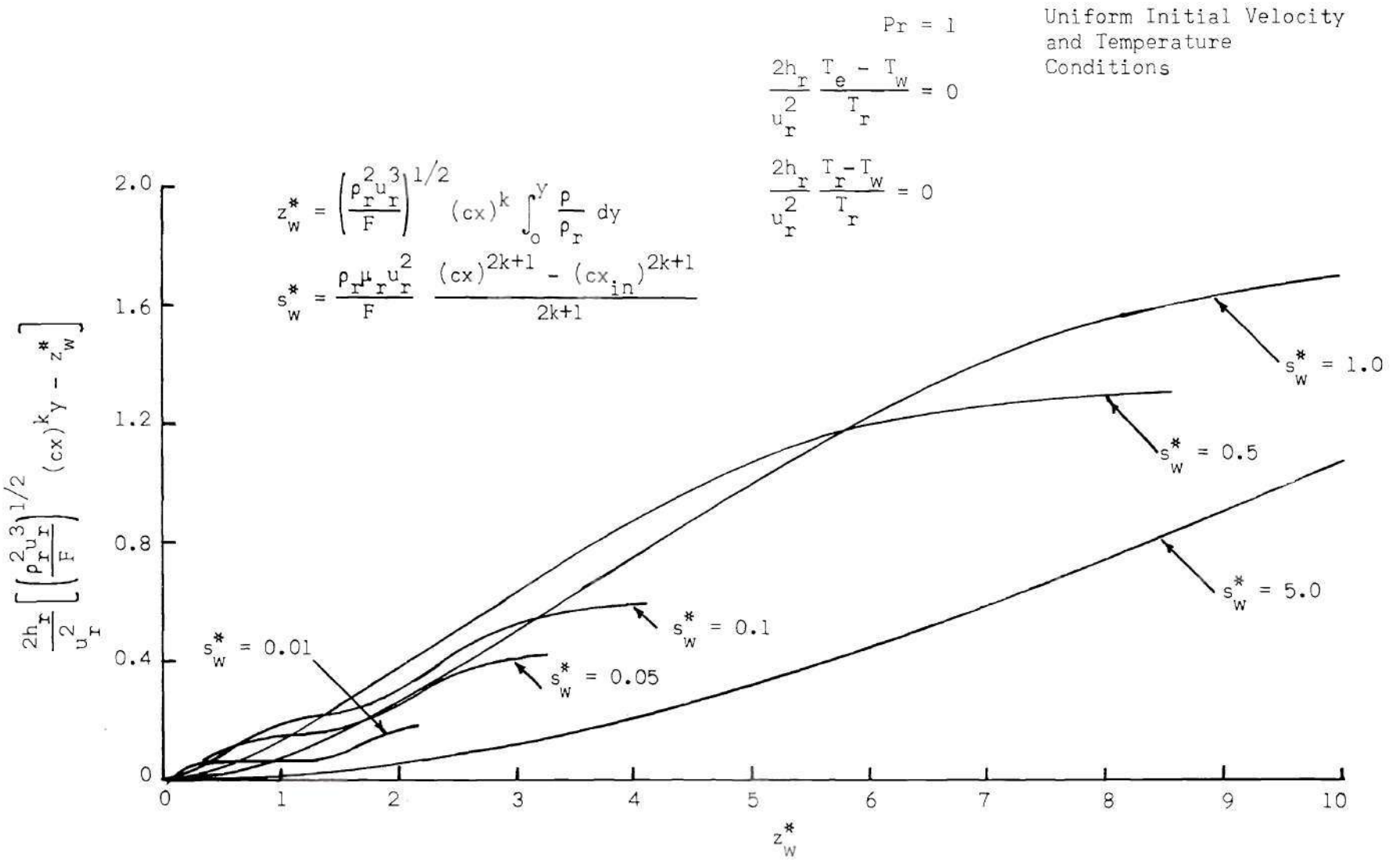

Figure 27. Normal Distance Parameter for the Compressible Wall Jet at Several Locations Downstream, $T_e = T_w$, $T_r = T_w$.

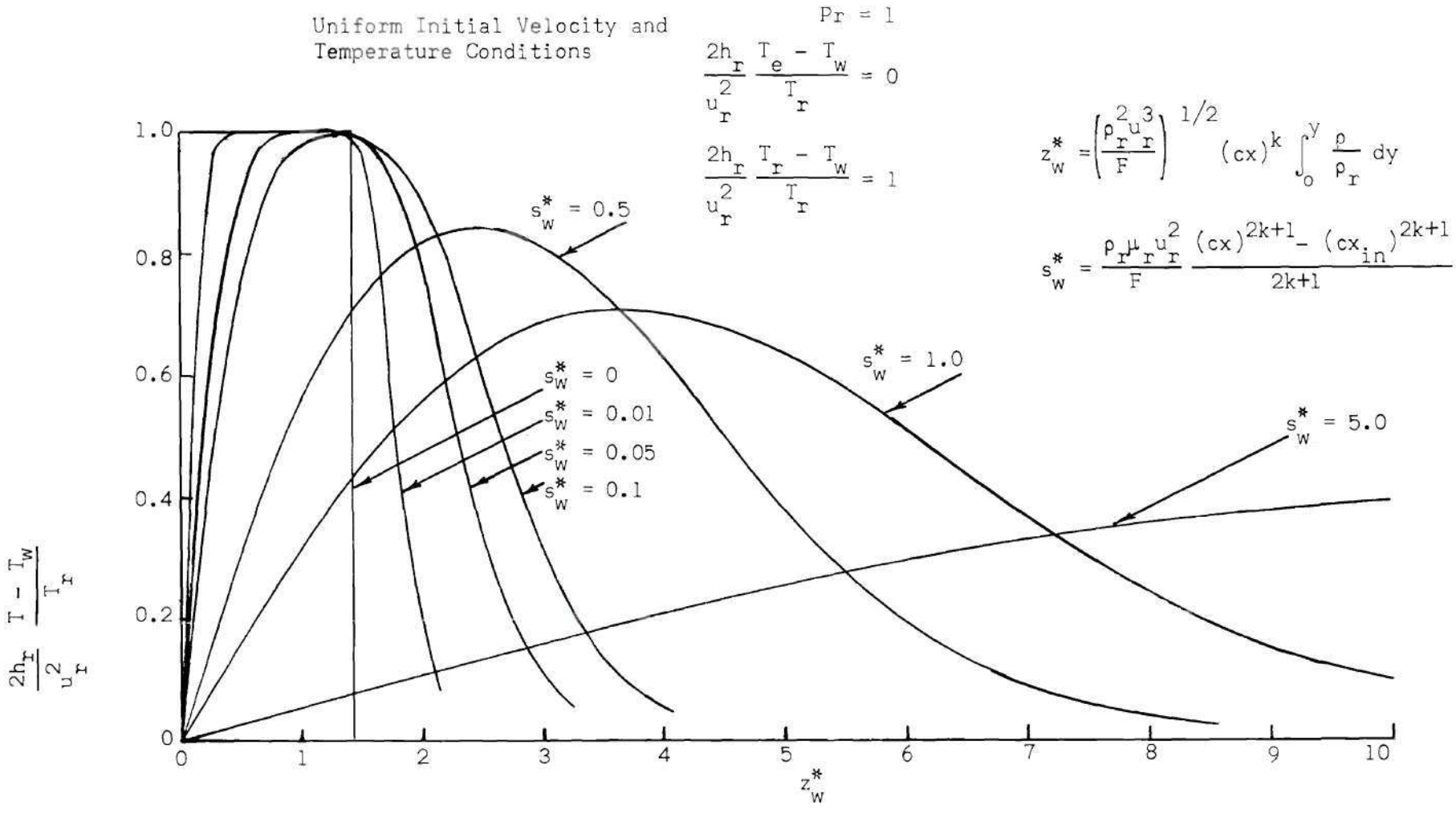

Figure 28. Temperature Distributions for the Compressible Wall Jet at Several Locations Downstream, $T_e = T_w$, $T_r \neq T_w$.

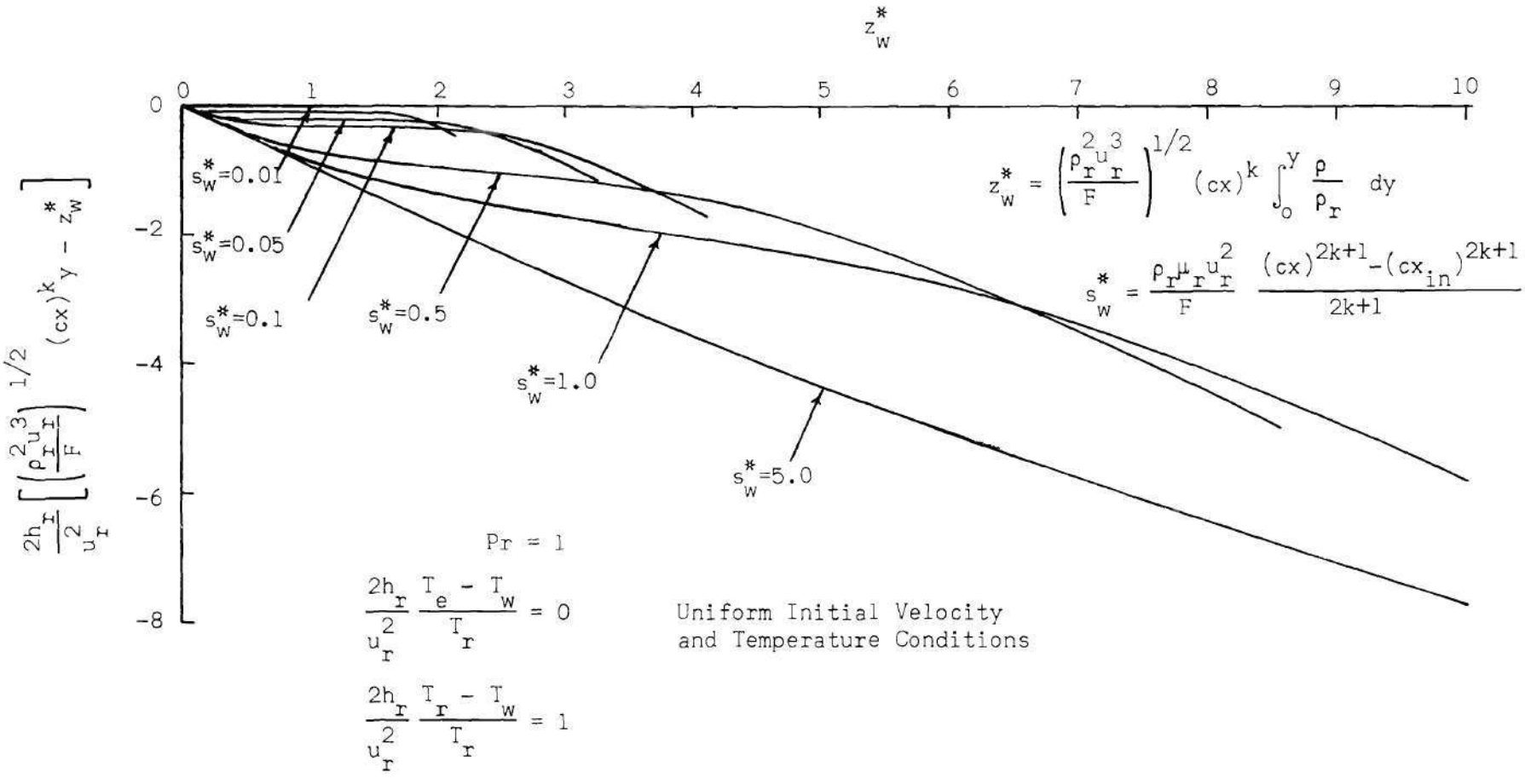

Figure 29. Normal Distance Parameter for the Compressible Wall Jet at Several Locations Downstream, $T_e = T_w$, $T_r \neq T_w$.

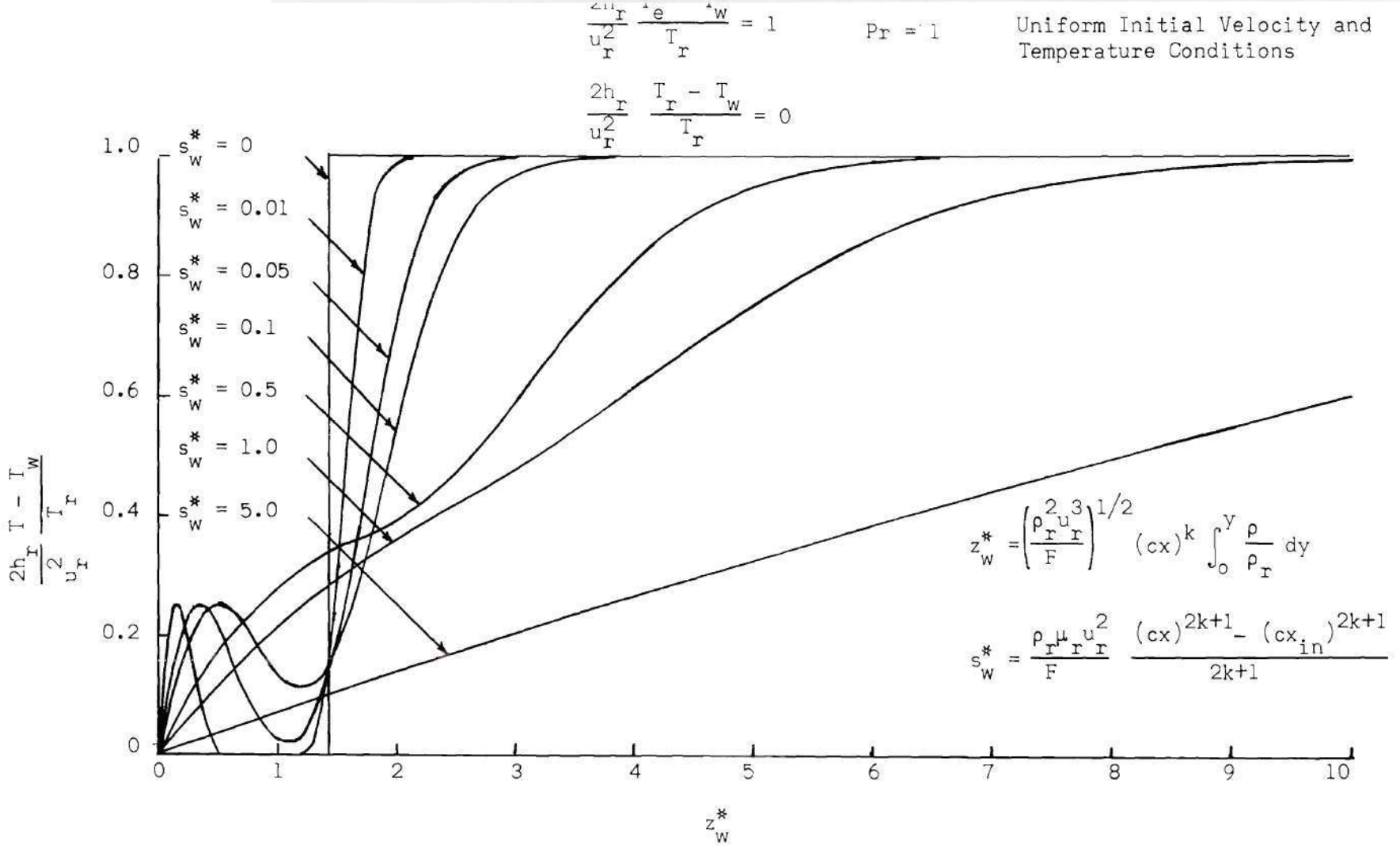

Figure 30. Temperature Distributions for the Compressible Wall Jet at Several Locations Downstream, $T_e \neq T_w$, $T_r = T_w$.

Uniform Initial Velocity and Temperature Conditions

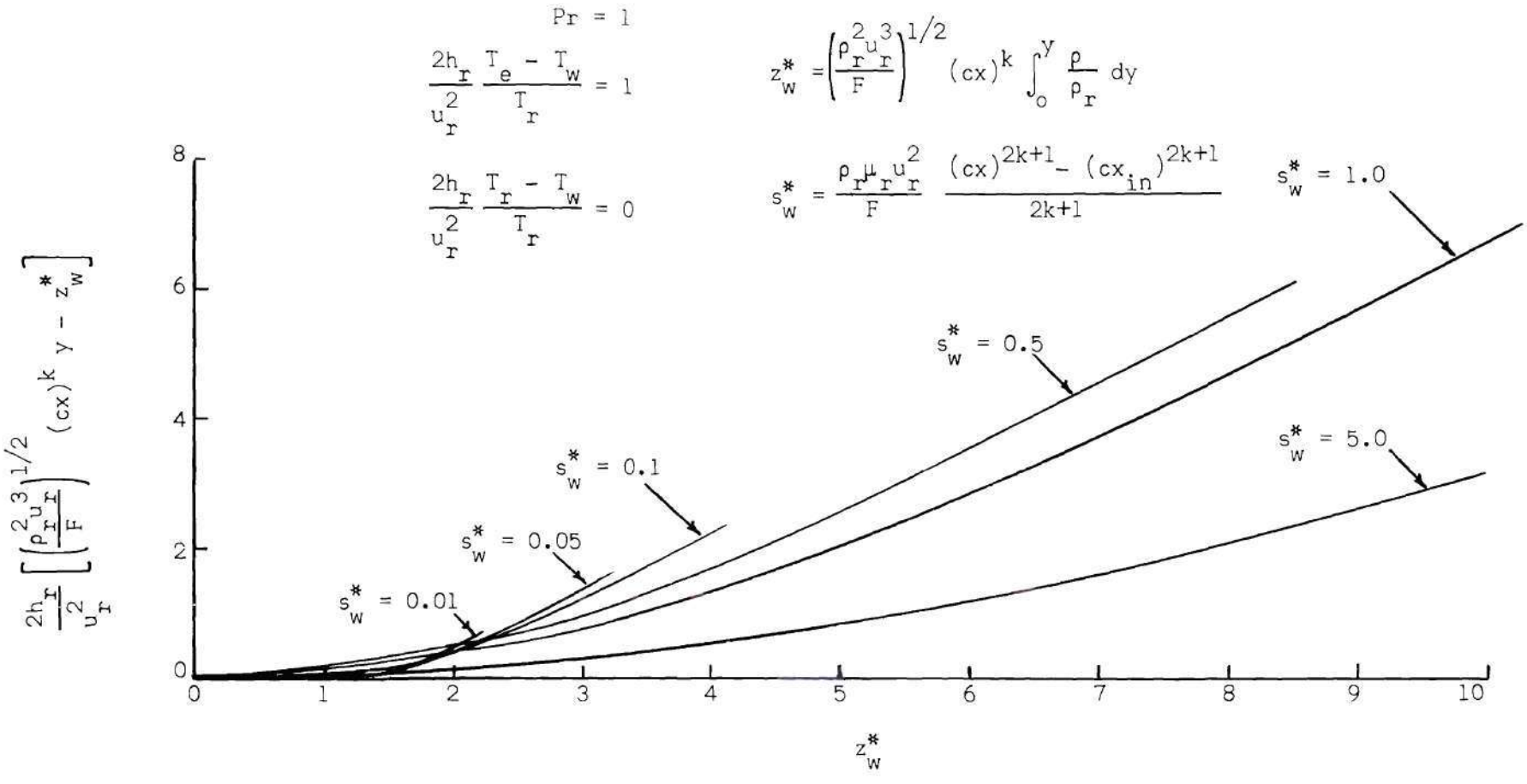

Figure 31. Normal Distance Parameter for the Compressible Wall Jet at Several Locations Downstream, $T_e \neq T_w$, $T_r = T_w$.

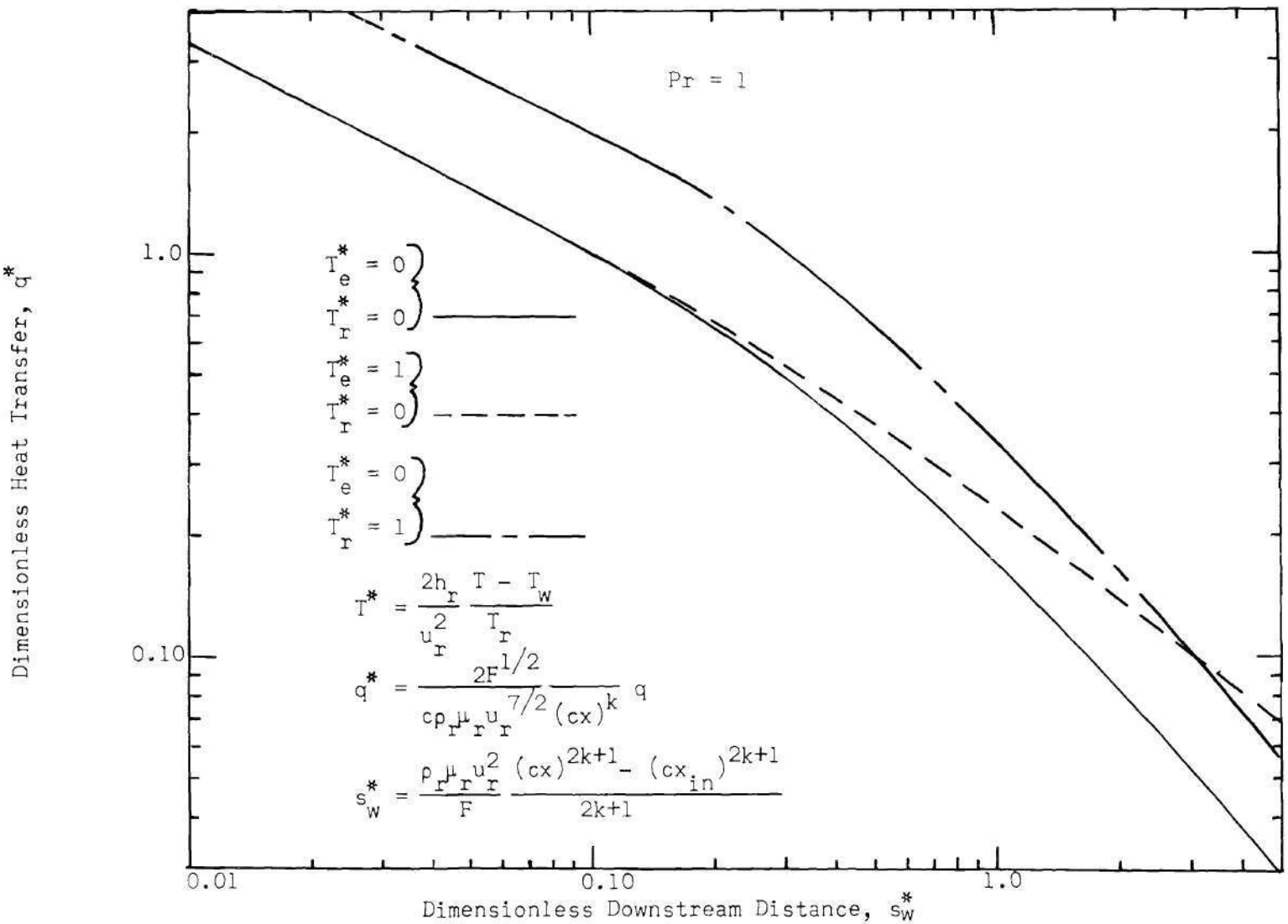

Figure 32. Heat Transfer Distributions for Wall Jets With Various External Fluid and Wall Conditions.

the case of a hot wall and a cold external fluid such that

$$T_r^* = -2$$

$$T_e^* = -1/4$$

is expressed as

$$\begin{Bmatrix} -1/4 \\ -2 \end{Bmatrix} = \begin{Bmatrix} 0 \\ 0 \end{Bmatrix} + (-2)\left(\begin{Bmatrix} 0 \\ 1 \end{Bmatrix} - \begin{Bmatrix} 0 \\ 0 \end{Bmatrix} \right) + (-1/4)\left(\begin{Bmatrix} 1 \\ 0 \end{Bmatrix} - \begin{Bmatrix} 0 \\ 0 \end{Bmatrix} \right)$$

The first term on the right hand side of this equation expresses the effect of the viscous dissipation on the temperature distribution, and the second and third terms express the effects of the wall temperature and the external fluid temperature, respectively, on the temperature distribution. Also, as in the case of the free jet, the transformation to the physical co-ordinates is linear in temperature and, therefore, the physical co-ordinates of the other solutions are obtained by adding the physical co-ordinates of the known solutions in the same way that the temperature solutions are added. The heat transfer characteristics of other solutions are obtained in the same way.

Approximate Solution

The approximate solution of the momentum equation for the wall jet is divided into two downstream regions in the same manner as in the case of the free jet. The region from the initial condition to the point downstream at which the maximum velocity of the jet begins to decay is termed region (I), and the region from that point on downstream is termed region (II).

The approximate solution of the wall jet in dimensionless form

for region (I) is

$$x^* > 0.0328$$

$$\frac{\delta_a}{d} = \delta_a^* = 4.64x^{*1/2}$$

$$\frac{\delta_b}{d} = \delta_b^* = 8.518x^{*1/2}$$

$$\frac{\delta}{d} = \delta^* = 1 - 3.164x^{*1/2}$$

$$\text{for } z^* \leq \delta_a^* \quad \text{then } u^* = 3/2\left(\frac{z^*}{\delta_a^*}\right) - 1/2\left(\frac{z^*}{\delta_a^*}\right)^3$$

$$\text{for } \delta_a^* < z^* \leq \delta^* \quad \text{then } u^* = 1$$

$$\text{for } z^* > \delta^* \quad \text{then } u^* = 2\left(\frac{z^* - \delta^*}{\delta_b^*}\right)^3 - 3\left(\frac{z^* - \delta^*}{\delta_b}\right)^2 + 1$$

and for region (II), is the numerical solution of the equations

$$u^*_{max}\frac{d\delta_a^{*2}}{ds^*} = 29.7446\left\{\frac{0.04118 + \frac{4.78506}{u^{*3}_{max}\delta_a^{*2}} - \sqrt{0.028358 + \frac{13.1811}{u^{*3}_{max}\delta_a^{*2}}}}{0.12758 + \frac{6.60608}{u^{*3}_{max}\delta_a^{*2}} - \sqrt{0.028358 + \frac{13.1811}{u^{*3}_{max}\delta_a^{*2}}}}\right\}$$

$$\delta_a^{*2}\frac{du^*_{max}}{ds^*} = 0.2010\, u^*_{max}\frac{d\delta_a^{*2}}{ds^*} - 4.330$$

$$\delta_b^* = \delta_a^* \left[-1.530 + \sqrt{0.028358 + \frac{13.1811}{u_{max}^{*3} \delta_a^{*2}}} \right]$$

for the unknowns δ_a^*, δ_b^*, and u_{max}^*, with

$$u^* = 3/2 \left(\frac{z^*}{\delta_a^*} \right) - 1/2 \left(\frac{z^*}{\delta_a^*} \right)^3$$

for $z^* \leq \delta_a^*$ and

$$u^* = 2 \left(\frac{z^* - \delta_a^*}{\delta_b^*} \right)^3 - 3 \left(\frac{z^* - \delta_a^*}{\delta_b^*} \right)^2 + 1$$

for $z^* > \delta_a^*$

A comparison of the velocity distribution of this solution with the velocity distribution of the exact solution is presented in Figure 33. As was the case with the approximate solution for the free jet, the maximum velocity compares well with the exact solution, but the layer thickness does not compare as well. The approximate and the exact wall shear, presented in Figure 34, compare well.

Experiment

A comparison of the exact solution of the momentum equation with the experimentally measured wall jet velocity distributions is presented in Figure 35. The measured condition at the nozzle exit plane was used as the initial condition of the theory, and comparisons are made at downstream locations of three, six, and nine inches. The comparisons of theory and experiment are very good for the first two locations. At

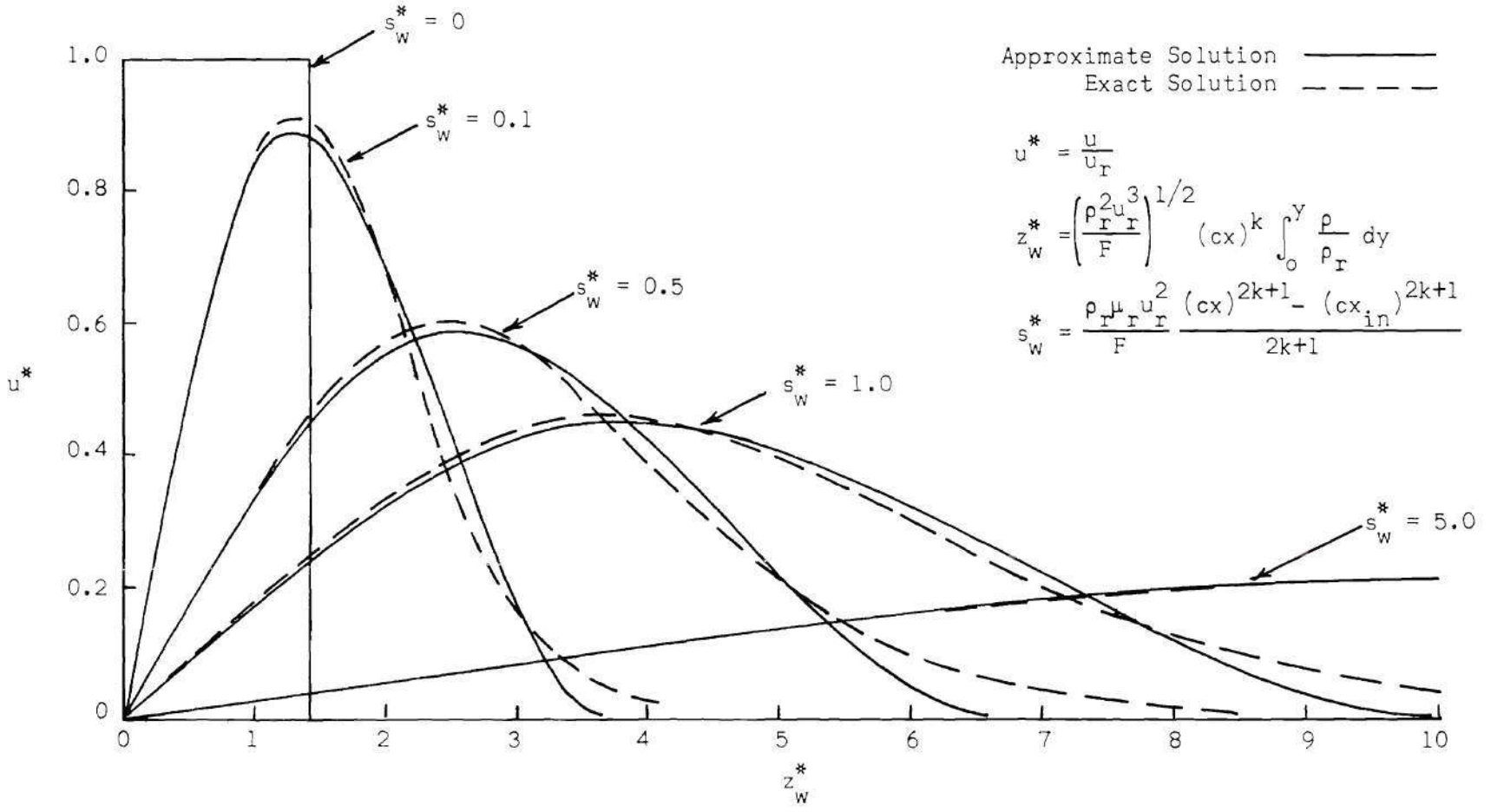

Figure 33. A Comparison of the Approximate and the Exact Velocity Distributions for the Wall Jet at Several Locations Downstream, Uniform Initial Velocity Condition.

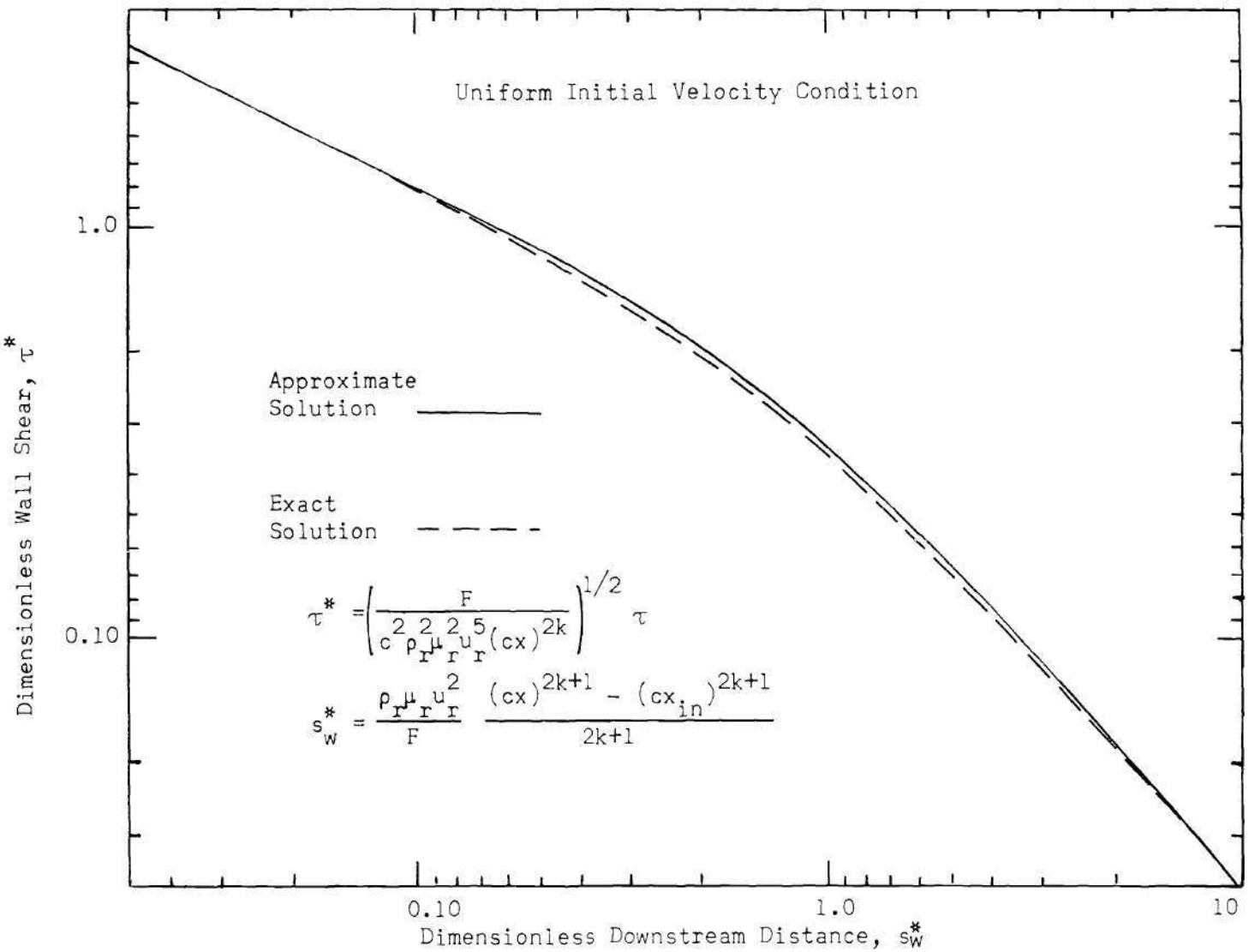

Figure 34. A Comparison of the Approximate and the Exact Wall Shear Distributions for the Wall Jet, Uniform Initial Velocity Condition.

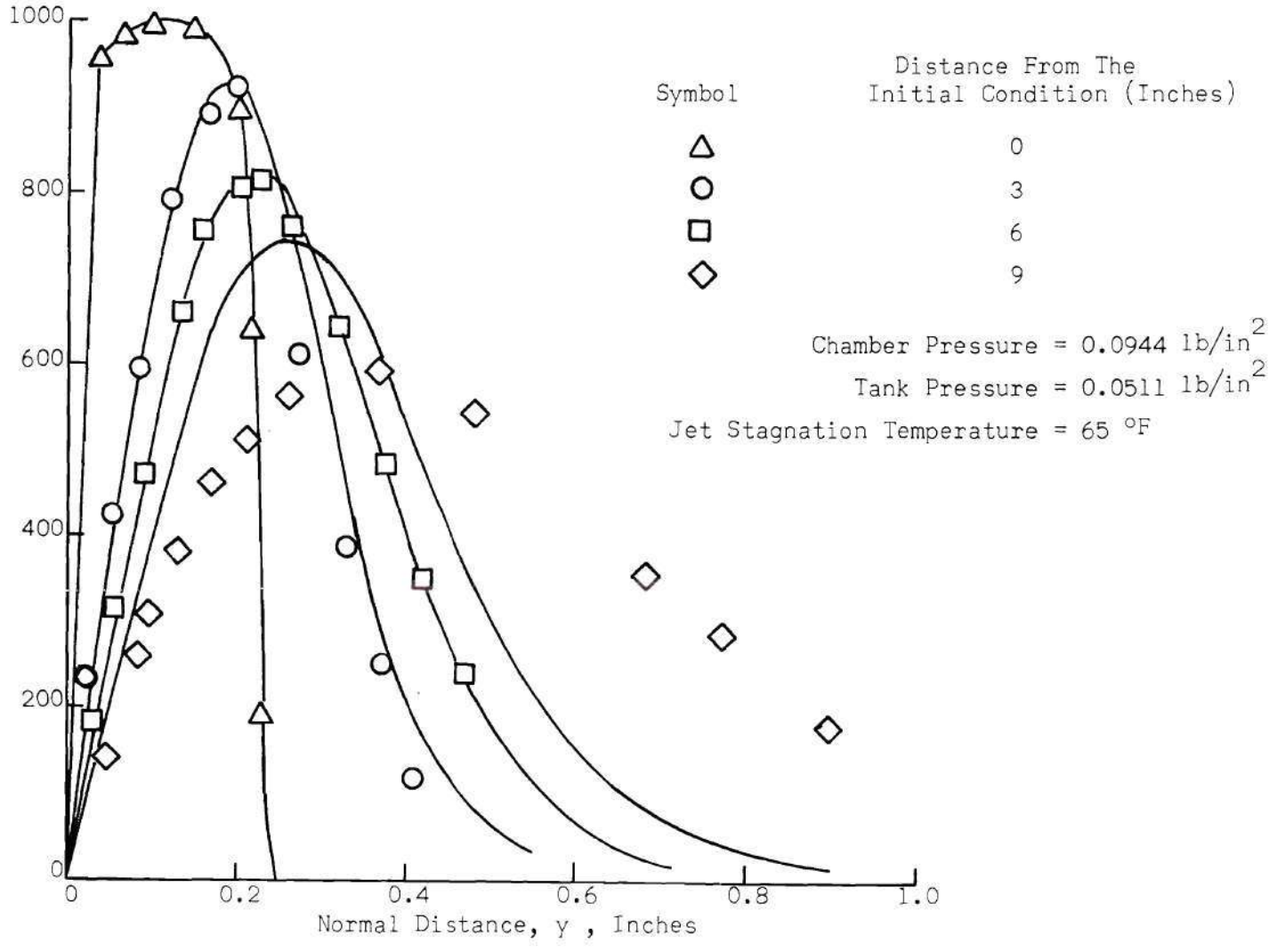

Figure 35. A Comparison of the Experimentally Measured Velocity Distribution With the Exact Theory.

the third location, however, the viscous layer is considerably thicker, and the velocity decay greater, than that predicted by the theory. The failure of the theory to continue to predict the experimental jet further downstream may be attributed to a breakdown of the two-dimensional jet into a three-dimensional jet due to the boundary layer development along the side walls, to the transition of the jet from a laminar wall jet to a turbulent wall jet, or to both. An estimation of the boundary layer development along the side walls indicates that nine inches from the initial condition this effect has influenced only about a quarter of the total width of the jet. Further, decay of the jet due to boundary layer development on the side walls fails to explain the sudden increase in the thickness of the measured viscous layer over that expected from the theory. It is concluded then, that the failure of the theory to predict the development of the wall jet further downstream is due to the transition of the laminar wall jet to a turbulent wall jet.

Figure 36 compares the maximum velocity of the jet from the exact theory with the measured values for various locations downstream. The early portion of the jet is laminar. However, as the jet becomes turbulent, it breaks away quickly from the laminar theory. The approximate location of transition for the wall jet of Figure 36 is about seven inches from the nozzle exit plane. A similar experiment for the free jet failed because the Reynolds number required to achieve a laminar free jet of air into air was too low to allow accurate measurements with the equipment available. Andrade, however, measured free jets of water into water and demonstrates the Reynolds number of transition to be about 30 based on the initial velocity and height of the jet (17). His

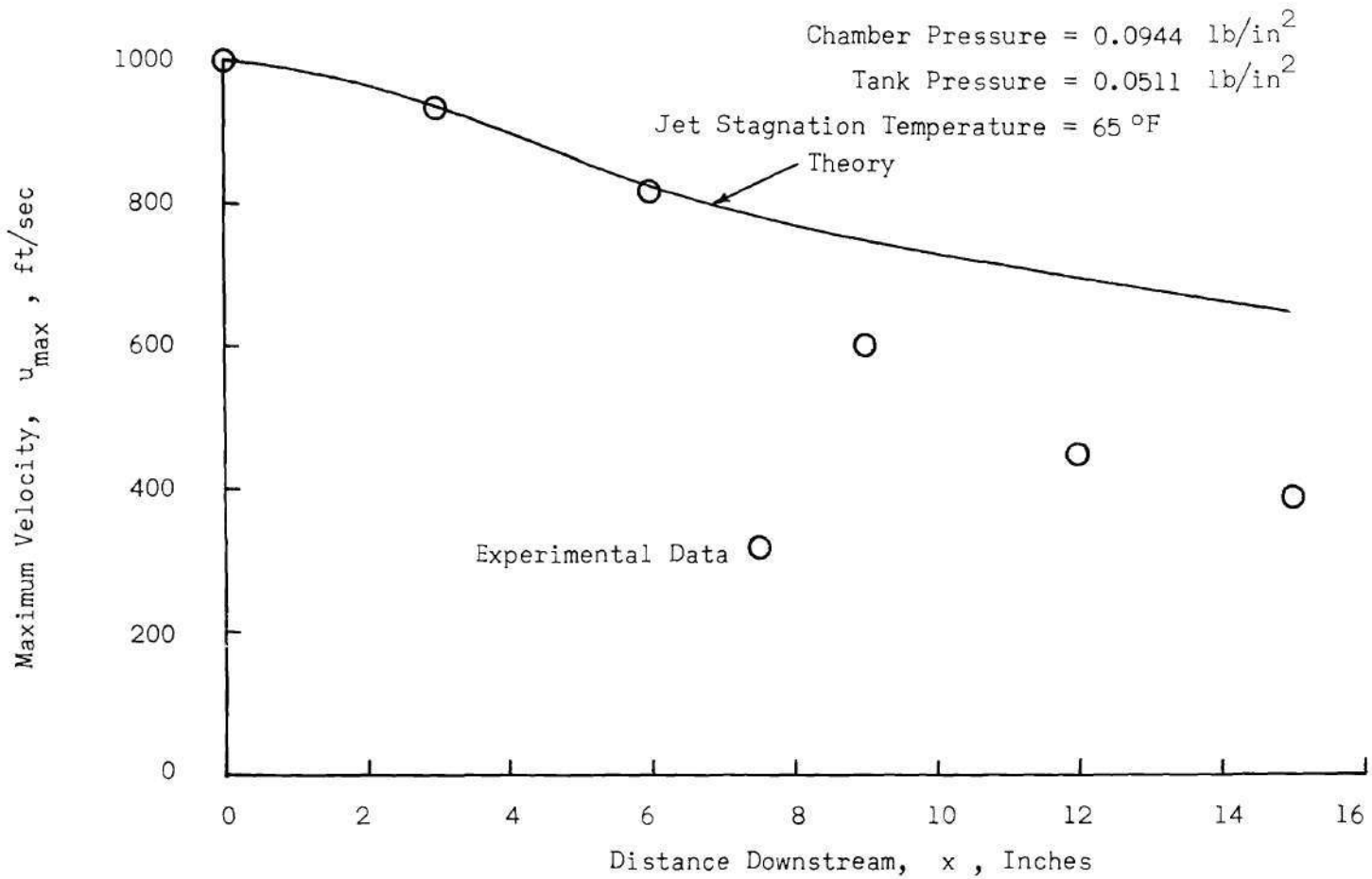

Figure 36. A Comparison of the Experimentally Measured Maximum Velocity Distribution With the Exact Theory.

work shows, further, that there is a small range of Reynolds numbers between fully laminar and fully turbulent free jets.

The Reynolds number of the wall jet studied was 450 based on the initial velocity and height of the jet. This jet was laminar over part of the downstream development region, whereas a laminar free jet at this Reynolds number could not be achieved. Therefore, the wall contributes appreciably to the stability of the wall jet. The Reynolds number of transition based on the initial velocity of the jet and the downstream distance to transition is about 12,600. A low value of the transition Reynolds number for the boundary layer is 300,000, so the finite dimension of the jet flow causes a loss of stability as compared to the infinite flow field of the boundary layer. The Reynolds numbers of transition for the wall jet are an order of magnitude above that for the free jet and an order of magnitude below that for the boundary layer.

CHAPTER V

CONCLUSIONS AND RECOMMENDATIONS

Theory

Under the assumptions of the theory, the momentum and energy equations for the two-dimensional (compressible and incompressible) and radial (compressible and incompressible) free jets and wall jets are transformed into a single set of two equations for the dimensionless longitudinal component of velocity and the dimensionless temperature. Since the transformed momentum equation is independent of the transformed energy equation then it can be solved first and the results used to solve the energy equation. The energy equation is linear in temperature, so solutions of this equation for various boundary conditions can be added to obtain new solutions.

Numerical solutions of the momentum equation are used to determine the velocity distributions in the development region of both free jets and wall jets. These results compare well with the asymptotic solutions far downstream of the initial condition. Further, this comparison indicates that the asymptotic solutions are good approximations to the exact solutions only after the maximum velocities of the jets have decayed to about one half of their original values for the free jets, and one third of their original values for the wall jets. The results for free jets and wall jets show that the solutions for the uniform initial velocity distribution are better approximations to the solutions for other initial velocity distributions than are the asymptotic solutions.

Further, it is argued that this will generally be the case regardless of the initial conditions of the jets. A comparison of the wall shear in the development region of the wall jet for several initial conditions yields a good correlation of the wall shear for a wide range of jet initial conditions.

An approximate integral solution for the free jet and the wall jet with a uniform initial velocity distribution results in a closed form solution for the free jet and a simple numerical solution for the wall jet. The integrals used are the integral momentum equation and the F relation of Glauert. These solutions predict the maximum velocity and general shape of the velocity distributions well but do not predict the thickness of the viscous layer as well. The wall shear for the wall jet predicted by this method is very close to the exact solution.

A possible extension of the solution of the energy equation is to include the effect of the Prandtl number different from unity (i.e., in particular for the Prandtl number of air). If, as for air, the Prandtl number is less than unity, however, then the thermal influence extends further into the external fluid than the velocity influence. That is, the change in the velocity at the outer edge of the viscous layer approaches zero faster than the change in temperature. Since the momentum approaches zero as the velocity, then $\left(\frac{\partial \theta^*}{\partial M^*}\Big|_{s_w^*}\right)_{z^* \to \infty} \longrightarrow \infty$, and thus the numerical approach in momentum co-ordinates, as used here, fails at the outer edge of the layer. This extension of the solution requires another approach to treat the outer edge of the layer.

Laminar free jets and wall jets occur less frequently in practice

than the corresponding turbulent jets since they become unstable at such low Reynolds numbers. Therefore, it is recommended that the theory presented herein be extended to obtain solutions for the turbulent jets.

Experiment

The theoretical results from the exact solution for the wall jet compare well with the experimentally measured velocity distributions until the jet becomes turbulent. Transition was observed approximately seven inches from the initial condition. The transition Reynolds number was 450 based on the initial jet width and 12,600 based on the distance downstream from the initial condition. These transition Reynolds numbers are an order of magnitude greater than that for the free jet and less than that for the boundary layer. The transition from laminar to turbulent flow occurs over a short longitudinal distance and is quite distinct.

There are two characteristic dimensions to consider regarding transition for the wall jet. These are the thickness of the initial jet and the longitudinal distance the jet has proceeded downstream. In order to understand the influence of these two dimensions consider the transition characteristics of two wall jets with uniform initial velocity distributions and identical flow conditions. One of the jets, termed the thin jet, has a much thinner initial velocity distribution than the other jet, termed the thick jet. Transition for the thin jet will occur at some position downstream after the maximum velocity of the jet has decayed from its initial value. An example of this case is the wall jet generated experimentally in this study. Now consider the transition characteristics of the thick jet. As the flow proceeds downstream the flow next to the wall would be boundary layer flow initially, and the flow at the exterior

fluid would be free layer flow initially. If the initial velocity distribution of this jet is thick enough, then transition from laminar to turbulent flow will occur for the boundary layer and free layer portions of the jet before the maximum velocity of the jet has decayed at all from its initial value. The velocity distribution of the wall jet at transition, then, can vary considerably depending on the thickness of the jet. Therefore, the thickness of the jet, as well as the distance from the initial condition, are parameters affecting transition. Further experiments with jets with various thicknesses would be of interest to study the effect of these two dimensions on the transition of the wall jet from laminar to turbulent flow.

APPENDIX A

CO-ORDINATE TRANSFORMATIONS

A Transformation of the Equations of Compressible Flow to the Equations of Incompressible Flow

The equations for compressible flow are

$$\rho u \left.\frac{\partial u}{\partial x}\right|_y + \rho v \left.\frac{\partial u}{\partial y}\right|_x = \left.\frac{\partial}{\partial y}\left(\mu \left.\frac{\partial u}{\partial y}\right|_x\right)\right|_x \tag{A.1}$$

$$\rho u \left.\frac{\partial T}{\partial x}\right|_y + \rho v \left.\frac{\partial T}{\partial y}\right|_x = \left.\frac{\partial}{\partial y}\left(\mu \left.\frac{\partial T}{\partial y}\right|_x\right)\right|_x + \frac{\mu}{c_p}\left(\left.\frac{\partial u}{\partial y}\right|_x\right)^2 \tag{A.2}$$

$$\left.\frac{\partial(\rho u x^k)}{\partial x}\right|_y + \left.\frac{\partial(\rho v x^k)}{\partial y}\right|_x = 0 \tag{A.3}$$

$$\rho T = \rho_r T_r \tag{A.4}$$

$$\frac{\mu}{T} = c\,\frac{\mu_r}{T_r} \tag{A.5}$$

These equations are transformed from the physical co-ordinates, x and y, to a new set of co-ordinates, X and Y, with

$$X = cx \tag{A.6}$$

$$Y = \int_o^y \frac{\rho}{\rho_r}\,dy \tag{A.7}$$

The transformation formulas for the first derivatives are

$$\left.\frac{\partial}{\partial x}\right|_y = c \left.\frac{\partial}{dX}\right|_Y + \frac{1}{\rho_r} \left(\int_o^Y \left.\frac{\partial \rho}{\partial x}\right|_y dy\right) \left.\frac{\partial}{\partial Y}\right|_X \tag{A.8}$$

$$\left.\frac{\partial}{\partial y}\right|_x = \frac{\rho}{\rho_r} \left.\frac{\partial}{\partial Y}\right|_X \tag{A.9}$$

Using equations (A.8) and (A.9) in equations (A.1) and (A.2) yields

$$c\rho_r u \left.\frac{\partial u}{\partial X}\right|_Y + (pv + u \int_o^Y \left.\frac{\partial \rho}{\partial x}\right|_y dy) \left.\frac{\partial u}{\partial Y}\right|_X = \left.\frac{\partial}{\partial Y}\left(\frac{\rho\mu}{\rho_r} \left.\frac{\partial u}{\partial Y}\right|_X\right)\right|_X \tag{A.10}$$

$$c\rho_r u \left.\frac{\partial T}{\partial X}\right|_Y + (pv + u \int_o^Y \left.\frac{\partial \rho}{\partial x}\right|_y dy) \left.\frac{\partial T}{\partial Y}\right|_X = \left.\frac{\partial}{\partial Y}\left(\frac{\rho\mu}{\rho_r} \left.\frac{\partial T}{\partial Y}\right|_X\right)\right|_X \tag{A.11}$$

$$+ \frac{\rho\mu}{\rho_r c_p} \left(\left.\frac{\partial u}{\partial Y}\right|_X\right)^2$$

Equation (A.3) is expressed as

$$ux^k \left.\frac{\partial \rho}{\partial x}\right|_y + \rho \left.\frac{\partial (ux^k)}{\partial x}\right|_y + \left.\frac{\partial (\rho v x^k)}{\partial y}\right|_x = 0$$

Integrating this equation with respect to y with $u = 0$ at $y = 0$ yields

$$\rho v + \int_o^Y u \left.\frac{\partial \rho}{\partial x}\right|_y dy = -\frac{1}{x^k} \int_o^Y \rho \left.\frac{\partial (ux^k)}{\partial x}\right|_y dy$$

Integrating the second term in this equation by parts yields

$$\rho v + u \int_o^Y \frac{\partial \rho}{\partial x}\Big|_y \, dy = - \int_o^Y \left(\frac{\rho}{x^k} \frac{\partial (ux^k)}{\partial x}\Big|_y - \int_o^Y \frac{\partial \rho}{\partial x}\Big|_y \, dy \, \frac{\partial u}{\partial y}\Big|_x \right) dy$$

which through equation (A.9) is expressed as

$$\rho v + u \int_o^Y \frac{\partial \rho}{\partial x}\Big|_y \, dy = - \frac{\rho_r}{X^k} \int_o^Y \left(\frac{\partial (uX^k)}{\partial x}\Big|_y \right.$$

$$\left. - \frac{1}{\rho_r} \int_o^Y \frac{\partial \rho}{\partial x}\Big|_y \, dy \, \frac{\partial (uX^k)}{\partial Y}\Big|_X \right) dY$$

From equation (A.8), the integrand of the right hand side of this equation is

$$\frac{\partial (uX^k)}{\partial x}\Big|_y - \frac{1}{\rho_r} \int_o^Y \frac{\partial \rho}{\partial x}\Big|_y \, dy \, \frac{\partial (uX^k)}{\partial Y}\Big|_X = c \, \frac{\partial (uX^k)}{\partial X}\Big|_Y$$

so that

$$\rho v + u \int_o^Y \frac{\partial \rho}{\partial x}\Big|_y dy = - \frac{c\rho_r}{X^k} \int_o^Y \frac{\partial (uX^k)}{\partial X}\Big|_Y \, dY \qquad \text{(A.12)}$$

Introducing equation (A.12) in equations (A.10) and (A.11) yields

$$c\rho_r u \frac{\partial u}{\partial X}\Big|_Y - \frac{c\rho_r}{X^k} \left(\int_o^Y \frac{\partial (uX^k)}{\partial X}\Big|_Y \, dY \right) \frac{\partial u}{\partial Y}\Big|_X = \qquad \text{(A.13)}$$

$$\frac{\partial}{\partial Y} \left(\frac{\rho \mu}{\rho_r} \frac{\partial u}{\partial Y}\Big|_X \right)\Big|_X$$

$$c\rho_r u \left.\frac{\partial T}{\partial X}\right|_Y - \frac{c\rho_r}{X^k}\left(\int_o^Y \left.\frac{\partial(uX^k)}{\partial X}\right|_Y dY\right)\left.\frac{\partial T}{\partial Y}\right|_X = \tag{A.14}$$

$$\frac{\partial}{\partial Y}\left(\frac{\rho\mu}{\rho_r}\left.\frac{\partial T}{\partial Y}\right|_X\right)\Bigg|_X + \frac{\rho\mu}{\rho_r c_p}\left(\left.\frac{\partial u}{\partial Y}\right|_X\right)^2$$

Equations (A.4) and (A.5) may be combined to obtain

$$\rho\mu = c\rho_r\mu_r$$

Using this expression in equations (A.13) and (A.14) yields

$$u \left.\frac{\partial u}{\partial X}\right|_Y - \frac{1}{X^k}\left(\int_o^Y \left.\frac{\partial(uX^k)}{\partial X}\right|_Y dY\right)\left.\frac{\partial u}{\partial Y}\right|_X = \frac{\mu_r}{\rho_r}\left.\frac{\partial^2 u}{\partial Y^2}\right|_X \tag{A.15}$$

$$u \left.\frac{\partial T}{\partial X}\right|_Y - \frac{1}{X^k}\left(\int_o^Y \left.\frac{\partial(uX^k)}{\partial X}\right|_Y dY\right)\left.\frac{\partial T}{\partial Y}\right|_X = \frac{\mu_r}{\rho_r}\left.\frac{\partial^2 T}{\partial Y^2}\right|_X + \frac{\mu_r}{\rho_r c_p}\left(\left.\frac{\partial u}{\partial Y}\right|_X\right)^2 \tag{A.16}$$

Equation (A.15) is the expression for an incompressible flow of constant viscosity, where X and Y are the physical co-ordinates of the system. This equation can be solved independently for $u(X,Y)$. Equation (A.16) can then be solved to obtain the solutions of the compressible flow problem. This solution is then used in equations (A.6) and (A.7) to obtain the physical co-ordinates of compressible flow.

A Transformation of the Equations of Radial Flow to the Equations of Two-dimensional Flow

If $\tilde{v}$ is defined as

$$\tilde{v} = -\frac{1}{X^k} \int_0^Y \left.\frac{\partial (uX^k)}{\partial X}\right|_Y dY \qquad (A.17)$$

then equations (A.15) and (A.16) are expressed as

$$u \left.\frac{\partial u}{\partial X}\right|_Y + \tilde{v} \left.\frac{\partial u}{\partial Y}\right|_X = \frac{\mu_r}{\rho_r} \left.\frac{\partial^2 u}{\partial Y^2}\right|_X \qquad (A.18)$$

$$u \left.\frac{\partial T}{\partial X}\right|_Y + \tilde{v} \left.\frac{\partial T}{\partial Y}\right|_X = \frac{\mu_r}{\rho_r} \left.\frac{\partial^2 T}{\partial Y^2}\right|_X + \frac{\mu_r}{\rho_r c_\rho} \left(\left.\frac{\partial u}{\partial Y}\right|_X\right)^2 \qquad (A.19)$$

Differentiating equation (A.17) with respect to Y yields

$$\left.\frac{\partial (uX^k)}{\partial X}\right|_Y + \left.\frac{\partial (\tilde{v}X^k)}{\partial Y}\right|_X = 0 \qquad (A.20)$$

where $k = 0$ is for two-dimensional flow, and $k = 1$ is for radial flow. Now let

$$s = \frac{X^{2k+1} - X_{in}^{2k+1}}{2k+1} \qquad (A.21)$$

$$z = X^k Y \qquad (A.22)$$

be the transformed independent variables, where X_{in} is the location of the initial condition in the incompressible co-ordinate. Then the transformation formulas for the first derivatives are

$$\left.\frac{\partial}{\partial X}\right|_Y = X^{2k} \left.\frac{\partial}{\partial s}\right|_z + kX^{k-1}Y \left.\frac{\partial}{\partial z}\right|_s$$

$$\left.\frac{\partial}{\partial Y}\right|_X = X^k \left.\frac{\partial}{\partial z}\right|_s$$

Applying this transformation to equations (A.18), (A.19), and (A.20) and dividing through by X^{2k} yields

$$u\left.\frac{\partial u}{\partial s}\right|_z + \left(\frac{\tilde{v}}{X^k} + \frac{kY}{X^{k+1}}\,u\right)\left.\frac{\partial u}{\partial z}\right|_s = \frac{\mu_r}{\rho_r}\left.\frac{\partial^2 u}{\partial z^2}\right|_s \qquad (A.23)$$

$$u\left.\frac{\partial T}{\partial s}\right|_z + \left(\frac{\tilde{v}}{X^k} + \frac{kY}{X^{k+1}}\,u\right)\left.\frac{\partial T}{\partial z}\right|_s = \frac{\mu_r}{\rho_r}\left.\frac{\partial^2 T}{\partial z^2}\right|_s + \frac{\mu_r}{\rho_r c_p}\left(\left.\frac{\partial u}{\partial z}\right|_s\right)^2 \qquad (A.24)$$

$$\frac{1}{X^k}\left.\frac{\partial \tilde{v}}{\partial z}\right|_s + \frac{kY}{X^{k+1}}\left.\frac{\partial u}{\partial z}\right|_s + \frac{ku}{X^{2k+1}} = -\left.\frac{\partial u}{\partial s}\right|_z \qquad (A.25)$$

The second and third terms of equation (A.25) are combined to yield

$$\frac{kY}{X^{k+1}}\left.\frac{\partial u}{\partial z}\right|_s + \frac{ku}{X^{2k+1}} = \frac{k}{X^{2k+1}}\left(z\left.\frac{\partial u}{\partial z}\right|_s + u\right) = \frac{k}{X^{2k+1}}\left.\frac{\partial (zu)}{\partial z}\right|_s$$

Introducing this into equation (A.25) and integrating with respect to z yields

$$\frac{\tilde{v}}{X^k} + \frac{kY}{X^{k+1}}\,u = -\int_o^z \left.\frac{\partial u}{\partial s}\right|_z dz \qquad (A.26)$$

Using equation (A.26) in equations (A.23) and (A.24) yields

$$u\left.\frac{\partial u}{\partial s}\right|_z - \left(\int_o^z \left.\frac{\partial u}{\partial s}\right|_z dz\right)\left.\frac{\partial u}{\partial z}\right|_s = \frac{\mu_r}{\rho_r}\left.\frac{\partial^2 u}{\partial z^2}\right|_s \qquad (A.27)$$

$$u \left.\frac{\partial T}{\partial s}\right|_z - \left(\int_o^z \left.\frac{\partial u}{\partial s}\right|_z dz \right) \left.\frac{\partial T}{\partial z}\right|_s = \frac{\mu_r}{\rho_r} \left.\frac{\partial^2 T}{\partial z^2}\right|_s + \frac{\mu_r}{\rho_r c_p} \left(\left.\frac{\partial u}{\partial z}\right|_s \right)^2 \tag{A.28}$$

A comparison of these equations with equations (A.15) and (A.16)with k=0 shows that (A.27) and (A.28) are the equations of two-dimensional flow with X and Y replaced by s and z . Radial flow results are therefore obtained from the two-dimensional flow results through the transformation equations (A.21) and (A.22).

The Transformation to

Momentum Co-ordinates

A transformation to momentum co-ordinates is applied to equations (A.27) and (A.28) with

$$M^* = \frac{\rho_r}{M_o} \int_o^z u^2 dz \tag{A.29}$$

where

$$M_o = \rho_r \int_o^\infty u^2 dz \tag{A.30}$$

is the total momentum at any s station downstream. The transformation formulas for the first derivatives are

$$\left.\frac{\partial}{\partial s}\right|_z = \left.\frac{\partial}{\partial s}\right|_M + \left.\frac{\partial M^*}{\partial s}\right|_z \left.\frac{\partial}{\partial M}\right|_s \tag{A.31}$$

$$\left.\frac{\partial}{\partial z}\right|_s = \left.\frac{\partial M^*}{\partial z}\right|_s \left.\frac{\partial}{\partial M}\right|_s \tag{A.32}$$

From equation (A.29)

$$\left.\frac{\partial M^*}{\partial z}\right|_s = \frac{\rho_r}{M_o} u^2 \qquad (A.33)$$

and

$$\left.\frac{\partial M^*}{\partial s}\right|_z = \frac{\rho_r}{M_o}\left[\int_o^z u \left.\frac{\partial u}{\partial s}\right|_z dz + \int_o^z u \left.\frac{\partial u}{\partial s}\right|_z dz - \frac{M^*}{\rho_r}\frac{dM_o}{ds}\right]$$

Integrating the third term of this expression by parts, and combining this with the second term yields

$$\left.\frac{\partial M^*}{\partial s}\right|_z = \frac{\rho_r}{M_o}\left\{u\int_o^z \left.\frac{\partial u}{\partial s}\right|_z dz + \int_o^z \left[u \left.\frac{\partial u}{\partial s}\right|_z - \left(\int_o^z \left.\frac{\partial u}{\partial s}\right|_z dz\right)\left.\frac{\partial u}{\partial z}\right|_s\right] dz - \frac{M^*}{\rho_r}\frac{dM_o}{ds}\right\}$$

The integrand of the second term on the right hand side of this equation is, from equation (A.17),

$$\left.\frac{\mu_r}{\rho_r}\frac{\partial^2 u}{\partial z^2}\right|_s$$

This expression is then integrated to yield

$$\left.\frac{\partial M^*}{\partial s}\right|_z = \frac{\rho_r}{M_o}\left[u\int_o^z \left.\frac{\partial u}{\partial s}\right|_z dz + \frac{\mu_r}{\rho_r}\left.\frac{\partial u}{\partial z}\right|_s - \frac{\mu_r}{\rho_r}\left(\left.\frac{\partial u}{\partial z}\right|_s\right)_{z=0} - \frac{M^*}{\rho_r}\frac{dM_o}{ds}\right] \qquad (A.34)$$

From equation (A.30),

$$\frac{dM_o}{ds} = \rho_r \int_o^\infty u \left.\frac{\partial u}{\partial s}\right|_z dz + \rho_r \int_o^\infty u \left.\frac{\partial u}{\partial s}\right|_z dz$$

After integrating the last term by parts and using $u=0$ as $y \to \infty$, this expression becomes

$$\frac{dM_o}{ds} = \rho_r \int_o^\infty \left[u \left.\frac{\partial u}{\partial s}\right|_z - \left(\int_o^z \left.\frac{\partial u}{\partial s}\right|_z dz \right) \left.\frac{\partial u}{\partial z}\right|_s \right] dz$$

Again, using equation (A.27), the integral may be evaluated to yield

$$\frac{dM_o}{ds} = \mu_r \left(\left.\frac{\partial u}{\partial z}\right|_s \right)_{z \to \infty} - \mu_r \left(\left.\frac{\partial u}{\partial z}\right|_s \right)_{z=0}$$

Since the flows of this study involve finite streams of fluid, then

$$\left(\left.\frac{\partial u}{\partial z}\right|_s \right)_{z \to \infty} = 0$$

and

$$\frac{dM_o}{ds} = - \mu_r \left(\left.\frac{\partial u}{\partial z}\right|_s \right)_{z=0} \qquad (A.35)$$

Then, combining equations (A.31), (A.32), (A.33), (A.34), and (A.35) yields the following transformation formulas:

$$\left.\frac{\partial}{\partial s}\right|_z = \left.\frac{\partial}{\partial s}\right|_{M^*} + \frac{\rho_r}{M_o}\left\{ u \int_o^z \left.\frac{\partial u}{\partial s}\right|_z dz \right. \tag{A.36}$$

$$\left. + \frac{\mu_r}{M_o}\left[u^2 \left.\frac{\partial u}{\partial M}\right|_s - (1-M^*)\left(u^2 \left.\frac{\partial u}{\partial M}\right|_s\right)_{M=0}\right]\right\} \left.\frac{\partial}{\partial M^*}\right|_s$$

$$\left.\frac{\partial}{\partial z}\right|_s = \frac{\rho_r}{M_o} u^2 \left.\frac{\partial}{\partial M^*}\right|_s \tag{A.37}$$

Applying these equations to equation (A.27) and simplifying yields

$$\frac{M_o^2}{\rho_r \mu_r} u \left.\frac{\partial u}{\partial s}\right|_{M^*} = u^2 \frac{\partial}{\partial M^*}\left(u^2 \left.\frac{\partial u}{\partial M^*}\right)\right|_s + \tag{A.38}$$

$$\left[(1-M^*)\left(u^2 \left.\frac{\partial u}{\partial M^*}\right|_s\right)_{M^*=0} - u^2 \left.\frac{\partial u}{\partial M^*}\right|_s\right] u \left.\frac{\partial u}{\partial M^*}\right|_s$$

Similarly, equations (A.36) and (A.37) applied to equation (A.28) yields

$$\frac{M_o^2}{\rho_r \mu_r} u \left.\frac{\partial T}{\partial s}\right|_{M^*} = u^2 \frac{\partial}{\partial M^*}\left(u^2 \left.\frac{\partial T}{\partial M^*}\right)\right|_s + \left[(1-M)\left(u^2 \left.\frac{\partial u}{\partial M^*}\right|_s\right)_{M^*=0}\right.$$

$$\left. - u^2 \left.\frac{\partial u}{\partial M^*}\right|_s\right] u \left.\frac{\partial T}{\partial M^*}\right|_s + \frac{1}{c_p}\left(u^2 \left.\frac{\partial u}{\partial M^*}\right|_s\right)^2 \tag{A.39}$$

Further, using equation (A.37) in equation (A.35) yields

$$\frac{dM_o}{ds} = \frac{\rho_r \mu_r}{M_o}\left(u^2 \left.\frac{\partial u}{\partial M^*}\right|_s\right)_{M^*=0}$$

This expression is now integrated to obtain

$$M_o^2 = M_{o_{in}}^2 - 2\rho_r\mu_r \int_o^s \left(u^2 \left.\frac{\partial u}{\partial M^*}\right|_s \right)_{M^*=0} ds \qquad (A.40)$$

where $M_{o_{in}}$ is the initial value of the total momentum.

APPENDIX B

INTEGRAL CONSERVATION EQUATIONS

The Conservation of Total Momentum

The momentum and continuity equations in terms of the transformed co-ordinates are expressed as

$$u \frac{\partial u}{\partial s} + v \frac{\partial u}{\partial z} = \frac{\mu_r}{\rho_r} \frac{\partial^2 u}{\partial z^2} \tag{B.1}$$

$$\frac{\partial u}{\partial s} + \frac{\partial v}{\partial z} = 0 \tag{B.2}$$

The first and second terms of equation (B.1) are expressed as

$$u \frac{\partial u}{\partial s} = \frac{\partial u^2}{\partial s} - u \frac{\partial u}{\partial s}$$

and

$$v \frac{\partial u}{\partial z} = \frac{\partial (uv)}{\partial z} - u \frac{\partial v}{\partial z}$$

Equation (B.1) then becomes

$$\frac{\partial u^2}{\partial s} - u \left(\frac{\partial u}{\partial s} + \frac{\partial v}{\partial z} \right) + \frac{\partial (uv)}{\partial z} = \frac{\mu_r}{\rho_r} \frac{\partial^2 u}{\partial z^2} \tag{B.3}$$

The second term in equation (B.3) is zero, from equation (B.2), so then

$$\frac{\partial u^2}{\partial s} = \frac{\mu_r}{\rho_r} \frac{\partial^2 u}{\partial z^2} - \frac{\partial (uv)}{\partial z} \tag{B.4}$$

Integrating this equation with respect to z from $z = 0$ to $z = \infty$ yields

$$\frac{\partial}{\partial s} \int_o^\infty u^2 dz = \frac{\mu_r}{\rho_r} \left[\left(\frac{\partial u}{\partial z} \right)_{z \to \infty} - \left(\frac{\partial u}{\partial z} \right)_{z=0} \right] \tag{B.5}$$

$$- \left[(uv)_{z \to \infty} - (uv)_{z=0} \right]$$

For the finite jet streams of this study,

$$(uv)_{z \to \infty} = \left(\frac{\partial u}{\partial z} \right)_{z \to \infty} = 0$$

Further, the boundary conditions of all the flows considered in this work demand that

$$(uv)_{z=0} = 0$$

so that equation (B.4) becomes

$$\frac{\partial}{\partial s} \int_o^\infty u^2 dz = \frac{-\mu_r}{\rho_r} \left(\frac{\partial u}{\partial z} \right)_{z=0} \tag{B.6}$$

Integrating equation (B.6) with respect to s from the initial condition, downstream yields

$$M_o = M_{o_{in}} - \mu_r \int_o^s \left(\frac{\partial u}{\partial z} \right)_{z=0} ds \tag{B.7}$$

where

$$M_o = \rho_r \int_o^\infty u^2 dz$$

is the total momentum at s , and

$$M_{o_{in}} = \rho_r \left[\int_o^\infty u^2 dz \right]_{s=0}$$

is the total momentum at the initial s .

Since

$$\left(\frac{\partial u}{\partial z} \right)_{z=0} = 0 \qquad (B.8)$$

is a boundary condition of the free jet, then equation (B.7) states that the total momentum is a constant and therefore conserved for every location downstream. Equation (B.8) is not zero for the wall jet, however, since there is a shear force on the wall. Therefore, the total momentum for the wall jet is not conserved.

The Conservation of F

Integration of equation (B.4) from z to infinity and multiplication by u yields

$$u \frac{\partial}{\partial s} \int_z^\infty u^2 dz = u^2 v - \frac{\mu_r}{\rho_r} u \frac{\partial u}{\partial z} \qquad (B.9)$$

Using

$$u \frac{\partial}{\partial s} \int_z^\infty u^2 dz = \frac{\partial}{\partial s} \left(u \int_z^\infty u^2 dz \right) - \left(\int_z^\infty u^2 dz \right) \frac{\partial u}{\partial s}$$

in equation (B.9) and integrating with respect to z from zero to infinity yields

$$\frac{\partial}{\partial s}\int_0^\infty u\int_z^\infty u^2 dz\,dz = \int_0^\infty \frac{\partial u}{\partial s}\left(\int_z^\infty u^2 dz\right)dz + \int_0^\infty u^2 v dz - \frac{1}{2}\frac{\mu_r}{\rho_r}(u^2)_{z=0} \tag{B.10}$$

From equation (B.2)

$$\frac{\partial u}{\partial s} = -\frac{\partial v}{\partial z}$$

so that the first term on the right hand side of equation (B.10) becomes

$$\int_0^\infty \frac{\partial u}{\partial s}\left(\int_z^\infty u^2 dz\right)dz = -\int_0^\infty \frac{\partial v}{\partial z}\left(\int_z^\infty u^2 dz\right)dz$$

Integrating this expression by parts yields

$$\int_0^\infty \frac{\partial u}{\partial s}\left(\int_z^\infty u^2 dz\right)dz = \left[-v\int_z^\infty u^2 dz\right]_0^\infty - \int_0^\infty u^2 v dz$$

Since $(v)_{z=0} = (v)_{z\to\infty} = 0$ then,

$$\int_0^\infty \frac{\partial u}{\partial s}\left(\int_z^\infty u^2 dz\right)dz = -\int_0^\infty u^2 v dz$$

Equation (B.10) integrated with respect to s from the initial condition to any condition downstream becomes

$$F = F_{in} - \frac{1}{2}\rho_r\mu_r\int_0^s (u^2)_{z=0}\,ds \tag{B.11}$$

where

$$F = \rho_r^2 \int_o^\infty u \int_z^\infty u^2 dzdz$$

is F at any s, and

$$F_{in} = \rho_r^2 \left[\int_o^\infty u \int_z^\infty u^2 dzdz \right]_{s=0}$$

is F at the initial s.

Since the velocity at $z = 0$ for the free jet is the maximum velocity of the jet, u_{max}, then equation (B.11) becomes

$$F = F_{in} - \frac{1}{2} \rho_r \mu_r \int_o^s u_{max}^2 ds \qquad (B.12)$$

F, then, is not conserved for the free jet but can be expressed by equation (B.12). A boundary condition of the wall jet is that the velocity at the wall, or $z = 0$, is zero, so then from equation (B.11), F is conserved for the wall jet.

Further, for the free layer used in the approximate solution, the velocity at $z = 0$ is a constant, u_r. Equation (B.11) in this case can be integrated to obtain

$$F = F_{in} - \frac{1}{2} \rho_r \mu_r u_r^2 s \qquad (B.13)$$

APPENDIX C

FINITE DIFFERENCE EQUATIONS

The Wall Jet

Momentum Equation

The momentum equation for the wall jet, as given in equations (2.54) and (2.55), is

$$\frac{M_o^2}{F}\frac{\partial \nu}{\partial s_w} = \nu \frac{\partial^2 \nu}{\partial M^2} + \frac{1}{3}\left[(1-M)\left(\frac{\partial \nu}{\partial M}\right) - \frac{\partial \nu}{\partial M}\right]\frac{\partial \nu}{\partial M} \tag{C.1}$$

where

$$M_o^2 = 1 - \frac{2}{3} F \int_o^{s_w} \left(\frac{\partial \nu}{\partial M}\right)_{M=0} ds_w \tag{C.2}$$

For the sake of simplicity, the superscript * has been dropped, however the variables are assumed dimensionless. The difference approximations used in these equations are

$$\left.\frac{\partial \nu}{\partial s_w}\right|_M \approx (\nu_{i,j+1} - \nu_{i,j})/\Delta s \tag{C.3}$$

$$\left.\frac{\partial \nu}{\partial M}\right|_{s_w} \approx \frac{1}{4\Delta M}\left[(\nu_{i+1,j+1} + \nu_{i+1,j} - \nu_{i,j+1} - \nu_{i,j})/\alpha\right. \tag{C.4}$$

$$\left. + (\nu_{i,j+1} + \nu_{i,j} - \nu_{i-1,j+1} - \nu_{i-1,j})/\beta\right]$$

$$\left.\frac{\partial^2 \nu}{\partial M^2}\right|_{s_w} \approx \frac{2}{(\alpha+\beta)\Delta M^2}\Big[(\nu_{i+1,j+1}+\nu_{i+1,j}-\nu_{i,j+1}-\nu_{i,j})/\alpha - (\nu_{i,j+1}+\nu_{i,j}-\nu_{i-1,j+1}-\nu_{i-1,j})/\beta\Big] \quad (C.5)$$

where Δs is the downstream increment, ΔM is the smallest increment in the momentum grid (10^{-4}), i is the M index, and j is the s index. The momentum grid control variables, α and β, are

$\alpha = \beta = 1$ for $0 < i < 100$

$\alpha = 100, \beta = 1$ for $i = 100$

$\alpha = \beta = 100$ for $100 < i < 199$

$\alpha = 1, \beta = 100$ for $i = 199$

$\alpha = \beta = 1$ for $199 < i < 298$

Applying equations (C.3), (C.4) and (C.5) to equations (C.1) and (C.2) then yields

$$\frac{M_o^2}{F}\frac{(\Delta M)^2}{\Delta s}(\nu_{i,j+1}-\nu_{i,j}) = \frac{\bar{\nu}_i}{(\alpha+\beta)}\Big[(\nu_{i+1,j+1}+\nu_{i+1,j}-\nu_{i,j+1}-\nu_{i,j})/\alpha - (\nu_{i,j+1}+\nu_{i,j}-\nu_{i-1,j+1}-\nu_{i-1,j})/\beta\Big]$$

$$+\frac{1}{24}\Big[2(i-M_i)\,\bar{\nu}_1 - (\bar{\nu}_{i+1}-\bar{\nu}_i)/\alpha - (\bar{\nu}_i-\bar{\nu}_{i-1})/\beta\Big]\times$$

$$\Big[(\nu_{i+1,j+1}-\nu_{i,j+1}+\nu_{i+1,j}-\nu_{i,j})/\alpha + (\nu_{i,j+1}-\nu_{i-1,j+1}+\nu_{i,j}-\nu_{i-1,j})/\beta\Big] \quad (C.6)$$

$$M_o^2 = 1 - \frac{2}{3}\frac{F\Delta s}{\Delta M}\sum_{j=1}^{s}(\bar{\nu}_1 - \bar{\nu}_o)_j \qquad (C.7)$$

where

$$\bar{\nu}_i = \nu_{i,j}$$

for the first computation of the $\nu_{i,j+1}$ at an s station. Then

$$\bar{\nu}_i = \frac{1}{2}(\nu_{i,j} + \nu_{i,j+1})$$

and the solution is repeated until the change in the $\bar{\nu}_i$ from one iteration to the next is less than 1 percent of the corrected values. If the known coefficients in equation (C.6) are designated as

$$K = \frac{24M_o^2}{F}\frac{(\Delta M)^2}{\Delta s} \qquad (C.8)$$

$$L = \frac{24\bar{\nu}_i}{(\alpha + \beta)} \qquad (C.9)$$

$$N = 2(1-M_i)\bar{\nu}_1 - (\bar{\nu}_{i+1} - \bar{\nu}_i)/\alpha - (\bar{\nu}_i - \bar{\nu}_{i-1})/\beta \qquad (C.10)$$

Then, equation (C.6) is expressed as

$$K(\nu_{i,j+1} - \nu_{i,j}) = L\left[(\nu_{i+1,j+1} + \nu_{i+1,j} - \nu_{i,j+1} - \nu_{i,j})/\alpha - (\nu_{i,j+1} - \nu_{i,j} - \nu_{i-1,j+1} - \nu_{i-1,j})/\beta\right]$$

$$+N\left[(\nu_{i+1,j+1} - \nu_{i,j+1} + \nu_{i+1,j} - \nu_{i,j})/\alpha + (\nu_{i,j+1} - \nu_{i-1,j+1} + \nu_{i,j} - \nu_{i-1,j})/\beta\right]$$

After simplification this becomes

$$\nu_{i-1,j+1} - \left(\frac{L(1+\beta/\alpha) - N(1-\beta/\alpha) + K\beta}{L - N} \right) \nu_{i,j+1} + \frac{\beta}{\alpha} \left(\frac{L+N}{L-N} \right) \nu_{i+1,j+1}$$

$$= -\nu_{i-1,j} + \left(\frac{L(1+\beta/\alpha) - N(1-\beta/\alpha) - K\beta}{L - N} \right) \nu_{i,j} - \frac{\beta}{\alpha} \left(\frac{L+N}{L-N} \right) \nu_{i+1,j} \qquad (C.11)$$

The right hand side of (C.11) contains all known quantities, whereas the left hand side contains the unknowns. Furtner defining

$$A(i,j) = -\left(\frac{L(1+\beta/\alpha) - N(1-\beta/\alpha) + K\beta}{L - N} \right) \qquad (C.12)$$

$$B(i,j) = \frac{\beta}{\alpha} \left(\frac{L+N}{L-N} \right) \qquad (C.13)$$

$$C(i,j) = -\nu_{i-1,j} + \left(\frac{L(1 + \beta/\alpha) - N(1 - \beta/\alpha) - K\beta}{L - N} \right) \nu_{i,j} \qquad (C.14)$$

$$- \frac{\beta}{\alpha} \left(\frac{L+N}{L-N} \right) \nu_{i+1,j}$$

equation (C.11) becomes

$$\nu_{i-1,j+1} + A(i,j)\nu_{i,j+1} + B(i,j)\nu_{i+1,j+1} = C(i,j) \qquad (C.15)$$

Equation (C.15) is the final difference approximation of equation (C.1). It is applied for each interior grid point at a particular s station. The result is a set of 297 equations and 297 unknowns. The matrix of coefficients governing these equations is tri-diagonal, however, and therefore the system is relatively easily solved.

Energy Equation

The energy equation (equation (2.57)) for the wall jet is

$$\frac{M_o^2}{F}\frac{\partial\theta}{\partial s_w} = \nu\frac{\partial^2\theta}{\partial M^2} + \frac{1}{3}\left[(1 - M)\left(\frac{\partial\nu}{\partial M}\right)_{M=0} + \frac{\partial\nu}{\partial M} - 2\frac{\nu}{\theta}\frac{\partial\theta}{\partial M}\right]\frac{\partial\theta}{\partial M} \tag{C.16}$$

If the analysis presented for equation (C.1) is repeated for equation (C.16) then the only change will be in the coefficient of the second term on the right hand side of equation (C.16). Equation (C.10) then must be replaced by

$$N = 2(1 - M_i)\bar{\nu}_1 - (\bar{\nu}_{i+1} - \bar{\nu}_i)/\alpha + (\bar{\nu}_i - \bar{\nu}_{i-1})/\beta - 2(\bar{\nu}_i/\bar{\theta}_i)\left[(\bar{\theta}_{i+1} - \bar{\theta}_i)/\alpha + (\bar{\theta}_i - \bar{\theta}_{i-1})/\beta\right] \tag{C.17}$$

where the $\bar{\theta}_i$ are averages computed in the same way that the $\bar{\nu}_i$ are computed. The result is the set of equations given by

$$\theta_{i-1,j+1} + A(i,j)\theta_{i,j+1} + B(i,j)\theta_{i+1,j+1} = C(i,j) \tag{C.18}$$

The $A(i,j)$, $B(i,j)$ and $C(i,j)$ are computed from equation (C.12), (C.13), and (C.14) combined with equations (C.8), (C.9), and (C.17).

The Free Jet

Momentum Equation

The momentum equation (equation(2.44))for the free jet is

$$\frac{\partial\nu}{\partial s_f} = \nu\frac{\partial^2\nu}{\partial M^2} - \frac{1}{3}\left(\frac{\partial\nu}{\partial M}\right)^2 \tag{C.19}$$

The analysis presented for equation (C.1) yields

$$K = 24 \frac{(\Delta M)^2}{\Delta s} \tag{C.20}$$

$$L = \frac{24\bar{\nu}_i}{(\alpha+\beta)} \tag{C.21}$$

$$N = -(\bar{\nu}_{i+1} - \bar{\nu}_i)/\alpha - (\bar{\nu}_i - \bar{\nu}_{i-1})/\beta \tag{C.22}$$

instead of equations (C.8), (C.9), and (C.10). Using these equations in equations (C.12), (C.13), and (C.14) then yields the coefficients of equation (C.15). The analysis is the same as that for the wall jet. The momentum grid control variables for the free jet are

$\alpha = \beta = 100$ for $0 < i < 100$

$\alpha = 100, \beta = 1$ for $i = 100$

$\alpha = \beta = 1$ for $100 < i < 199$

Energy Equation

The energy equation (equation(2.45))for the free jet is

$$\frac{\partial\theta}{\partial s_f} = \nu \frac{\partial^2\theta}{\partial M^2} + \frac{1}{3}\left\{\frac{\partial\nu}{\partial M} - 2\frac{\nu}{\theta}\frac{\partial\theta}{\partial M}\right\}\frac{\partial\theta}{\partial M}$$

As in the case of the wall jet, the only difference from the analysis of equation (C.19) is in the non-linear coefficient, N , expressed in equation (C.22). This equation is replaced by

$$N = (\bar{\nu}_{i+1} - \bar{\nu}_i)/\alpha + (\bar{\nu}_i - \bar{\nu}_{i-1})/\beta$$

$$-2(\bar{\nu}_i / \bar{\theta}_i) \left[(\bar{\theta}_{i+1} - \bar{\theta}_i)/\alpha + (\bar{\theta}_i - \bar{\theta}_{i-1})/\beta \right]$$

Introducing this expression for N into equations (C.12), (C.13), and (C.14) yields the coefficients for equation (C.18).

APPENDIX D

DETAILS OF THE APPROXIMATE ANALYSIS

The Boundary Layer

The boundary layer velocity distribution is approximated by

$$u_a^* = \frac{u_a}{u_r} = A\left(\frac{z}{\delta_a}\right)^3 + B\left(\frac{z}{\delta_a}\right)^2 + C\left(\frac{z}{\delta_a}\right) + D \qquad (D.1)$$

where δ_a is the transformed boundary layer thickness, and u_r is the free stream velocity. Requiring that the boundary conditions

$$z = 0, \qquad u = \frac{\partial^2 u_a}{\partial z^2} = 0$$

$$z = \delta_a, \qquad \frac{\partial u_a}{\partial z} = \frac{\partial^2 u_a}{\partial z^2} = 0$$

are satisfied by equation (D.1) then yields

$$u_a^* = \frac{3}{2}\eta - \frac{1}{2}\eta^3 \qquad (D.2)$$

where $\eta = z/\delta_a$. The unknown boundary layer thickness, δ_a, is obtained from the integral momentum equation for the boundary layer which is

$$\frac{d}{ds}\left[\delta_a u_r^2 \int_0^1 (1-u_a^*)u_a^*\, d\eta\right] = \frac{\mu_r}{\rho_r}\frac{u_r}{\delta_a}\left(\frac{\partial u_a^*}{\partial \eta}\right)_{\eta=0} \qquad (D.3)$$

The integral in equation (D.3) with u_a^* given by equation (D.2) yields

$$\int_0^1 (1 - u_a^*)u_a^* \, d\eta = \frac{39}{280} \tag{D.4}$$

Also, from equation (D.2),

$$\left(\frac{\partial u_a^*}{\partial \eta}\right)_{\eta=0} = \frac{3}{2} \tag{D.5}$$

Substituting equations (D.4) and (D.5) in equation (D.3) yields

$$\frac{39}{280} u_r^2 \frac{d\delta_a}{ds} = \frac{3}{2} \frac{\mu_r}{\rho_r} \frac{u_r}{\delta_a}$$

This equation can be integrated directly to obtain

$$\frac{\delta_a}{d} = 4.64 \sqrt{\frac{\mu_r}{\rho_r u_r s}} \left(\frac{s}{d}\right) \tag{D.6}$$

where d is a reference length. The velocity distribution for any downstream position, s, is obtained from this solution and equation (D.2).

The Free Layer

The free layer velocity distribution is approximated by

$$u_b^* = \frac{u_b}{u_r} = A\left(\frac{z - \delta}{\delta_b}\right)^3 + B\left(\frac{z - \delta}{\delta_b}\right)^2 + C\left(\frac{z - \delta}{\delta_b}\right) + D \tag{D.7}$$

where δ_b is the transformed thickness of the free layer, and δ is the transformed distance from a reference line to the viscous layer

as defined in Figure 2. Requiring that the conditions

$$z = \delta, \qquad u_b = u_r \quad \text{and} \quad \frac{\partial u_b}{\partial z} = 0$$

$$z = \delta + \delta_b, \qquad u_b = \frac{\partial u_b}{\partial z} = 0$$

be satisfied by equation (D.7) yields

$$u_b^* = 2\eta^3 - 3\eta^2 + 1 \tag{D.8}$$

where $\eta = \frac{z-\delta}{\delta_b}$. The two unknowns δ_b and δ can be obtained from the integral momentum equation and F relation, which are expressed as

$$M_o/\rho_r = (d-\delta)u_r^2 = \delta_b \int_o^1 u_b^{*2}\, d\eta \tag{D.9}$$

$$\frac{F}{\rho_r^2} = u_r^3\delta^2 \int_o^1 \int_\eta^1 d\eta d\eta + u_r\delta\,\delta_b \int_o^1 \int_o^1 u_b^{*2}\, d\eta d\eta \tag{D.10}$$

$$+ \delta_b^2 u_r^3 \int_o^1 u_b^* \int_\eta^1 u_b^{*2}\, d\eta d\eta = \frac{1}{2} u_r^3 d^2 - \frac{1}{2}\frac{\mu_r}{\rho_r} u_r^2 s$$

where d is the thickness of the initial velocity distribution. The integrals in equations (D.9) and (D.10) are

$$\int_o^1 u_b^{*2}\, d\eta = \frac{13}{35} \tag{D.11}$$

$$\int_o^1 \int_\eta^1 d\eta d\eta = \frac{1}{2} \tag{D.12}$$

$$\int_0^1 \int_0^1 u_b^{*2}\, d\eta d\eta = \frac{13}{35} \tag{D.13}$$

$$\int_0^1 u_b^* \int_\eta^1 u_b^{*2}\, d\eta d\eta = 0.07587 \tag{D.14}$$

Substituting these constants into equations (D.9) and (D.10) and solving for δ_b and δ yields

$$\frac{\delta_b}{d} = 8.518 \left(\frac{\mu_r}{\rho_r u_r s} \right)^{1/2} \left(\frac{s}{d} \right) \tag{D.15}$$

$$\frac{\delta}{d} = 1 - 3.164 \left(\frac{\mu_r}{\rho_r u_r s} \right)^{1/2} \left(\frac{s}{d} \right) \tag{D.16}$$

With δ_b and δ the velocity distribution is then available from equation (D.8).

Region (II) of the Free Jet

The velocity distribution for region (II) of the free jet defined in Figure 2 is of the same form as equation (D.8) with $u_b^* = u/u_{max}$ and $\eta = z/\delta_b$. The two unknowns, the maximum velocity, u_{max}, and the transformed jet thickness, δ, are obtained from the conservation of total momentum equation and the F relation differentiated with respect to s. These equations are expressed as

$$M_o/\rho_r^2 = u_r^2 d = u_{max}^2\, \delta_b \int_0^1 u_b^{*2}\, d\eta \tag{D.17}$$

$$0 = \frac{d}{ds}\left[U_{max}^3 \, \delta_b^2 \int_o^1 u_b^* \int_\eta^1 u_b^{*2} \, d\eta d\eta \right] - \frac{1}{2} \frac{\mu_r}{\rho_r} \qquad (D.18)$$

The integrals are the same as those presented in (D.11) through (D.14). Solving equation (D.17) for δ_b yields

$$\frac{\delta_b}{d} = 2.692 \left(\frac{u_r}{u_{max}} \right)^2 \qquad (D.19)$$

Using this expression in (D.18) yields

$$\frac{1}{u_{max}^4} \frac{du_{max}}{ds} = - 0.9092 \, u_r^2 d$$

which is integrated directly to obtain

$$\frac{u_{max}}{u_r} = \left(\frac{1}{2.727 \frac{\mu_r}{\rho_r u_r d} \left(\frac{x}{d} \right) + 1} \right)^{1/3} \qquad (D.20)$$

The shear layer thickness, δ_b, is obtained by combining equations (D.19) and (D.20). The velocity distribution is then obtained from equation (D.8).

Region (II) for the Wall Jet

The velocity profile for region (II) of the wall jet is divided into two parts. The portion of the profile next to the wall is of the form of equation (D.2),

$$u_a^* = \frac{3}{2} \eta - \frac{1}{2} \eta^3 \qquad (D.21)$$

where $u_a^* = \frac{u}{u_{max}}$ and $\eta = z/\delta_a$. The top portion of the profile, from the maximum velocity away from the wall, is of the form of equation (D.8),

$$u_b^* = 2\xi^3 - 3\xi^2 + 1 \qquad (D.22)$$

where $u_b^* = \frac{u}{u_{max}}$ and $\xi = \frac{z - \delta_a}{\delta_b}$. The δ_a and δ_b are the transformed layer thicknesses from the wall to the maximum velocity point and from that point to the end of the layer, respectively. The three unknowns, δ_a , δ_b and u_{max} are computed from the integral momentum equation taken over the entire profile, which is expressed as

$$\frac{d}{ds}\left[u_{max}^2\, \delta_a \int_0^{\delta_a} u_a^{*2}\, d\eta + u_{max}^2\, \delta_b \int_{\delta_a}^{\delta_a+\delta_b} u_b^{*2} d\xi \right] \qquad (D.23)$$

$$= \frac{\mu_r}{\rho_r} \frac{u_r}{\delta_a} \left(\frac{\partial u_a^*}{\partial \eta}\right)_{\eta=0}$$

the integral momentum equation taken over the top portion of the profile, which is expressed as

$$\frac{d}{ds}\left[u_{max}^2\, \delta_b \int_0^1 u_b^{*2}\, d\xi \right] = \qquad (D.24)$$

$$- u_{max} \frac{d}{ds}\left[u_{max}\, \delta_a \int_0^1 u_a^*\, d\eta \right]$$

and the F relation over the entire profile, which is expressed as

$$\frac{F}{\rho_r^2} = \frac{1}{2} u_r^3 d^2 = u_{max}^3 \delta_a^2 \int_o^1 u_a^* \left[\int_\eta^1 u_a^{*2} \, d\eta \right] d\eta \qquad (D.25)$$

$$+ u_{max}^3 \delta_a \delta_b \int_o^1 u_a^* \left[\int_o^1 u_b^{*2} \, d\xi \right] d\eta$$

$$+ u_{max}^3 \delta_b^2 \int_o^1 u_b^* \left[\int_\xi^1 u_b^{*2} \, d\xi \right] d\xi$$

The two momentum equations are expressed differentiated with respect to s . The integrals contained in these three equations have already been presented with the exception of the following:

$$\int_o^1 u_a^* \, d\eta = \frac{5}{8}$$

$$\int_o^1 u_a^* \left[\int_\eta^1 u_a^{*2} \, d\eta \right] d\eta = \frac{4863}{27720}$$

$$\int_o^1 u_a^* \left[\int_o^1 u_b^{*2} \, d\xi \right] d\eta = \frac{13}{56}$$

With these expressions, then, equation (D.25) can be expressed as

$$\frac{\delta_b}{\delta_a} = -1.530 + \sqrt{0.028358 + 6.5906 \left(\frac{u_r}{u_{max}} \right)^3 \left(\frac{d}{\delta_a} \right)^2} \qquad (D.26)$$

Equation (D.24) can be used in equation (D.23) and the result expressed as

$$\delta_a^2 \frac{du_{max}}{ds} = 0.2010\, u_{max} \frac{d\delta_a^2}{ds} - 4.330 \frac{\mu_r}{\rho_r} \qquad (D.27)$$

Equations (D.26) and (D.27) in equation (D.24) yield

$$u_{max} \frac{d\delta_a^2}{ds} = 29.7446 \frac{\mu_r}{\rho_r} \left\{ \frac{0.04118 - \left[0.028358 + 6.5906 \left(\frac{u_r}{u_{max}} \right)^3 \left(\frac{d}{\delta_a} \right)^2 \right]^{1/2}}{0.12758 - \left[0.028358 + 6.5906 \left(\frac{u_r}{u_{max}} \right)^3 \left(\frac{d}{\delta_a} \right)^2 \right]^{1/2}} \right.$$

$$\left. \frac{+ 2.3925 \left(\frac{u_r}{u_{max}} \right)^3 \left(\frac{d}{\delta_a} \right)^2}{+ 3.3035 \left(\frac{u_r}{u_{max}} \right)^3 \left(\frac{d}{\delta_a} \right)^2} \right\} \qquad (D.28)$$

An explicit finite difference scheme can be used to solve equations (D.26), (D.27), and (D.28) for the three unknowns, δ_a , δ_b , and u_{max} . The velocity distributions then can be obtained from equations (D.21) and (D.22).

LITERATURE CITED

1. H. Schlichting, Boundary Layer Theory, McGraw-Hill Inc., 1960, p. 164.

2. W. Bickley, "The Plane Jet," The Philosophical Magazine, Series 7, p. 727, 1937.

3. M. B. Glauert, "The Wall Jet," Journal of Fluid Mechanics, 1, 1956, p. 625.

4. N. Riley, "Effects of Compressibility on a Laminar Wall Jet," Journal of Fluid Mechanics, 4, 1958, p. 615.

5. S. I. Pai, Fluid Dynamics of Jets, D. Van Nostrand Company, Inc., 1954.

6. L. Howarth, "Concerning the Effect of Compressibility on Laminar Boundary Layers and Their Separation," Proceeding of The Royal Society of London, 194, 1958, p. 16.

7. D. R. Chapman, "Laminar Mixing of a Compressible Fluid," NACA TN 1800, 1950.

8. A. M. Kuethe and J. D. Schetzer, Foundations of Aerodynamics, Second edition, John Wiley and Sons, Inc., 1959.

9. W. Mangler, "Zusammehang swischen eben und rotations symmetrischen Grenzschichten in kompressiblen Flussigkeiten," ZAMM, 28, 1948, p. 7.

10. N. Riley, "An Application of Mangler's Transformation," Quarterly Journal of Mechanics and Applied Mathematics, 14, 1961, p. 197.

11. C. F. Dewey, S. I. Schlesinger, and L. Sashkin, "Temperature Profiles in a Finite Solid with Moving Boundary," Journal of the Aerospace Sciences, 27, 1960, p. 59.

12. M. R. Denison and E. Baum, "Compressible Free Shear Layer with Finite Initial Thickness," AIAA J., 1, 1963, p. 342.

13. L. Crocco, "Su di un valore massimo del coefficiente di transmissione del calore da una lamina piana a un fluido scorrente," Rendicent: R. Accademia dei Lindei, 14, 1931, p. 490.

14. L. Crocco, "Sulla transmissione del calore da una lamina piana un fluido scorrente ad alta velocita," L'Aerotecnica, 12, 1932, p. 181.

15. E. R. G. Eckert and R. M. Drake, Jr., Heat and Mass Transfer, McGraw-Hill Inc., 1959, p. 140.

16. F. S. Sherman, "New Experiments on Impact-Pressure Interpretation in Supersonic and Subsonic Rarefied Air Streams," NACA TN 2995, 1953.

17. E. N. da C. Andrade, "The Velocity Distribution in a Liquid-into-Liquid Jet. Part 2: The Plane Jet," Proceeding Physical Society, London, 51, 1939, p. 784.

VITA

John Patrick Crenshaw was born in Atlanta, Georgia on April 24, 1938. He attended the public schools of Atlanta and DeKalb County and graduated from Southwest DeKalb High in June of 1956. He entered the Georgia Institute of Technology the following fall. He was awarded the degree of Bachelor of Aeronautical Engineering under the Co-operative plan in June of 1961. In the fall of 1961, he was granted an assistantship to continue his study. He was awarded the Master of Science Degree in Aerospace Engineering in June of 1963. In the fall of 1963, he was granted a NASA traineeship to continue his study and pursue the Doctor of Philosophy in the School of Aerospace Engineering. He is a member of the Sigma Gamma Tau and Sigma Xi honorary societies.

Mr. Crenshaw spent his work periods under the co-operative plan, as well as two summers as an engineer, with the Marshall Space Flight Center in Huntsville, Alabama. He spent another summer as an engineer with the Aeronutronics Division of the Philco Corporation in Newport Beach, California.

Mr. Crenshaw was married in 1965 to the former Miss Carolyn Lorenda Bass of New Orleans, Louisiana. They have a daughter, Elizabeth Anne.